Energy Functional for Nuclear Masses

A Thesis Presented for

The Doctor of Philosophy

Degree

The University of Tennessee, Knoxville

Michael Giovanni Bertolli

December 2011

To Alicia,

my $\max_x\{f(\mathbf{x})\}$.

$\forall f$.

Acknowledgements

In the process of this work, and all that led up to it, I was supported by many. I would like to thank:

- Colleagues, for help and discussions on problems of physics and mathematics, both simple and complex
- My thesis committee, for their oversight and guidance academically and professionally
- The Department of Energy and University of Tennessee, Department of Physics and Astronomy, for funding
- My collaborator, Stefan Wild at ANL, for insightful discussions, teaching and work on the minimization of this functional
- My advisor, Thomas Papenbrock, for the opportunity to work in a fascinating field of research
- Family and friends, for support that words cannot do justice.

Abstract

An energy functional is formulated for mass calculations of nuclei across the nuclear chart with major-shell occupations as the relevant degrees of freedom. The functional is based on Hohenberg-Kohn theory. Motivation for its form comes from both phenomenology and relevant microscopic systems, such as the three-level Lipkin Model. A global fit of the 17-parameter functional to nuclear masses yields a root-mean-square deviation of χ[chi] = 1.31 MeV, on the order of other mass models. The construction of the energy functional includes the development of a systematic method for selecting and testing possible functional terms. Nuclear radii are computed within a model that employs the resulting occupation numbers.

Contents

List of Tables

List of Figures

Chapter 1

Motivation and background

The bulk properties (i.e. masses and radii) of a nucleus are fundamental aspects of nuclear structure. The interest, both theoretically and experimentally, in nuclear masses is the focus of this work. The mass $M(N, Z)$ of some nucleus with a total number of neutrons N and protons Z is in fact less than the sum of masses of its constituent nucleons. The difference is known as the binding energy $BE(N, Z)$

$$BE(N, Z) = NM_n + ZM_p - M(N, Z) \tag{1.1}$$

where M_n and M_p are the masses of the free neutron and proton respectively. This so-called "mass-defect" was discovered by Aston in the first part of the 1900's when his measurements revealed that the atomic mass of helium was at 4.000 atomic units (to within 1 part in 1000), while that of hydrogen was at 1.008 atomic units [Aston, 1920]. This led to a discrepancy with the current view of helium consisting of four hydrogen nuclei. Aston's contemporary, Eddington, interpreted this "defect" in terms of the binding energy. Eddington's suggestion from this that the transformation of hydrogen into helium could provide an energy excess sufficient to power stellar processes indicates the foundational relationship between nuclear masses and astrophysics [Lunney et al., 2003].

This relationship continues. Understanding the process of nucleosynthesis relies on accurate calculations of the reactions involved. The rapid neutron capture process (r-process) results in the formation of roughly half of the elements heavier than iron. The r-process occurs in a high temperature and neutron-rich environment, possibly supernovae or merging neutron stars. The process entails consecutive capture of neutrons on a seed nucleus, followed by β-decay. The r-process follows a path governed by the competition between these neutron capture and β-decay rates. Necessary inputs for modeling this process are nuclear masses and β-decay half-lives of nuclei the vast majority of which are inaccessible by experiment [Martinez-Pinedo and Langanke, 1999, Thielemann et al., 2001, Stone and Reinhard, 2007].

Binding energy calculations for nuclei can be applied to the study of compact stars (e.g. white dwarfs, neutron stars) [Stone and Reinhard, 2007]. The Equation of State (EoS) for modeling compact stars relies on the effective interaction and its density dependence. The effective interaction provides a means by which one can approximate a solution to the many-body Schödinger equation. Moreover, a primary input for the EoS is the energy per particle, whose value includes the nuclear mass.

Outside of the realm of astrophysics masses play a crucial role in Q-value calculations for other branches of physics. Particle physics, for example, relies on mass differences between parent and daughter nuclei to determine the location of the double-β peak in neutrino-less double-β decay [Klapdor-Kleingrothaus et al., 2001, Aalseth et al., 2002]. Within nuclear structure itself, decay modes for a given system can be determined through the energy released in a reaction [Giovinazzo et al., 2002, Pfützner et al., 2002].

Additionally, there are fundamental nuclear phenomena that remain to be fully understood on a theoretical basis. Increased binding at certain N and Z values (the magic numbers) has been described via the shell-model (see Section 4.1.2 for details). However, questions still remain whether changes in magic numbers are to be discovered beyond areas explored by experiment, or if the effect of the current magic

numbers will be lessened as one moves further towards the proton or neutron drip-lines [Ozawa et al., 2000, Sorlin et al., 2000, Myers and Swiatecki, 2001]. Pairing, too, remains to be satisfactorily understood for both the case of a proton and neutron coupled in an isospin $T = 0$ state and the case of the different binding found in nuclei with even numbers of nucleons verses odd numbers (so-called "odd-even staggering") [Duguet et al., 2001a, Duguet et al., 2001b]. Furthermore, a precise location of the proton and neutron drip-lines remains unknown beyond $Z = 50$ and $Z = 8$, respectively, and thus we lack an understanding of the behaviour of nuclei far from the line of stability.

While the study of nuclear masses is an extensive and interesting field, the focus of this work is to describe the systematics of masses at a global scale. Furthermore, we maintain a focus on extrapolation to regions of the nuclear chart that remain unknown. The research work presented here takes several forms and the thesis is organized as follows: Section 1.1 gives a brief overview of some of the previously developed nuclear mass models. Chapter 2 provides the foundation for our approach to nuclear mass calculations via shell-model energy density functionals. In Chapter 3 we show the analytical derivation of the energy functional for the three-level Lipkin model. The primary purpose of this work was to gain further understanding into analytical systems and their energy functionals. The realistic framework and method for developing the energy functional for nuclei, which is the major thrust of this work, are described in Chapter 4. This work consisted of the coding and implementation of a FORTRAN program that minimizes the functional, as well as designing and executing a methods by which large numbers of terms could be tested. Chapter 5 then details the fitting procedures used to obtain the parameters of our functional. The parameter fitting was performed in collaboration with Stefan Wild of Argonne National Lab. Here the main effort was to insure minimal numerical noise. The model for calculating nuclear charge radii is presented in Chapter 6. The model is implemented in FORTRAN and post-processes the data from the minimization of the functional. Finally, results and concluding remarks are given in Chapters 7 and 8.

This thesis is an extended version of the papers: *Energy functional for the three-level Lipkin model* [Bertolli and Papenbrock, 2008] and *Occupation number-based energy functional for nuclear masses* [Bertolli et al., 2011]. Throughout the thesis "we" refers to myself and my collaborators with whom this work was done. My own contributions included: the development and implementation of the method for determining new terms for the functional (Section 4.3), which led to the inclusion of new terms and a significant lowering of the χ value; the analytical work necessary to insure proper scaling of terms and provide their analytical gradients for the minimizations; the majority of the coding and testing of the functional; and major contributions to the writing of the publications, including first drafts.

1.1 Approaches to nuclear mass calculations

There are very good mass models available, however improvements are desired for more accurate contributions to astrophysical calculations and predictions in nuclear structure. In this chapter we introduce the methods of constructing mass models and describe our new approach to shell-model based mass formulae.

The first mass formula was the Weizsäcker semi-empirical mass formula introduced in 1935, shown in the form given by Bethe and Bacher [Bethe and Bacher, 1936] :

$$BE(N,Z) = a_v A - a_s A^{2/3} - a_c \frac{Z(Z-1)}{(A)^{1/3}} - a_A \frac{(N-Z)^2}{A} + a_P \frac{\delta}{\sqrt{A}} \tag{1.2}$$

where $BE(N,Z)$ is the binding energy of a nucleus with N neutrons and Z protons, and $A = N + Z$ is the total number of nucleons.

The liquid drop model provides motivation for the terms in Equation 1.2 (See Section 4.1.1 for details). The radius of a nucleus is proportional to $A^{1/3}$, therefore the first term $a_v A$ represents a volume and accounts for the saturation of the nuclear force. The remaining terms then represent a surface term (a_s), a Coulomb contribution (a_c),

an isospin term to account for asymmetry between protons and neutrons (a_A) and a pairing term (a_P). In the pairing term δ is 1, 0, and -1 for even-even, odd mass, and odd-odd nuclei, respectively. The coefficients are determined empirically by fitting to known nuclear binding energies. Performing a χ^2 minimization fit of the parameters a_i yields a least-squares error of $\chi \simeq 2.9$ MeV. Expansion of the nuclear binding energy with terms of physically transparent meaning (volume, surface, etc.) has also been studied in the leptodermous, or "light-skin", expansion (see Reference [Reinhard et al., 2006] for a discussion).

The Bethe-Weizsäcker formula does not depend on orbital occupation of proton and neutrons, but rather simply on the total proton and neutron number. One shortcoming of the Bethe-Weizsäcker formula is that it does not include shell effects. Figure 1.1 shows the oscillations about zero for $E^{\mathrm{BW}} - E^{\mathrm{exp}}$ that result from no shell closures being represented in the Bethe-Weizsäcker formula. The lack of shell-corrections can be approached in ways such as the Strutinsky method [Strutinsky, 1967] or within the Skyrme-Hatree-Fock theories (see for example [Kruppa et al., 2000]). One way to account for the shell effects, and that adopted in this work, is by explicit dependence on proton and neutron orbital occupation.

The Bethe-Weizsäcker mass formula is presented here as an historical benchmark for the mass model work discussed later. It gives a simple interpretation of the mass dependencies. One will expect that a more sophisticated mass formula must improve on the χ value from the Bethe-Weizsäcker formula.

Since the Bethe-Weizsäcker model there have been many developments in nuclear mass formulae, resulting in χ values of several hundred keV (for a review see Reference [Lunney et al., 2003]). It is known that a thorough understanding of nuclei requires the inclusion, both experimentally and theoretically, of rare isotopes [Bertsch et al., 2007]. Yet the important ability to extrapolate to rare isotopes is thus far difficult to achieve in mass formulae.

One can obtain good extrapolation in a mass model through a firm microscopic foundation. A model has "good extrapolation" when the applicaiton to larger

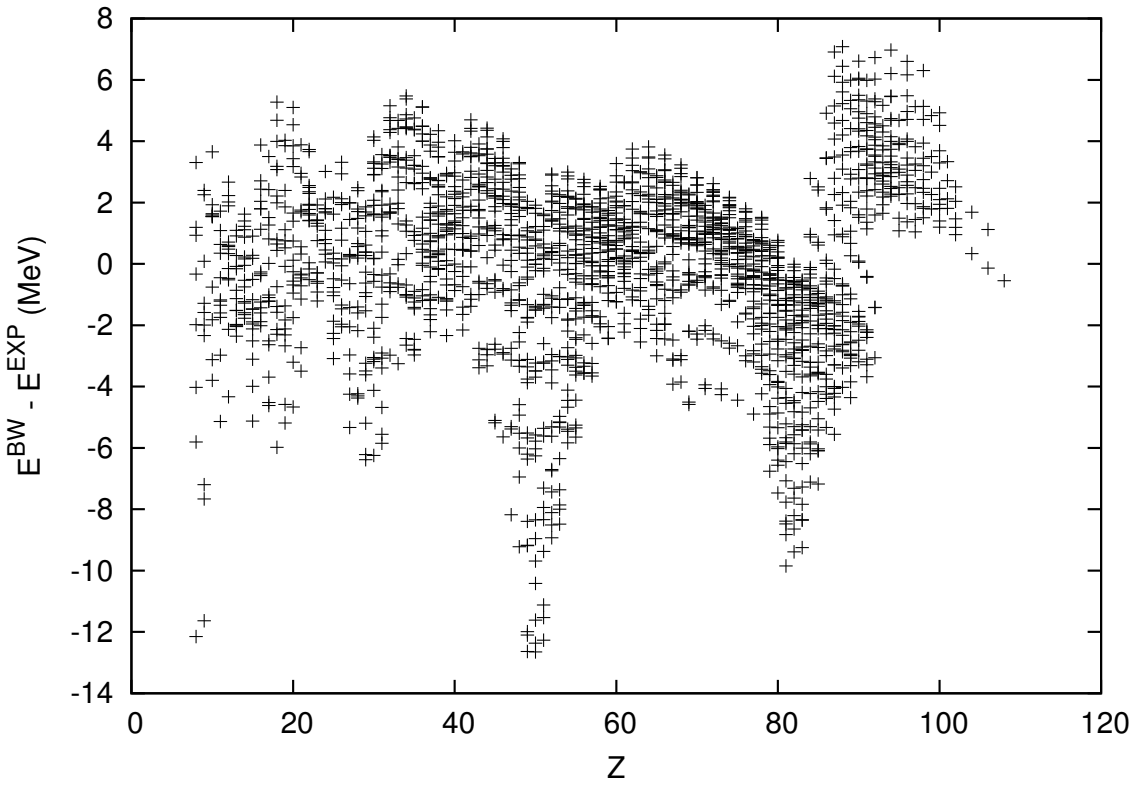

Figure 1.1: Difference between Bethe-Weizsäcker calculations and experimental binding energies (range from -14 MeV to $+8$ MeV) as a function of proton number Z (range from 0 to 120). One can clearly see the oscillations around zero that result from no shell closure in the Bethe-Weizsäcker formula.

datasets does not significantly increase the chi value.. One method of providing this foundation is through ab initio approaches. *Ab initio* ("from the beginning") methods describe nuclei through solutions to the non-relativistic Schrödinger equation, or relativistic Dirac equation, currently with two-and three-body potentials [Fritz et al., 1993, Navrátil et al., 2001, Machleidt, 1989, Brueckner and Gammel, 1958].

Ab initio approaches to nuclear mass calculations face exceptional hurdles in the quickly expanding size of the model sspace as heavier nuclei are considered [Bertsch et al., 2007]. As a result, the techniques (no-core shell-model, Green function Monte Carlo) have been successful for the light nuclei ($A \leq 12$ [Wiringa et al., 2000, Pieper et al., 2001]) and other models with more efficient treatments of the many-body system are needed for heavier nuclei [Bertsch et al., 2007, Lunney et al., 2003, Stone and Reinhard, 2007]. For example, the coupled-cluster method works well for doubly magic nuclei up to $A \sim 40$.

Methods which extend past light nuclei can be found in mean-field approaches, which have been used for over 70 years. For a recent review see Reference [Bender et al., 2003a]. The underlying concept behind mean-field approaches is the treatment of nucleons as non-interacting particles in an effective density-dependent potential (for reviews see References [Pandharipande et al., 1997, Bender et al., 2003a]). The Hartree-Fock (HF) approximation assumes the many-body system can be described by a product wavefunction, constructed as a single Slater determinant of the independent particle wavefunctions. Each independent particle moves in a mean-field potential generated by the remaining particles [Hartree, 1929, Mayer and Jensen, 1955]. Nuclei are self-bound and therefore generate their own mean-field [Bertsch et al., 2007].

While the HF method seems very much in line with initial inceptions of the shell-model (the interacting particle model), it is not sufficient in describing nuclear systems where pairing correlations are significant. Generalizing the concepts of the HF approximation to include a pairing component is given by the Hartree-Fock-Bogoliubov (HFB) method [Mang, 1975, Bender et al., 2003a]. Both HF and HFB methods employ the variational principle to obtain ground state energies.

In recent years, significant progress has been made in developing global nuclear mass models; see, for example, References [Goriely et al., 2009, Kortelainen et al., 2010b]. The Skyrme-Hartree-Fock-Bogoliubov mass functionals by Goriely *et al.* [Goriely et al., 2009] achieve a least-squares error of about $\chi = 0.58$ MeV with 14 parameters fit to nuclei with $N, Z \geq 8$. The UNEDF functionals UNEDFnb (12 parameters) and UNEDF0 (10 parameters) of Reference [Kortelainen et al., 2010b] have a least-squares deviation of $\chi = 0.97$ MeV and $\chi = 1.46$ MeV, respectively, when fit to a set of 72 even-even nuclei. The fitted functionals, when applied to 520 even-even nuclei of a mass table, yield least-squares deviations of $\chi = 1.45$ MeV and $\chi = 1.61$ MeV, respectively. The refit [Bertsch et al., 2005] of the Skyrme functional Sly4 to even-even nuclei exhibits a root-mean-square deviation of about $\chi = 1.7$ MeV. Somewhat older mass models also perform well, such as HFB-2 [Goriely et al., 2002] based on a parameterization of a Skyrme interaction, achieves a least-squares error of $\chi \simeq 0.6$ MeV. The Finite Range Droplet Model (FRDM) [Möller et al., 1995] employs a macroscopic-microscopic method where microscopic shell corrections are grafted onto to a macroscopic liquid drop energy through the Strutinsky method and achieves a similar least-squares error at $\chi \simeq 0.6$ MeV. For a recent review on this matter, see Reference [Stone and Reinhard, 2007].

Using an occupation-number approach, the mass formula by Duflo and Zuker computes the binding energy in terms of the shell-model occupations [Duflo and Zuker, 1995]. The occupations are parameters—not variables—and their values are taken from the noninteracting shell-model (with modifications due to deformations). The form of the Duflo-Zuker mass formula is motivated by semiclassical scaling arguments, which ensure that the binding energy scales linearly with the mass number in leading order; see Reference [Mendoza-Temis et al., 2010] for details. The Duflo-Zuker mass formula achieves an impressive root-mean-square deviation of $\chi \simeq 0.35$ MeV with 28 fit parameters. The ability of any of these mass models to extrapolate to new nuclei is of primary interest (see Table 1.1). Working with a strong microscopic foundation for the model proposed in this thesis, its terms should be limited to those

with microscopic physical significance. As will be discussed later, this microscopic guidance will also come from exactly solvable models.

Table 1.1: A comparison of the χ values for three models fitted to the 1995 compilation of nuclear binding eneries (1768 nuclei) and the resulting χ values for calculations of the 382 new nuclei available in 2001. In this case it is seen that the FRDM appears rather stable to extrapolations, while the remaining models are not as good. * HFB-2 was fit to the entire 2001 compilation (2135 nuclei) and it's performance is compared to the calculations of the 382 nuclei not available in 1995.

	χ (MeV)	
	(1995 data)	(2001 new nuclei)
HFB-2*	0.674	0.769
FRDM	0.678	0.655
Duflo-Zuker	0.346	0.479

1.2 Density functional theory

The mean-field approach we are most interested in here is density functional theory (DFT). DFT has proved remarkably successful in condensed matter and quantum chemistry as well as in describing nuclei across the nuclear chart [Bender et al., 2003a, Lunney et al., 2003, Bertsch et al., 2007]. By utilizing the density as the degree of freedom for the system has allowed it to overcome many of the computional obstacles faced by *ab initio* techniques (see Figure 1.2) [Bertsch et al., 2007]. Introduced in 1964 by Hohenberg and Kohn, the theory is centered on the (one-body) ground state density [Hohenberg and Kohn, 1964]. The energy density can be shown to be a functional of the applied external potential. Moreover an energy functional of the density can be constructed that is valid for any number of particles in any external potential [Hohenberg and Kohn, 1964]. If the energy density functional is known the ground state energy of a system can be found by the minimization of the functional with the external potential incorporated through an additive term (via the variational principle) [Hohenberg and Kohn, 1964, Eschrig, 2003]. Of course the determination of

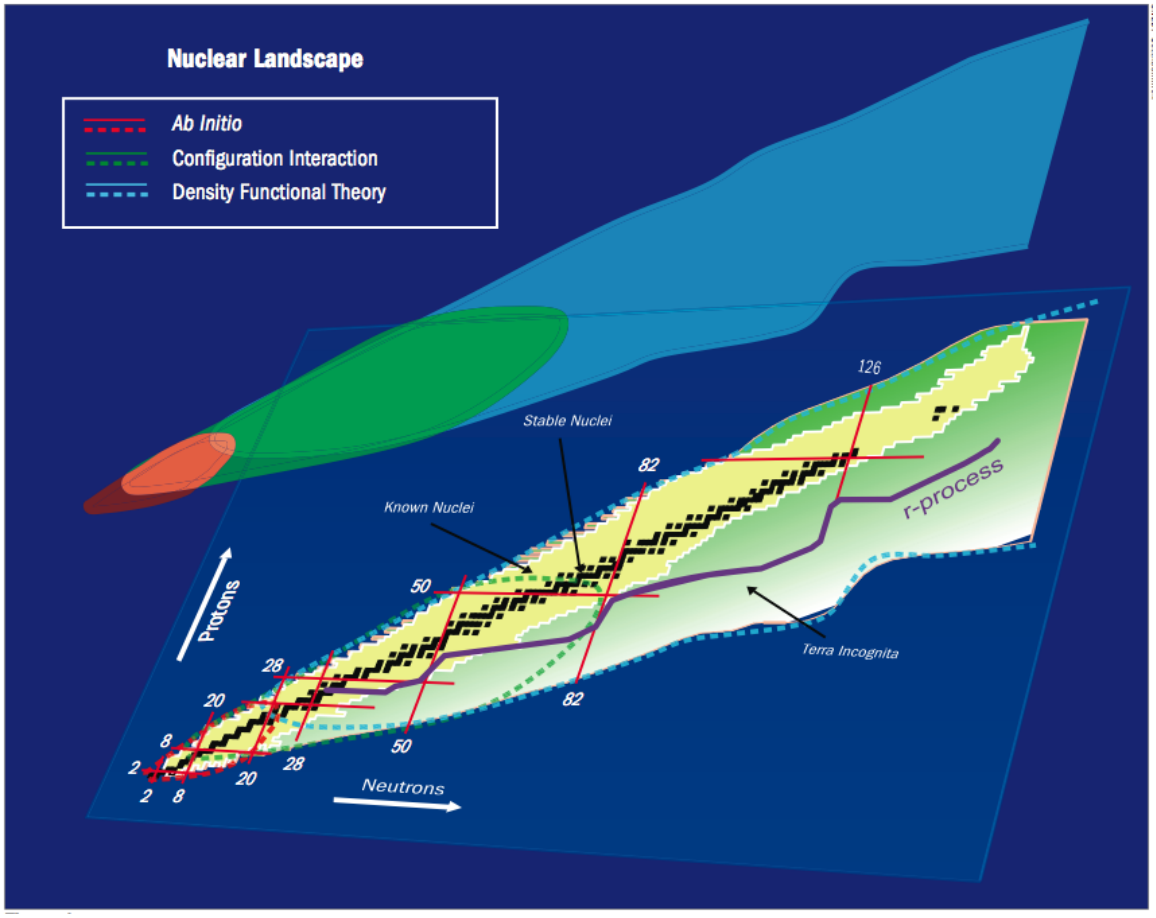

Figure 1.2: The nuclear landscape and various methods used in describing it. DFT works well across the entire chart, except in areas of the lightest nuclei. (coloured squares) Shown are both stable (black) and unstable (yellow) nuclei which are readily studied in the laboratory [Bertsch et al., 2007].

the functional for a system is non-trivial and is the focus of this work. In Section 2.1 of the following chapter we detail the specifics of the theoretical foundation of this work.

Difficulties in expressing the Hohenberg-Kohn functional, where the density for a many-body system in an arbitrary potential is not always known, were addressed by Kohn and Sham. Kohn and Sham introduced a method of expressing the kinetic energy in terms of single-particle wavefunction orbitals. The Kohn-Sham (KS) equations are solved self-consistently to determine the particle density that satisfies the one-particle Schrödinger equation with appropriate effective and exchange

correlation potentials, starting from an assumed approximate density [Kohn and Sham, 1965, Argaman and Makov, 2000]. While the KS approach should be mentioned for its wide application to many fields, the work proposed here falls well within the Hohenberg-Kohn formalism (details of which follow in the next chapter).

Many approaches to the nuclear energy-density functional are empirical [Skyrme, 1956, Vautherin and Brink, 1972, Vautherin, 1973, Dobaczewski et al., 1984, Oliveira et al., 1988, Anguiano et al., 2001, Duguet et al., 2002], but guidance can be found from analytical solutions to simpler models (see Chapter 3). The complete ground-state energy of a quantum many-body system as a functional of any external potential is available for only a few solvable or weakly interacting systems. Furnstahl and colleagues [Furnstahl et al., 2007, Puglia et al., 2003, Bhattacharyya and Furnstahl, 2005] derived energy-density functionals for dilute Fermi gases with short-ranged interactions. For Fermi gases in the unitary regime, simple scaling arguments suggest the form of the energy-density functional [Carlson et al., 2003, Papenbrock, 2006, Bhattacharyya and Papenbrock, 2006, Bulgac, 2007]. We similarly use scaling arguments in the development of our functional.

We develop a functional in the shell-model to describe the full nuclear mass table. Within the shell-model the variables of interest in the functional are the proton and neutron occupation numbers in each shell-model orbital. By working with a shell-model representation and providing greater microscopic motivation we are able to obtain a competitive global mass functional with a least-squares error for binding energies on the order of those from mean-field approaches, using 17 fitted parameters. Additionally, the microscopic aspects of the functional might improve upon its ability to extrapolate to regions of unfitted nuclei over a purely liquid drop model and lend to more physical transparency of terms.

Chapter 2

Methodology

2.1 Theoretical foundation

In this section we present the basis for our work: Hohenberg-Kohn DFT. We present our new approach of shell-model based functionals in Section 2.2.

We now briefly introduce the framework of DFT in which our work is formulated. According to Hohenberg and Kohn, for a many-body system with density ρ in an external potential v there exists a functional of the density $\mathcal{F}_{\mathcal{HK}}(\rho)$ independent of v such that the system's ground state energy can be expressed as [Hohenberg and Kohn, 1964, Fiolhais et al., 2003]

$$E_{g.s.} = \min_{\rho}\{\mathcal{F}_{\mathcal{HK}} + \int d\mathbf{r} v(\mathbf{r})\rho(\mathbf{r})\}. \tag{2.1}$$

Consider the Hamiltonian for an A-body system:

$$\hat{H} = \hat{T} + \hat{U} + \hat{V} \tag{2.2}$$

with kinetic energy $\hat{T}$ and internal energy $\hat{U}$ and some external potential $\hat{V} = v(\mathbf{r})$. From the variational principle, the ground state energy can be expressed as a functional of $v(\mathbf{r})$:

$$E_{g.s.}(v) = \min\{\langle\psi|\hat{H}|\psi\rangle\} \tag{2.3}$$

Via the Hellman-Feynman theorem [Hellman, 1937, Feynman, 1939] we can obtain the density from the functional derivative of $E(v)$ with respect to v. We write the expectation value as

$$\begin{aligned}\langle\psi|\hat{H}|\psi\rangle &= \langle\psi|\hat{T}+\hat{U}|\psi\rangle + \langle\psi|\hat{V}|\psi\rangle \\ &= \langle\psi|\hat{T}+\hat{U}|\psi\rangle + \int d\mathbf{r} v(\mathbf{r})\rho(\mathbf{r}).\end{aligned} \tag{2.4}$$

Then

$$\frac{\delta}{\delta v(\mathbf{r})}E(v) = \frac{\delta}{\delta v(\mathbf{r})}\langle\psi|\hat{H}|\psi\rangle = \rho(\mathbf{r}). \tag{2.5}$$

The first theorem by Hohenberg and Kohn states that Equation (2.5) can be inverted to give the external potential as a unique function of the density: $v = v(\rho)$ [Hohenberg and Kohn, 1964]. With this, we can then define the universal functional in terms of the density [Hohenberg and Kohn, 1964].

$$\begin{aligned}\mathcal{F}_{\mathcal{HK}}(\rho) &= \min_{|\psi\rangle}\{\langle\psi|\hat{T}+\hat{U}|\psi\rangle\} \\ &= E_{g.s.}(\rho) - \int d\mathbf{r} v(\mathbf{r})\rho(\mathbf{r})\end{aligned} \tag{2.6}$$

As one can see from Equation (2.6), the functional is the functional Legendre transform of the ground state energy with respect to the external potential. A Legendre transform of a function f is defined as

$$\mathcal{L}\{f(x_1,...,x_N)\} = f(x_1,...,x_N) - \sum_i x_i \frac{\partial f}{\partial x_i}. \tag{2.7}$$

and it is understood that all x_i are replaced by $\frac{\partial f}{\partial x_i}$. This view of functionals was introduced by Lieb as a constructive path in constructing functionals [Lieb, 1983].

$\mathcal{F}_{\mathcal{HK}}$ is termed universal in that a term $\int d\mathbf{r}\tilde{v}(\mathbf{r})\rho(\mathbf{r})$ must be added to it when describing a system in some arbitrary potential $\tilde{v}(\mathbf{r})$. That is, the only explicit dependence of E on $\tilde{v}$ can be incorporated simply through an additive term [Kutzelnigg, 2006].

Assuming a knowledge of the ground state energy for any given external potential in constructing the functional would already assume a solution to the many-body problem. In the following section we present our approach to obtaining the form of the functional.

2.2 Functionals in a shell-model basis

Motivated by the various benefits of accurate theoretical descriptions of nuclear masses (see Chapter 1), we turn to the primary focus of this work. We developed an energy functional in the framework of Hohenberg-Kohn DFT for the calculation of nuclear binding energies (and thus masses) with a competitive least-squares error in global calculations. The functional is formulated in the harmonic oscillator basis with shell-model occupations in protons and neutrons as the degrees of freedom. Both macroscopic and microscopic parameters are determined via a least-squares fit to experimental binding energies, where we emphasize the global nature of the functional by providing equal treatment of all nuclei with no restrictions on N, Z or deformation. This section will begin by presenting and motivating our chosen framework. The specific form of the functional will be presented in Chapter 4.

In this thesis a new representation of density functionals is proposed. The mass calculations with current DFT models [Goriely et al., 2002, Goriely et al., 2009, Kortelainen et al., 2010b, Dobaczewski et al., 1984] are based on Skyrme interactions [Skyrme, 1956, Vautherin and Brink, 1972, Vautherin, 1973, Beiner et al., 1975, Brack et al., 1985, Chabanat et al., 1997, Tondeur et al., 1984]. Such models use

densities $\rho(\mathbf{r})$ represented through the spatial coordinate $\mathbf{r}$. These densities include particle density, spin density and others. See Reference [Bender et al., 2003b] for a review. The use of spatial densities seems a natural choice, particularly in quantum chemistry and condensed matter systems, where DFT has also found much success. However, this may not be the most natural space with which to represent nuclei. Rather, we consider functionals based on occupations of shell-model orbitals.

2.2.1 Approach

The functional is founded on Hohenberg-Kohn DFT (see Section 2.1) that states one can obtain the ground-state energy for a many-body system from the minimum of a functional in an external field, according to Equation (2.1), and is developed with shell-model degrees of freedom. The choice of this approach to many-body systems is taken from the success of DFT in global mass calculations for nuclei. Hohenberg-Kohn DFT provides a firm theoretical foundation on which the nuclear many-body problem can be approached. Furthermore, our occupation-number-based approach does not require us to invoke the theorems of Kohn-Sham and we obtain relative computational simplicity once our fit parameters are fixed (see Chapter 5 for a discussion on the numerical nature of the functional).

Since the 1950's, Jensen and Goeppert-Mayer's shell-model description of nuclei [Mayer and Jensen, 1955] has proved remarkably successful. Shell-model calculations of light nuclei can be treated fully microscopically through diagonalizations of the shell-model Hamiltonian (see below). While the size of the model space is a limiting factor, excellent results have been found for *sd*- [Retamosa et al., 1997, Caurier et al., 1998, Caurier et al., 2005] and *fp*- [Caurier et al., 1999] shell nuclei. Larger nuclei can be approached via stochastic methods still in a shell-model basis, such as the Monte Carlo shell-model approach of Reference [Otsuka, 2001, Otsuka et al., 2001]. All of these methods are based on the shell-model Hamiltonian (see Reference [Brown and Richter, 2006] for a more recent formulation).

$$H_{SM} = \sum_i \varepsilon_i a_i^\dagger a_i + \frac{1}{4} \sum_{i,j,k,l} v_{i,j,k,l} a_i^\dagger a_j^\dagger a_l a_k \tag{2.8}$$

Here ε_i are single-particle energies and $v_{i,j,k,l}$ are two-body matrix elements. The shell-model Hamiltonian is expressed in terms of the creation and annihilation of nucleons in single-particle orbits. Therefore, the occupation of these orbits is the natural degree of freedom for the functionals of shell-model systems. More details on the shell-model and it's source of motivation for our work is given in Section 4.1.2.

The shell-model for nuclei was first speculated, from atomic physics, in the 1930's [Elsasser, 1933, Elsasser, 1934a, Elsasser, 1934b]. The model was developed in the late 1940's and early 1950's, motivated in part by experimental mass measurements, in an effort to describe the increased binding of magic nuclei ($N, Z = 2, 8, 20, 28, 50, 82$) over that predicted by the smooth systematics of the liquid drop model [Mayer, 1966, Haxel et al., 1950, Mayer and Jensen, 1955]. Shell structure in any system of particles relies on the presence of a common field in which the particles are able to move approximately independently. The electric charge of a nucleus can generate the necessary field for electron shell-structure in atoms. However, the less obvious case is the extent to which the short-range interaction of nucleons smooth themselves out to provide a similar mean-field [Gomes et al., 1958]. As one sees from Figure 1.1 a purely liquid drop model inspired mass formula such as the Bethe-Weizsäcker formula is unable to account for increased binding at the magic numbers that result from nuclear shell structure. The discrete shell closures require more sophisticated methods to reconcile shell-model and liquid drop model systematics.

The Duflo and Zuker mass formula is based on shell-model occupation numbers [Duflo and Zuker, 1995]. This microscopic mass formula is based on a phenomenological description of the shell-model Hamiltonian, which can be expanded into what Reference [Duflo and Zuker, 1995] call the monopole and multipole terms. The form of the monopole, which can reproduce exact energies for closed (fully filled) shells, is quadratic in occupation number and isospin. Through scaling arguments

and asymptotic forms, Duflo and Zuker were able to obtain a least-squares error of $\chi \simeq 0.375$ MeV. The formula is fitted with 28 parameters, as opposed to the 18 and 19 fit parameters of the HFB-2 and FRDM mass models, respectively [Goriely et al., 2002, Möller et al., 1995]. Furthermore, the Bethe-Weizsäcker formula is reproduced in the asymptotic limit [Duflo and Zuker, 1995].

The seemingly natural approach of the orbital occupations to the shell-model Hamiltonian, and the success of Duflo and Zuker, leads us to investigate if a mean-field description in a shell-model basis is a promising direction in global nuclear mass calculations. By its nature this approach is able to account for shell structure directly, and motivation from phenomenology may provide the necessary smoothness suggested by the liquid drop model.

Our functional follows from the approach in the Duflo and Zuker mass formula and is based on shell-model occupation numbers, though we must make a distinction in our work. We emphasize the difference between an energy functional for nuclear masses and a mass formula. Mass formulae, such as the Duflo and Zuker mass formula [Duflo and Zuker, 1995], calculate nuclear masses from an assumed nuclear structure. The mass formula by Duflo and Zuker computes the binding energy in terms of the shell-model occupations. The occupations are parameters—not variables—and their values are taken from the non-interacting shell-model (with modifications due to deformations). In this work we instead have a functional. That is, the occupations are determined so as to minimize the ground-state energy according to Equation (2.1), where the minimization is over occupation numbers.

The nuclear shell-model is suitable for mean-field calculations, where the nucleonic interactions themselves provide a common, smooth field in which we approximate nucleons moving independently. This provides us with a framework in which to execute a shell-model approach beyond light nuclei and into a global description of the nuclear chart. To present our concept formally, we consider the ground state energy $E(\{\varepsilon_\alpha\})$ of an A-body system described by a shell-model Hamiltonian with

single-particle energies ε_α, see Equation (2.8). The occupation number of a given orbital β is given by

$$n_\beta = \frac{\partial}{\partial \varepsilon_\beta} E(\{\varepsilon_\alpha\}) \tag{2.9}$$

Inverting Equation (2.9), the functional can be defined through the Legendre transform:

$$\mathcal{F}(\{n_\alpha\}) = E(\{\varepsilon_\alpha(\{n_\beta\})\}) - \sum_\alpha n_\alpha \varepsilon_\alpha(\{n_\beta\}) \tag{2.10}$$

Equation (2.10) is a functional of occupation number, where the mean-field becomes the equivalent of an external potential. In this work we make a formal analogy between Hohenberg-Kohn DFT and occupation number functionals. The Hohenberg-Kohn theorems remain valid where we exchange $v(\mathbf{r}) \leftrightarrow \varepsilon_\alpha$ and $\rho(\mathbf{r}) \leftrightarrow n_\alpha$. In the following chapter we discuss the development of our occupation-number functional. In Section 4.2 we will show explicitly the dependence of our functional on orbital occupations.

Chapter 3

Application to a toy model

In order to construct the functional for the full mass table we look for microscopic guidance. We begin by finding the occupation-number based functional for a simple system. The three-level Lipkin model is an exactly solvable system applicable to atomic nuclei. Through the Lipkin model we are able to gain insight into the form of functionals for two-body and symmetry-breaking one-body interactions. First we show the formulation of the energy functional for the Lipkin model with degenerate excited energy levels and then for non-degenerated excited levels. The energy functional has been developed in the Hohenberg-Kohn framework, and with Lieb's approach to functionals as Legendre transforms and we follow [Bertolli and Papenbrock, 2008].

3.1 The 3-level Lipkin Model

3.1.1 Degenerate energy levels

We consider the three-level Lipkin model [Lipkin et al., 1965, Li et al., 1970, Holozwarth and Yukawa, 1974, Meredith et al., 1988, Hagino and Bertsch, 2000]. This model consists of N fermions that are distributed over three levels (labeled as 0, 1, and 2) consisting of N degenerate, single-particle states each. The single-particle

energies are $\varepsilon_0 = 0$, and the two excited levels are degenerate, $\varepsilon_1 = \varepsilon_2 \equiv \varepsilon$. The Hamiltonian is

$$H = \varepsilon(\hat{n}_1 + \hat{n}_2) - \frac{V}{2}(K_1 K_1 + K_2 K_2 + K_1^\dagger K_1^\dagger + K_2^\dagger K_2^\dagger) \ . \tag{3.1}$$

Here,

$$\hat{n}_\alpha = \sum_{i=1}^{N} a_{\alpha i}^\dagger a_{\alpha i}, \quad \alpha = 0, 1, 2 \tag{3.2}$$

is the number operator of level α, while

$$K_\alpha = \sum_{i=1}^{N} a_{\alpha i}^\dagger a_{0 i}, \quad \alpha = 1, 2 \tag{3.3}$$

transfer fermions from the level 0 to the level $\alpha > 0$. We assume $\varepsilon \geq 0$ for the spacing to the degenerate levels 1 and 2. The operators $a_{\alpha i}^\dagger$ and $a_{\alpha i}$ create and annihilate a fermion in state i of level α. The Hamiltonian is invariant under the simultaneous orthogonal transformation of the N orbitals belonging to each level, and this symmetry facilitates the numerical solution of this problem [Meredith et al., 1988]. Note that the Hamiltonian (3.1) is invariant under orthogonal transformations of states belonging to the degenerate levels 1 and 2, i.e.

$$\begin{pmatrix} c_{1i}^\dagger \\ c_{2i}^\dagger \end{pmatrix} \rightarrow \begin{pmatrix} \cos\phi & \sin\phi \\ -\sin\phi & \cos\phi \end{pmatrix} \begin{pmatrix} c_{1i}^\dagger \\ c_{2i}^\dagger \end{pmatrix} \ . \tag{3.4}$$

This symmetry will be broken by the Hartree-Fock (HF) solution for sufficiently strong V (see below), and we will study the explicit breaking of this symmetry by additional one-body terms of the Hamiltonian in Section 3.2.

The energy functional is the Legendre transform

$$F(n) = E(\varepsilon) - \varepsilon n(\varepsilon) \ . \tag{3.5}$$

Here

$$n(\varepsilon) \equiv \frac{\partial E(\varepsilon)}{\partial \varepsilon} \tag{3.6}$$

is the occupation of levels 1 and 2 in the ground-state, while $E(\varepsilon)$ is the ground-state energy as a function of the spacing ε. The exact ground-state energy can be obtained numerically by diagonalizing a matrix of modest dimensions [Meredith et al., 1988], and one can thus construct easily the exact energy functional. However, we are interested in gaining analytical insight into the problem. For this reason, we employ the analytical expression that provides the ground-state energy in terms of the HF energy and corrections due to the Random Phase Approximation (RPA) [Hagino and Bertsch, 2000]. The HF result depends on the size of the parameter ε/v where

$$v \equiv V(N-1) \tag{3.7}$$

is the effective strength of the two-body coupling V in the N-body system. That is, the HF result depends on the size of the level spacing ε normalized by the effective interaction strength. The spherical phase is found for $\varepsilon/v > 1$, while one deals with a deformed phase for $\varepsilon/v < 1$. In the spherical (deformed) phase, the HF solution preserves (breaks) the symmetry (3.4) of the Hamiltonian. The results are [Hagino and Bertsch, 2000]

$$E = \sqrt{\varepsilon^2 - v^2} - \varepsilon \quad \text{for} \quad \varepsilon > v \ , \tag{3.8}$$

$$E = -\frac{N+4}{4} v + \sqrt{\frac{v^2 - \varepsilon^2}{2}} + \frac{2N-1}{4}\varepsilon - \frac{N-1}{4}\frac{\varepsilon^2}{v} \quad \text{for} \quad \varepsilon < v \ . \tag{3.9}$$

Figure 3.1 compares the approximate ground-state energies (3.8) and (3.9) with the exact result as a function of ε/V for a system of $N = 20$ fermions. The approximate solution exhibits a cusp at the boundary $\varepsilon/v \approx 1$ between the spherical and deformed phases, but it agrees well with the exact result away from the phase boundary. Note

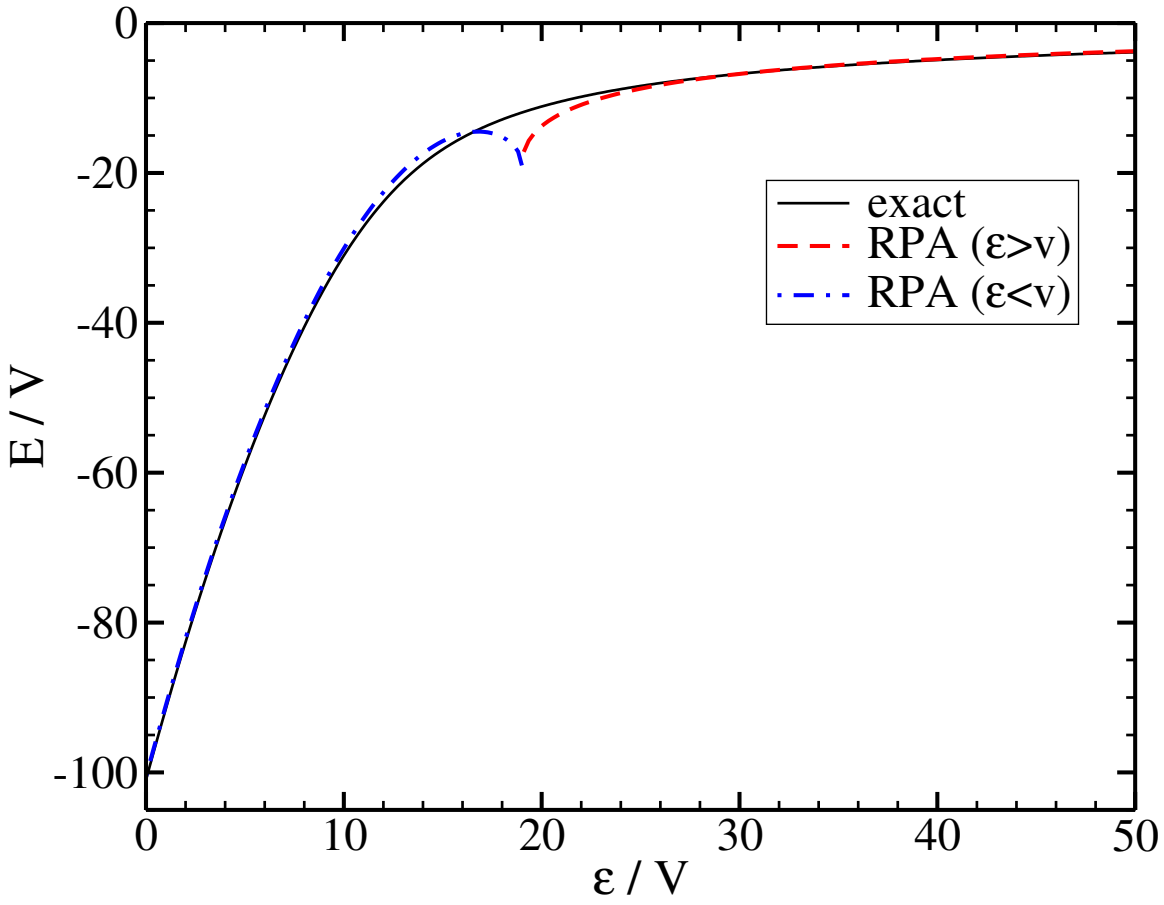

Figure 3.1: Comparison of the exact ground-state energy to the RPA approximation for a system of $N = 20$ fermions. The RPA result shows a cusp at $\varepsilon \approx v \equiv (N-1)V$, corresponding to the boundary between the spherical ($\varepsilon > v$) and the deformed phase ($\varepsilon < v$) [Bertolli and Papenbrock, 2008].

that the cusp (a phase transition) renders the RPA solution non-convex, and its Legendre transform is therefore not possible close to the phase boundary. Within the RPA formalism, the occupation number (3.6) attains non-physical negative values close to the cusp. We will avoid this problem in the construction presented below.

Let us start with the analytical construction of the energy functional (3.5) in the spherical phase. Here, the RPA solution is convex. We have

$$n \equiv \frac{\partial E}{\partial \varepsilon} = \frac{\varepsilon}{\sqrt{\varepsilon^2 - v^2}} - 1 \ . \tag{3.10}$$

This equation can easily be solved for $\varepsilon(n)$, and the functional thus reads

$$F(n) = -|v|\sqrt{n(n+2)} \ . \tag{3.11}$$

Thus, for small occupation numbers (i.e. the weak coupling limit $v \ll \varepsilon$), the functional is nonanalytical and exhibits a square-root singularity. This is a rather generic feature of energy functionals and is also seen in the energy functional for the pairing Hamiltonian [Papenbrock and Bhattacharyya, 2007].

We next turn to the deformed case ($\varepsilon < v$). The occupation number is

$$n(\varepsilon) = \frac{2N-1}{4} - \frac{N-1}{2}\frac{\varepsilon}{v} - \frac{\varepsilon}{\sqrt{2(v^2-\varepsilon^2)}} \ . \tag{3.12}$$

Equation (3.12) is difficult to invert analytically because of the term involving the square root. Note that this term also renders the occupation number negative as ε approaches v. We avoid this problem by expanding Equation (3.12) in powers of ε/v, approximate $\varepsilon/v \ll 1$, and keep up to orders $O(\varepsilon/v)$ in the resulting expression. The result is

$$\varepsilon(n) = \frac{N-2n-1/2}{N-1+\sqrt{2}}v \ . \tag{3.13}$$

Insertion of this result and Equation (3.9) into Equation (3.5) yields the density functional in the deformed phase.

Note that the energy functional is analytical in the strong coupling limit $v \gg \varepsilon$. Again, this is a generic feature of energy functionals and was also exhibited in the pairing problem.

Figure 3.2 compares the exact energy functional with the RPA solutions obtained in the spherical and deformed phase for $N = 20$. Note that the spherical (deformed) phase corresponds to sufficiently small (large) occupation numbers. The inset shows that the RPA solution has a kink at the critical occupation number $n \approx 0.7$ at the phase transition. Note also that the solution of the deformed phase is a good

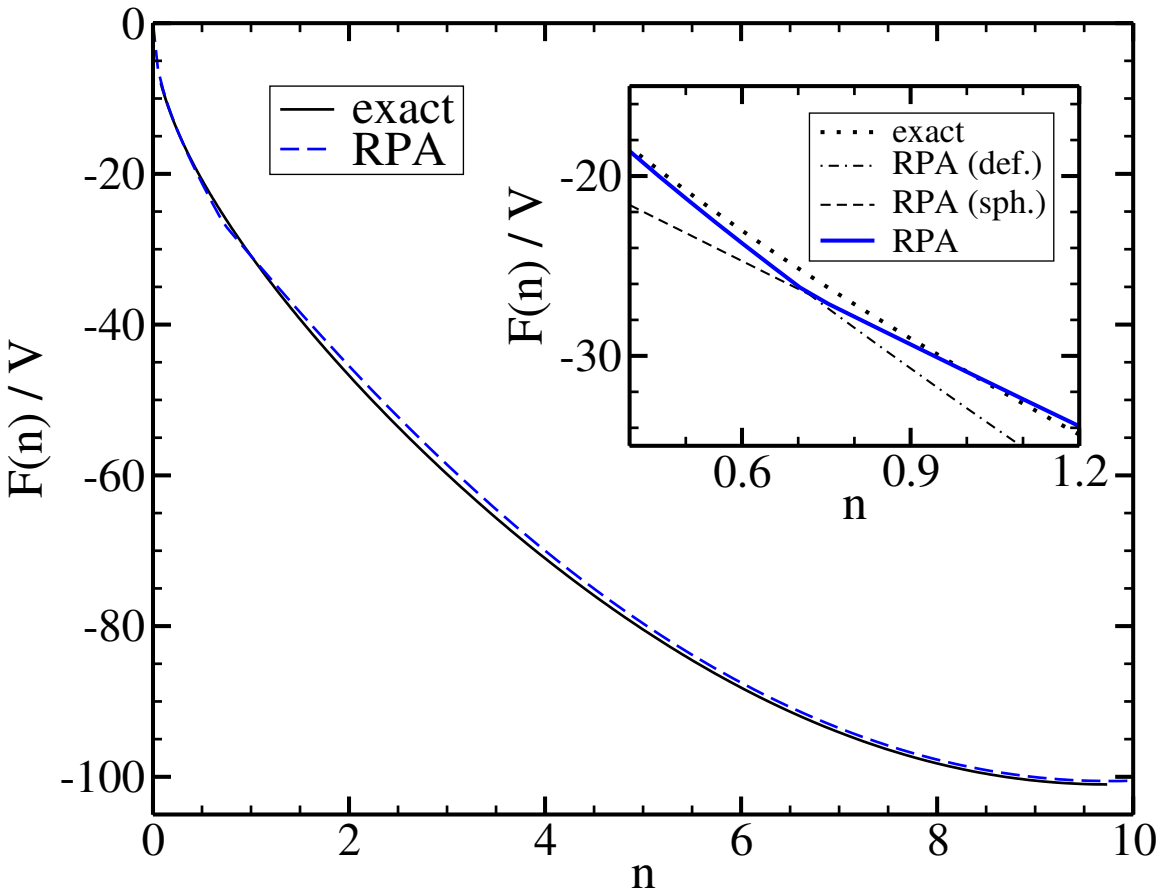

Figure 3.2: Comparison of the exact energy functional (solid line) and RPA-obtained functional (dashed line) for $N = 20$ fermions. Inset: The phase transition is clearly seen at the intersection of the deformed and spherical RPA solutions. [Bertolli and Papenbrock, 2008].

approximation over the entire range $n > 0.7$, although its derivation employed the approximation $\varepsilon \ll v$ corresponding to $n \approx N/2$, see Equation (3.12).

To address the question of the severity of the kink present at $n \approx 0.7$, we employ the RPA functional in practical calculations. We add the one-body term εn to the functional and numerically determine the occupation number n that minimizes the ground-state energy

$$E(n) = F(n) + \varepsilon n \ . \tag{3.14}$$

The energy taken at the minimum is plotted as a function of the minimizing occupation number n in Fig. 3.3. The result is also compared to the exact numerical

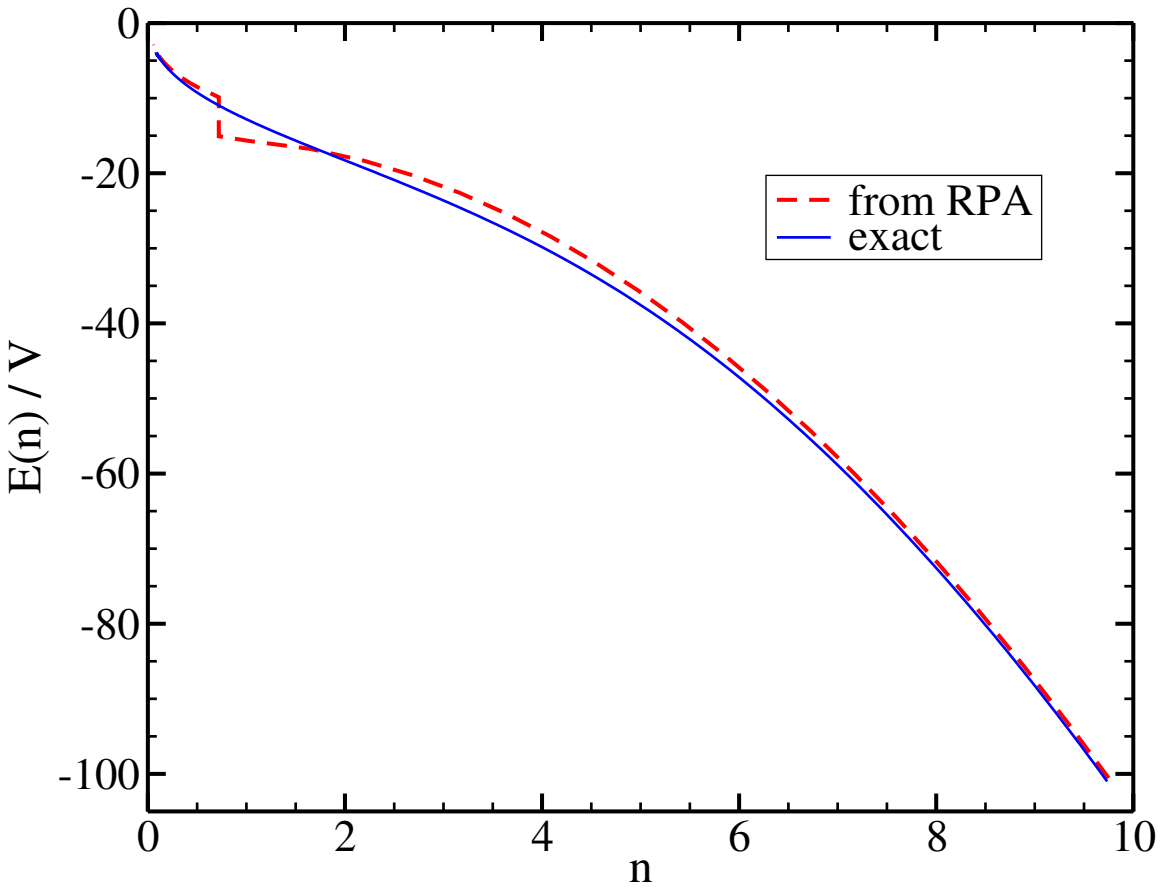

Figure 3.3: Ground-state energy as a function of occupation number obtained from the exact functional (solid line) and the RPA functional (dashed line) for $N = 20$ fermions. The RPA solution fails at the phase transition [Bertolli and Papenbrock, 2008].

result. We see that the energy functional, obtained via RPA, provides a good prediction of the ground state energy function of the three-level Lipkin model. At the phase transition, however, the functional predicts multiple values for the ground state energy, due to the discontinuity in the derivative at the phase transition. Thus, for external potentials $\varepsilon \approx v$ the energy functional does not provide good predictive power, owing to the relatively small kink visible in the inset of Fig. 3.2.

3.2 Non-degenerate energy levels and symmetry-breaking

The two-body interaction and the one-body terms of the Hamiltonian (3.1) are invariant under the symmetry transformation (3.4). In this section we study the breaking of this symmetry by a one-body potential, i.e. we lift the degeneracy of levels 1 and 2 in the Hamiltonian (3.1) and modify its one-body term as follows

$$\varepsilon(\hat{n}_1 + \hat{n}_2) \to \varepsilon_1 \hat{n}_1 + \varepsilon_2 \hat{n}_2 \ . \tag{3.15}$$

The two-body interaction remains the same. Technically it is convenient to substitute $\varepsilon \to (\varepsilon_1 + \varepsilon_2)/2$ in Equation (3.1) and to add the term

$$\frac{\varepsilon_1 - \varepsilon_2}{2}(\hat{n}_1 - \hat{n}_2) \tag{3.16}$$

to the resulting expression. This approach is particularly convenient for the RPA calculation.

The energy functional corresponds to the symmetry-preserving two-body interaction that is probed by a symmetry-breaking one-body potential. Thus, the functional depends on two variables (the occupation numbers of levels 1 and 2), and we are interested in the form of this functional and in its relation to the functional of the symmetry-preserving case. We thereby hope to gain insight into energy functionals for atomic nuclei. The nuclear shell-model, for instance, employs a spherically symmetric two-body interaction, but deformed nuclei might be described within a deformed mean-field basis that breaks the rotational invariance through one-body terms.

The numerical calculations are simple and require only a minor modification of the matrix elements corresponding to the one-body terms. For the analytical construction of the functional, we have to perfom the HF and RPA calculations. Extending the work of Reference [Hagino and Bertsch, 2000] to the case of non-degenerate levels

and obtain the HF energy surface:

$$E(\alpha,\beta) \;=\; N\sin^2\alpha(\varepsilon_1\cos^2\beta+\varepsilon_2\sin^2\beta)-vN\sin^2\alpha\cos^2\alpha \tag{3.17}$$

as a function of the two angles α and β of the HF transformation. In the case $\varepsilon_1=\varepsilon_2$ of degenerate levels, the energy surface (3.17) becomes independent of β.

In what follows, we assume $\varepsilon_1 \le \varepsilon_2$. The minimum of the energy surface Equation (3.17) occurs at $\alpha=0$ (where β is arbitrary and can be chosen as zero) for $\varepsilon_1 > v$, and at $\cos 2\alpha = \varepsilon_1/v$ and $\beta=0$ for $\varepsilon_1 < v$. Again, we refer to these cases as the weak-coupling regime and the strong-coupling regime, respectively. The Hartree-Fock energy becomes

$$E_{\rm HF}=\begin{cases} 0\ , & \varepsilon_1 > v \\ -\frac{N}{4}v+\frac{N}{2}\varepsilon_1-\frac{N}{4}\varepsilon_1^2/v\ , & \varepsilon_1 < v \end{cases}\ . \tag{3.18}$$

Thus, within the HF approximation, all particles stay in level 0 in the weak-coupling regime, while the fermions occupy level 0 and level 1 in the strong-coupling regime. The RPA equation takes the well-known form [Hagino and Bertsch, 2000]

$$\begin{pmatrix} A & B \\ -B & -A \end{pmatrix}\begin{pmatrix} X \\ Y \end{pmatrix}=\omega\begin{pmatrix} X \\ Y \end{pmatrix}\ . \tag{3.19}$$

The nonzero matrix elements of the 2×2 matrices A and B are

$$\begin{aligned} A_{11} &= \varepsilon_1\cos 2\alpha+\frac{3}{2}v\sin^2 2\alpha\ , \\ A_{22} &= \varepsilon_2-\varepsilon_1\sin^2\alpha+\frac{v}{2}\sin^2 2\alpha\ , \\ B_{11} &= -v(\cos^4\alpha+\sin^4\alpha)\ , \\ B_{22} &= -v\cos^2\alpha\ . \end{aligned}$$

Solving for the eigenfrequencies ω yields

$$\omega_1^2 = \begin{cases} \varepsilon_1^2 - v^2 \ , & \varepsilon_1 > v \\ 2(v^2 - \varepsilon_1^2) \ , & \varepsilon_1 < v \end{cases} \tag{3.20}$$

$$\omega_2^2 = \begin{cases} \varepsilon_2^2 - v^2 \ , & \varepsilon_1 > v \\ (\varepsilon_2 - \varepsilon_1)(\varepsilon_2 + v) \ , & \varepsilon_1 < v \ . \end{cases} \tag{3.21}$$

The total energy is

$$E = E_{\rm HF} + \frac{1}{2}\left(\sum_{i=1}^{2}\omega_i - {\rm Tr}A\right) \ , \tag{3.22}$$

and the result thus becomes

$$E = \frac{1}{2}\sum_{j=1}^{2}\left(\sqrt{\varepsilon_j^2 - v^2} - \varepsilon_j\right) \quad \text{for} \quad \varepsilon_1 > v \ , \tag{3.23}$$

$$E = -\frac{N+4}{4}v + \frac{1}{2}\sqrt{\varepsilon_2 - \varepsilon_1}\sqrt{v + \varepsilon_2} + \sqrt{\frac{v^2 - \varepsilon_1^2}{2}} + \frac{2N+1}{4}\varepsilon_1 - \frac{\varepsilon_2}{2} - \frac{N-1}{4}\frac{\varepsilon_1^2}{v} \quad \text{for} \quad \varepsilon_1 < v \ . \tag{3.24}$$

In the weak-coupling regime, the energy (3.23) is very simply related to the energy for the spherical phase (3.8), while the energy of the strong-coupling regime differs mainly from its deformed counterpart (3.9) through the term that is nonanalytical in the level splitting $\varepsilon_2 - \varepsilon_1$. It seems that the non-analyticity is an artifact of the RPA approximation.

The energy functional results from the Legendre transform

$$F(n_1, n_2) = E(\varepsilon_1, \varepsilon_2) - \sum_{j=1}^{2} n_j \varepsilon_j \ , \tag{3.25}$$

and it is understood that $\varepsilon_j = \varepsilon_j(n_1, n_2)$ results from the inversion of the occupation numbers

$$n_j \equiv \frac{\partial E}{\partial \varepsilon_j} \ . \tag{3.26}$$

We start with the weak-coupling regime $\varepsilon_1 > v$ and find

$$n_j = \frac{1}{2}\left(\frac{\varepsilon_j}{\sqrt{\varepsilon_j^2 - v^2}} - 1\right) \ . \tag{3.27}$$

Thus, the occupation number of the two energy levels depends only on the energy of the level itself, and the strength of the two-body interaction. Note that the occupation numbers are symmetric under exchange of level 1 and level 2. The inversion of Equation (3.27) is straightforward, and we obtain the energy functional

$$F(n_1, n_2) = -|v| \sum_{j=1}^{2} \sqrt{n_j(n_j+1)} \ . \tag{3.28}$$

Note that the functional (3.28) is symmetric under exchange of level 1 and level 2, and that it is simply the sum of two functionals. Its form could have almost been guessed from the functional (3.11) for degenerate levels.

We turn to the strong-coupling regime $\varepsilon_1 < v$ which once again proves more difficult. The occupation numbers

$$n_1 = \frac{2N+1}{4} - \frac{x}{4} - \frac{N-1}{2}\frac{\varepsilon_1}{v} - \frac{\varepsilon_1}{\sqrt{2(v^2 - \varepsilon_1^2)}} \tag{3.29}$$

$$n_2 = \frac{1}{4}\left(x + x^{-1} - 2\right) \tag{3.30}$$

do not decouple as in the weak-coupling limit. Here, we employed the shorthand

$$x \equiv \sqrt{\frac{\varepsilon_2 + v}{\varepsilon_2 - \varepsilon_1}} \ . \tag{3.31}$$

We solve Equation (3.30) for x and obtain

$$x(n_2) = 2n_2 + 1 + 2\sqrt{n_2(n_2+1)} \ . \tag{3.32}$$

We insert this result into Equation (3.29), approximate $\varepsilon_1 \ll v$ and solve for ε_1. This expansion again renders the resulting functional convex, and we obtain

$$\varepsilon_1(n_1, n_2) = \frac{N - 2n_1 + 1/2 - x/2}{N - 1 + \sqrt{2}} v \ . \tag{3.33}$$

where $x \equiv x(n_2)$. Finally, we insert this result into Equation (3.31) and find

$$\varepsilon_2(n_1, n_2) = \frac{v + x^2 \varepsilon_1}{x^2 - 1} \ . \tag{3.34}$$

The insertion of the expressions (3.33) and (3.34) into the functional (4.43) thus yields the desired expression. Figure 3.4 shows the resulting functional and compares it to the exact solution. The agreement between the exact result and the RPA result is quite satisfactory. Note that the boundary between the regimes of strong and weak coupling is a one-dimensional line in the region of small occupation numbers $n_{1,2} < 1$.

We constructed the energy functional for the three-level Lipkin model with degenerate and non-degenerate excited levels, with analytical results based on RPA calculations and subsequent Legendre transformations. They agree well with exact numerical results in the limits of strong and weak coupling, respectively, but the RPA fails at the boundary between the two regimes.

The results shown here should be useful in the construction of an occupation-number based energy functional for nuclear masses. The nuclear shell-model employs a spherically symmetric two-body interaction, but deformed nuclei might be described within a deformed mean-field basis with the rotational invariance broken through one-body terms. In Chapter 4 we will see how our insights into the Lipkin model provide specific motivation for terms in our global energy functional for nuclear masses.

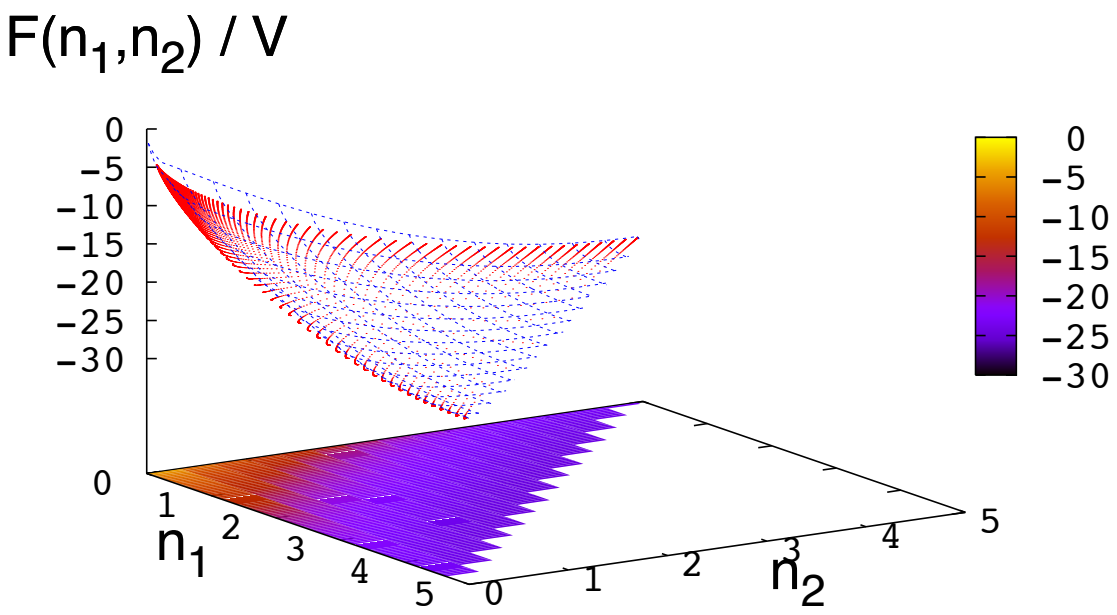

Figure 3.4: Energy functional $F(n_1, n_2)$ of the three-level Lipkin model with non-degenerate single-particle levels for $N = 10$ fermions. The exact result is shown as dots, while the RPA result is shown as a mesh and the corresponding contour [Bertolli and Papenbrock, 2008].

Chapter 4

Realistic energy functional for the full mass table

Based on our investigation of the three-level Lipkin model we have gained valuable insight into the form of a functional whose degrees of freedom are level occupations. In this chapter we will extend our work to calculate masses across the nuclear chart, and reveal further details of nuclear structure in the form of major-shell occupations.

Our functional is developed in a spherical harmonic oscillator basis. This basis is convenient for our choice of orbital occupations as the relevant degree of freedom. The harmonic oscillator Hamiltonian

$$H = \frac{\hat{p}^2}{2m} + \frac{1}{2}m\omega^2\hat{x}^2 \tag{4.1}$$

is easily written in terms of fermionic creation, $a^\dagger$, and annihilation, a, operators (as defined in Section 3.1.1):

$$\hat{x} = \sqrt{\frac{\hbar}{2m\omega}}(a + a^\dagger) \tag{4.2}$$

$$\hat{p} = -i\sqrt{\frac{\hbar m\omega}{2}}(a - a^\dagger). \tag{4.3}$$

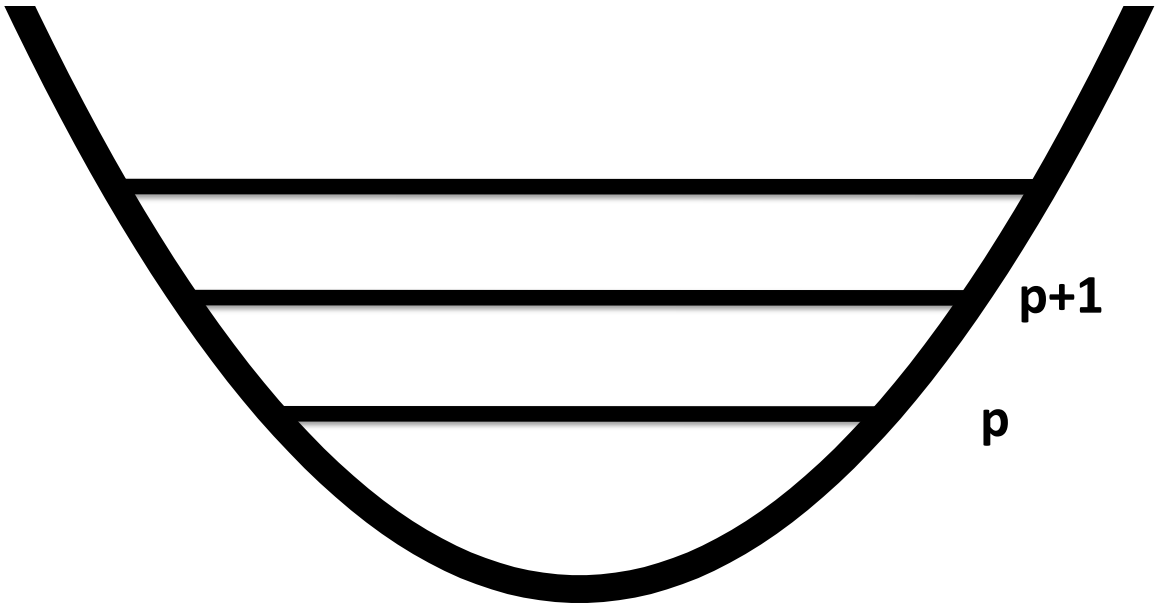

Figure 4.1: Harmonic oscillator shells with principle quantum number p. Each shell has dimensionality $d_p = (p+1)(p+2)$.

In this representation solutions to the eigenvalue problem $H|\psi = E\psi$ are easily found in terms of the principle quantum number p:

$$E = \langle\psi|H|\psi\rangle \tag{4.4}$$

$$= \hbar\omega(p + 3/2) \tag{4.5}$$

The quantum number p defines the oscillator shells (see Fig. 4.1), each with degeneracy $d_p = (p+1)(p+2)$.

The degeneracy d_p provides shell closure as $2, 8, 20, 40, \ldots$. In order to describe known nuclear shell closures at magic numbers we have chosen the prescription of Reference [Duflo and Zuker, 1995]. We define shells of the harmonic oscillator as the low-j subshells of some orbital p plus the intruding highest-j subshell of the $p+1$ orbital. Figure 4.2 illustrates below, with the specific example given in Fig. 4.2b. Such a methodology provides us with shell closures that more closely resemble those

of the nuclear magic numbers at $2, 6, 14, 28, 50, 82, 126 \ldots$. We note that 6 and 14 are not traditional magic numbers, but remain as shell closures in our model in place of 8 and 20.

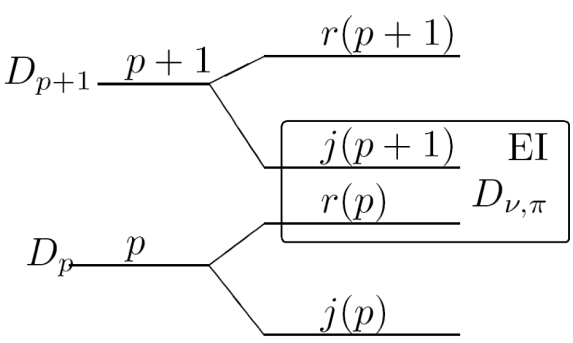

(a) Intruder-Extruder closures taken from [Duflo and Zuker, 1995]

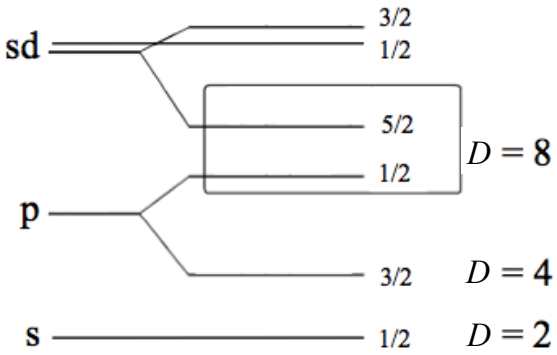

(b) Shell closure example for *sd*-nuclei

Figure 4.2: Modified closures for major oscillator shells where $D_p \equiv d_p$ is the dimensionality of the shell. We define shells of the harmonic oscillator as the low-j subshells of some orbital p plus the intruding highest-j subshell of the $p+1$ orbital.

With our shell structure defined we may now approach the problem of saturation. It is a well known phenomenon that nuclear binding energy per particle saturates at about 8 MeV [Aston, 1933]. The short-range nature of the nuclear force implies that a given nucleon affects its nearest neighbour greatest, with binding to farther nucleons quickly diminishing. The result is an observed saturation of the binding energy such that it can increase at most as the total number of nucleons, $A = N + Z$, to leading order. Therefore, while terms of our functional are motivated by several factors (see Section 4.1), we must ensure that no term contributes to the energy faster than linearly in A.

Our functional is guided by semi-classical scaling arguments in order to achieve nuclear saturation. We present a development of the semi-classical scaling that comes out of the Thomas-Fermi approximation. For the harmonic oscillator ($V = \frac{1}{2}m\omega^2 r^2$) one can obtain the density of states $g(\varepsilon)$ as a function of the single particle energy ε:

$$g(\varepsilon) = \frac{1}{2\pi^2}\left(\frac{2m}{\hbar^2}\right)^{3/2} \int d^3r \ (\varepsilon - \frac{1}{2}m\omega^2 r^2)^{1/2}\Theta(\varepsilon - \frac{1}{2}m\omega^2 r^2) \tag{4.6}$$

$$= \frac{\varepsilon^2}{(\hbar\omega)^3}. \tag{4.7}$$

We can then obtain the particle number up to some Fermi level from the density of states given in Equation (4.7):

$$A = \int_0^{\varepsilon_f} d\varepsilon \ g(\varepsilon) \tag{4.8}$$

$$= \int_0^{\varepsilon_f} d\varepsilon \ \frac{\varepsilon^2}{(\hbar\omega)^3} \tag{4.9}$$

$$= \frac{\varepsilon_f^3}{3(\hbar\omega)^3}. \tag{4.10}$$

Inverting Equation (4.10) we find $\varepsilon_f \propto A^{1/3}$. Therefore, working in an harmonic oscillator basis, a nucleus of A particles has about $A^{1/3}$ occupied shells below the Fermi level, and about $A^{2/3}$ particles in the final shell. See Refence [Ring and Schuck, 1980] for a more detailed discussion. We consider the scaling of a possible functional term dependent on proton and neutron occupations, Equation (4.11). Such a term may describe the energy of z_p protons in the shell with principle quantum number p, where z_p is the proton occupation of the p^{th} shell and scales as p^2 to leading order.

$$pz_p \sim p^3 \tag{4.11}$$

where $\sim$ indicates "scales as". We take a semi-classical approach as our primary guide in selecting terms. In this approach, which is valid for large number of oscillator shells, we can approximate the summation as an integral with an upper bound at $A^{1/3}$.

$$\sum_p p^3 \simeq \int_0^{A^{1/3}} dp\ p^3 \tag{4.12}$$

$$\sim A^{4/3}. \tag{4.13}$$

So we see that the sum $\sum_p pz_p$ requires a factor of $A^{-1/3}$ to scale correctly as A to leading order.

Working in a harmonic oscillator basis, Equation (4.1), with modified shell closures, we choose our relevant degrees to be the proton and neutron occupations in 15 major shells. The choice of 15 major shells was taken to insure convergence of the minimization of the functional (see Section 5.2). The modified shell closures do not alter our semi-classical scaling, as a given j-orbital contains about $A^{1/3}$ particles. Its addition or subtraction from a major shell is therefore negligible. These degrees of freedom identify the density by which can employ the Hohenberg-Kohn theorems. The ground-state energy of the nucleus is obtained via the Hohenberg-Kohn theorem, Equation (2.1), through a minimization of the functional over the proton and neutron occupations. The motivation governing the terms and details of the functional form are presented in the following sections.

4.1 Motivation for terms

In this section we describe more specific motivations for the form of the functional from the foundations set forth previously. Motivation for the functional, beyond semi-classical scaling to ensure saturation, comes from several sources. The first we have already considered in Chapter 3: investigations of analytically solvable models such as the three-level Lipkin Model. The other two we briefly present here. The liquid drop model, which motivates bulk terms of the functional, and the shell-model Hamiltonian, which motivates the microscopic terms, are able to provide analytic

motivations for the forms of functional terms. In Section 4.2 we present further detail on the selection of specific terms.

4.1.1 Liquid drop model

We begin at the macroscopic level with the liquid drop model, which proposes the nucleus be viewed as a water drop-like system. Originally proposed by Gamow in 1930 [Gamow, 1930], the model is associated with the saturation property discussed previously. The short range of the nuclear force implies that nuclei at the surface experience a different level of binding than those at the center. This leads to a surface energy which can be associated with a surface tension as one might find in a water drop. Empirical observations that the nuclear radius is proportional to $A^{1/3}$ provides a scale in terms of nucleon number to describe the surface and volume of the nucleus in the context of a spherical liquid drop.

One considers the volume and surface of a uniform sphere:

$$V_{sph} = \frac{4}{3}\pi r^3 \tag{4.14}$$

$$S_{sph} = 4\pi r^2 \tag{4.15}$$

If one uses the empirical radius of the nucleus $r = r_0 A^{1/3}$, where $r_0 = 1.25$ fm, we obtain

$$V_{sph} = \frac{4}{3}\pi (r_0 A^{1/3})^3 \sim A \tag{4.16}$$

$$S_{sph} = 4\pi (r_0 A^{1/3})^2 \sim A^{2/3} \tag{4.17}$$

The volume and surface energy of the nucleus then go as A and $A^{2/3}$ respectively. We recall the Bethe-Weizsacker mass formula which employed terms proportional to A and $A^{2/3}$ to account for volume and surface energy (see Section 1.1 for more detail):

$$a_v A + a_s A^{2/3}. \tag{4.18}$$

However, the nucleus being composed of both protons and neutrons we must also include the effects of charged particles in our macroscopic description. Let us consider the energy associated with the repulsion between two charged particles in a sphere:

$$E_C \propto \frac{Q^2}{R}. \tag{4.19}$$

We allow the distance between the particles in Equation (4.19), R, to be proportional to the nuclear radius and the charge, Q, of the nucleus to be proportional to the total number of protons Z.

$$Q \propto Z \tag{4.20}$$

$$R \propto A^{1/3} \tag{4.21}$$

Where every proton repels every other we obtain $Z(Z-1)$ interactions, and thus arrive at the form of the Coulomb term to the liquid drop model:

$$E_C = a_C \frac{Z(Z-1)}{A^{1/3}}. \tag{4.22}$$

The necessary pre-factors of the Coulomb interaction are contained in the coefficient a_C, which are determined (for instance, by fits to experiment) to be of the order $a_C = 0.69$ MeV.

The next term present in the liquid drop model is isospin and is the result of the Pauli exclusion principle [Roy and Nigam, 1967]. Assuming a Fermi gas model with fermionic statistics we calculate the number of protons and neutrons with momenta $p = 0$ to some maximum p_F (the Fermi momentum):

$$N, Z = \int_0^{\pi_F} dp \frac{2V 4\pi p^2}{(2\pi\hbar)^3} = \frac{V 8\pi p_F^3}{3h^3} \tag{4.23}$$

where V is again the volume of the spherical nucleus, Equation (4.16). We define $\rho_Z = Z/V$ and $\rho_N = N/V$ as the proton and neutron densities, respectively. We then find the Fermi momentum for protons ($p_{F,Z}$) and neutrons ($p_{F,N}$) in terms of the density

$$p_{F,Z} = h\left(\frac{3}{8\pi}\rho_Z\right)^{1/3} \tag{4.24}$$

$$p_{F,N} = h\left(\frac{3}{8\pi}\rho_N\right)^{1/3} \tag{4.25}$$

From Eqs. (4.24) and (4.25) we can calculate the total kinetic energy for Z protons and N neutrons to be

$$\begin{aligned} K.E. &= \int_0^{p_{F,Z}} dp \frac{2V 4\pi p^2}{h^3} \frac{p^2}{2M} + \int_0^{p_{F,N}} dp \frac{2V 4\pi p^2}{h^3} \frac{p^2}{2M} \\ &= \frac{4\pi}{5M}\left(\frac{3}{8\pi}\right)^{5/3} \frac{h^2}{V^{2/3}}(Z^{5/3} + N^{5/3}) \end{aligned} \tag{4.26}$$

where we have employed $A = N + Z$. Utilizing $V \sim A$ from Equation (4.16) and defining

$$T = (N - Z)/2 \tag{4.27}$$

as the isospin we can rewrite Equation (4.26) as:

$$K.E. = c\frac{1}{A^{2/3}}\left(\frac{A}{2}\right)^{5/3}\left[\left(1 - \frac{N-Z}{A}\right)^{5/3} + \left(1 + \frac{N-Z}{A}\right)^{5/3}\right] \tag{4.28}$$

Then for the case of $A \gg T$ we obtain the final form of

$$\begin{aligned} K.E. &\propto \frac{A}{2^{2/3}}\left[1+\frac{20}{9}\frac{T^2}{A^2}\right] \\ &\sim bA + c\frac{T^2}{A} \end{aligned} \tag{4.29}$$

where the necessary pre-factors are retained in the constants b and c. We see in the second term of Equation (4.29) the form of the isospin contribution to the nuclear energy found in the liquid drop model. An investigation of the potential energy can be performed resulting in a similar form, and implies the proton-neutron interaction is on average stronger than proton-proton or neutron-neutron interactions [Bohr and Mottelson, 1969]. This last term will be shown as crucial in the development of functional in Section 4.2.2. Finally, we discuss the last term in the liquid drop model: the pairing term.

Once again a result of the Pauli exclusion principle, the pairing term accounts for the lower energy observed for nuclei with even numbers of protons and neutrons. An even number of nucleons allows for spin coupling and thus a reduction in energy. The form of the pairing term is

$$a_P \frac{\delta(A,Z)}{\sqrt{A}} \tag{4.30}$$

where

$$\delta(A,Z) = \begin{cases} +1 & Z,N \text{ even } (A \text{ even}) \\ 0 & A \text{ odd} \\ -1 & Z,N \text{ odd } (A \text{ even}) \end{cases}. \tag{4.31}$$

The factor of $A^{-1/2}$ is emperically determined, along with the leading coefficient a_P.

With the development of Eqs. (4.18)-(4.30) we are able to arrive at the final form of the liquid drop model:

$$BE_{LD}(N,Z) = a_v A - a_s A^{2/3} - a_c \frac{Z(Z-1)}{A^{1/3}} - a_A \frac{(N-Z)^2}{A} + a_P \frac{\delta}{\sqrt{A}} \tag{4.32}$$

Equation (4.32) is the same as the Bethe-Weizsäcker formula, Equation (1.2), whose performance in describing nuclear masses was discussed in Chapter 1. The macroscopic treatment of nuclear masses discussed above will be incorporated into the the shell-model based functional developed in this work. We recall the failure of the Bethe-Weizsäcker formula to accurately reproduce shell effects. As will be seen in Chapter 7, our shell-model approach has much better performance in describing shell closures. This improved performance comes in part from the motivation obtained from the shell-model, described in the following Section 4.1.2.

4.1.2 Shell-model

In addition to the macroscopic terms provided by the liquid drop model, we know microscopic effects must be included to account for shell structure. The shell-model Hamiltonian has already been shown in Equation (2.8) (Section 2.2). As the motivation of the shell-model and its role in nuclear structure has been discussed in Section 2.2.1, we will now turn to specific motivations from the form of the shell-model Hamiltonian. We present here again Equation (2.8) [Mayer and Jensen, 1955]:

$$H_{SM} = \sum_i \varepsilon_i a_i^\dagger a_i + \frac{1}{4} \sum_{i,j,k,l} v_{ijkl} a_i^\dagger a_j^\dagger a_l a_k.$$

By applying the fermionic anticommutator relations

$$\{a_i, a_j\} = \{a_i^\dagger, a_j^\dagger\} = 0 \tag{4.33}$$

$$\{a_i, a_j^\dagger\} = \delta_{ij} \tag{4.34}$$

we can rewrite H_{SM} as

$$H_{SM} = \sum_i \varepsilon_i a_i^\dagger a_i + \frac{1}{4} \sum_{i,j,k,l} v_{ijkl} \left(a_i^\dagger a_k \delta_{lj} - a_i^\dagger a_l a_j^\dagger a_k \right). \tag{4.35}$$

We now define the number operator $\hat{m}_i = a_i^\dagger a_i$ which counts the number of fermions in some state i. If we then restrict ourselves to look at only those terms of the summation in Equation (4.35) in which $i = l$ and $j = k$ we obtain:

$$\begin{aligned} H_{SM} &= \sum_i \varepsilon_i \hat{m}_i + \frac{1}{4} \sum_{i,j,l=i,k=j} v_{ijij} \left(a_i^\dagger a_j \delta_{ij} - a_i^\dagger a_i a_j^\dagger a_j \right) + \frac{1}{4} \sum_{i,j,l\neq i,k\neq j} v_{ijkl} a_i^\dagger a_j^\dagger a_k a_l \\ &= \sum_i \varepsilon_i \hat{m}_i + \frac{1}{4} \sum_{i,j} v_{ij} \left(a_i^\dagger a_j \delta_{ij} - \hat{m}_i \hat{m}_j \right) + \frac{1}{4} \sum_{i,j,l\neq i,k\neq j} v_{ijkl} a_i^\dagger a_j^\dagger a_k a_l \end{aligned} \tag{4.36}$$

This separation is motivated by the linear and quadratic forms in occupation numbers of References [Duflo and Zuker, 1995] and [Duflo, 1994], where the diagonal terms ($i = l,\ j = k$) are termed the monopole contributions and the off-diagonal ($i \neq l,\ j \neq k$) are termed the multipole contributions. Following the prescription of Reference [Duflo and Zuker, 1995], we remain primarily motivated by the monopole term of Equation (4.36) which reproduces the exact energy of closed shells and closed shells plus or minus 1 particle [Duflo and Zuker, 1995]. As we see in Equation (4.36), the monopole term contains linear ($\hat{m}$) and quadratic ($\hat{m}^2$) forms of the number operator $\hat{m}$. These terms may provide contributions to the energy from single-particle and particle-particle interactions respectively. As such, we anticipate any functional

in a shell-model basis to employ linear and quadratic forms in neutron and proton number.

4.2 Functional form

The functional employs bulk terms taken from the liquid drop model, which are independent of orbital occupations, and a microscopic interaction which rely on the proton and neutron occupations. We first introduce the functional as macroscopic Coulomb and pairing terms plus a microscopic interaction, $\mathcal{F}(n,z)$:

$$F(c;n,z) = c_c \frac{Z(Z-1)}{A^{1/3}} + c_P \frac{\delta}{\sqrt{A}} + \mathcal{F}(c;n,z) \tag{4.37}$$

where δ is 1 or -1 for even-even or odd-odd nuclei, respectively, and 0 otherwise. The 17 fit parameters of the full functional are denoted as the shorthand coefficients

$$c \equiv \{c_1, c_2, \ldots, c_{11}, c_c, c_P, c_s, c_{as}, c_{ss}, \tilde{c}_s\}, \tag{4.38}$$

while

$$z \equiv \{z_1, z_2, \ldots\} \tag{4.39}$$

$$n \equiv \{n_1, n_2, \ldots\} \tag{4.40}$$

denote the occupations of proton and neutron shells, respectively. The microscopic functional $\mathcal{F}(c;n,z)$ has the form

$$\begin{aligned} \mathcal{F}(c;n,z) &= \hbar\omega(V + T_{kin} + I_{2B} + D + D_{4B} + \mathcal{T} + M_{4Bex} + L_{val}) \\ &\quad + \hbar\tilde{\omega}(\tilde{D}_{2B} + L + \tilde{L}) \end{aligned} \tag{4.41}$$

The coefficients c are determined via a fit to experimental data, discussed in the following section. The microscopic interactions contained in $\mathcal{F}(c;n,z)$ are dependent on major oscillator shell occupations of protons and neutrons. To achieve a desirable χ value from our functional we have found the need to scale the microscopic energy by one of two non-trivial $\hbar\omega$ functions, $\hbar\omega$ and $\hbar\tilde{\omega}$. Both forms are independent of shell occupations, but contain fit parameters. Their forms and physical meaning are presented in the following section.

4.2.1 Microscopic terms

We begin our detailed discussion of terms with those that scale as A, or our volume terms. The scaling of the functional terms presented here follow similarly to Equation (4.11).We begin with the volume terms that scale as A:

$$V \equiv c_1 A, \tag{4.42}$$

$$T_{\text{kin}} \equiv c_2 A^{-1/3} \sum_p p(z_p + n_p), \tag{4.43}$$

$$I_{\text{2B}} \equiv c_3 A^{-1/3} \sum_p \left(\frac{z_p(z_p-1)}{p} + \frac{n_p(n_p-1)}{p} + \frac{2n_p z_p}{p} \right), \tag{4.44}$$

$$\begin{aligned} D \equiv\ & c_4 \sum_p \left(\frac{\sqrt{d_p}}{2} - \frac{2}{d_p^{3/2}}(z_p - d_p/2)^2 \right) \\ & \times \sum_q \left(\frac{\sqrt{d_q}}{2} - \frac{2}{d_q^{3/2}}(n_q - d_q/2)^2 \right), \end{aligned} \tag{4.45}$$

$$D_{\text{4B}} \equiv c_6 \sum_p \frac{z_p(d_p - z_p) n_p (d_p - n_p)}{d_p^3}, \tag{4.46}$$

$$L \equiv c_7 \sum_p \left(\sqrt{(z_p+\varepsilon)(n_p+1)} + \sqrt{(n_p+\varepsilon)(z_p+1)} \right), \tag{4.47}$$

$$\mathcal{T} \equiv c_9 \sum_p \sqrt{(n_p - z_p)^2 + \varepsilon^2}. \tag{4.48}$$

Note that $\varepsilon = 10^{-3}$ is a regularization parameter in Eqs. (4.42)-(4.48), to ensure differentiability.

As is evident, V in Equation (4.42), is simply a bulk volume term which provides a smoothing of the energy surface. A fermion in the major shell p has energy p and so the next term, T_{kin} of Equation (4.43), represents a kinetic energy contribution from single-particle energies. Such a one-body term is expected from our discussion of achieving the ground-state energy from a functional.

Equation (4.44) begins our treatment of two-body interactions in the shell-model that scale as the volume. Such a two-body term is motivated by the shell-model and strongly suggested by the form of the monopole hamiltonian present in the Duflo and Zuker mass formula [Duflo and Zuker, 1995]. I_{2B} is a mean-field like term where we see the single particle self-energy is deducted from the two-body proton-proton, neutron-neutron contributions.

The term D of Equation (4.45) is technically a two-, three- and four-body interaction and serves to include deformation effects, which result in shell oscillations around mid-shell [Strutinsky, 1967]. The form of this term has a linear onset, that maximizes at mid-shell with half-filled occupations. In practice it behaves in the same manner as a function of the form $\min(n_p, d_p - n_p)$, however we have chosen this form to eliminate the discontinuity present in the first derivative of a min function. Similarly in D_{4B}, Equation (4.46), we see higher-order contributions. This four-body term once again provides a maximum at mid-shell, and is present for accurate descriptions of higher-order nuclear deformation

Equation (4.47) is strongly motivated by the work in References [Bertolli and Papenbrock, 2008, Papenbrock and Bhattacharyya, 2007]. The minimum energy for a two-level system results in fractional occupations of the higher level due to a square-root term. Such a term was readily seen analytically in both the derivation of the energy functional for the three-level Lipkin model and the pairing Hamiltonian [Bertolli and Papenbrock, 2008, Papenbrock and Bhattacharyya, 2007]. Furthermore, we see a connection to the solid state field where studies in Reference [Lacroix and Hupir, 2010] show a similar form for mesoscopic pairing in superconductors. Both studies exhibit a square-root singularity for small occupations. The inclusion of such

square-root terms not only has this analytical motivation, but has proved helpful for the functional's accurate reproduction of experimental energies.

Finally $\mathcal{T}$ is an isospin term, also referred to as a Wigner term [Wigner, 1937, Satula et al., 1997, Zeldes, 1998]. This is straightforward in calculating the isospin of each individual orbital. Not surprisingly, $\mathcal{T}$ has proven necessary to accurately describe of nuclei far from the $N = Z$ line. We note that Equation (4.48) is written in terms of square roots (rather than absolute values) for computational purposes, where in the case of $|n_p - z_p| \gg \varepsilon$ we have $\sqrt{(n_p - z_p)^2 + \varepsilon^2} \simeq |n_p - z_p|$

We also need to include surface corrections independent of the volume terms. Technically, surface terms scale as $A^{2/3}$. We employ

$$\tilde{D}_{2\mathrm{B}} \equiv c_5 \sum_p \left(\frac{z_p(d_p - z_p)}{d_p^{3/2}} + \frac{n_p(d_p - n_p)}{d_p^{3/2}} \right), \tag{4.49}$$

$$\tilde{L} \equiv c_8 A^{-2/3} \sum_p \left(z_p \sqrt{z_p + 1} + n_p \sqrt{n_p + 1} \right), \tag{4.50}$$

$$M_{4\mathrm{Bex}} \equiv c_{10} \sum_p \frac{1}{p^{23}} \Big[(z_p(z_p - 1)(z_p - 2)(z_p - 3))^3 + (n_p(n_p - 1)(n_p - 2)(n_p - 3))^3 \Big], \tag{4.51}$$

$$L_{\mathrm{val}} \equiv c_{11} \left(\sqrt{(d_f - n_f)n_{f+1} + \varepsilon^2} + \sqrt{(d_f - z_f)z_{f+1} + \varepsilon^2} \right). \tag{4.52}$$

$\tilde{D}_{2B}$, Equation (4.49), provides a term that accounts at least in part for microscopic pairing. It takes a form motivated by Talmi's seniority model [Talmi, 1962], again with a maximum contribution at mid-shell as with the volume term Equation (4.45) Likewise, $\tilde{L}$ of Equation (4.50) is a surface corrective term motivated along the same lines as Equation (4.47) above.

In Equation (4.51) we present an extended mean-field energy term. The cubic nature of this term indicates its effect (as determined via the method described in Section 4.3) is present as a higher order correction. The powers of p are in place to insure appropriate scaling.

Finally we consider the term L_{val} in Equation (4.52). This term is unique in that it involves no summation over shells, but involves only the last filled shell according to a naive level filling (the Fermi surface) and the shell immediately above, e.g. n_f and n_{f+1} respectively. Equation (4.52) represents a particle-hole like contribution to the surface energy and has shown useful in providing finer corrections to energy calculations.

4.2.2 Anatomy of $\hbar\omega$ terms

A key component to our mass functional is the scaling of the microscopic terms by

$$\hbar\omega(c_s, c_{as}, c_{ss}) = 1 - c_s A^{-1/3} - \frac{c_{as}}{1 + c_{ss}A^{-1/3}} \frac{T(T+1)}{A^2} \tag{4.53}$$

$$\hbar\tilde{\omega}(\tilde{c}_s) = 1 - \tilde{c}_s A^{-1/3} \tag{4.54}$$

Both forms, Eqs. (4.53) and (4.54), are functions of total neutron (N) and proton number (Z) as well as the set of fit coefficients c. The presence of both Eqs. (4.53) and (4.54) are found to be crucial in obtaining a desirable χ value. The motivation of these forms of $\hbar\omega$ and $\hbar\tilde{\omega}$ is not immediately obvious. In this section we will provide the necessary physical motivations for their inclusion.

We will begin with Equation (4.54) which is the simpler of the two. The leading 1 of Equation (4.54) allows for each microscopic term it affects to contribute at leading order. As we have ensured all terms scale at most as A, saturation is always maintained by the term itself. The second term of Equation (4.54), $\tilde{c}_s A^{-1/3}$, provides a smooth bulk surface correction to each microscopic term. That is, any term scaling as A will now also have a smaller contribution that scales as $A^{-1/3}A = A^{2/3}$, which is a surface term (see Section 4.1.1). Those terms which already scale as $A^{2/3}$ will now have radial correction scaling as $A^{1/3}$.

The second form, Equation (4.53), is more complex and requires some motivation. Like Equation (4.54), Equation (4.53) contains in its first two terms, $1 + c_s A^{-1/3}$, leading contributions and surface corrections for each of the microscopic terms it scales. However, its final term

$$\frac{c_{ss}}{1 + c_{as} A^{-1/3}} \frac{T(T+1)}{A^2}$$

also provides an isospin correction [Danielewicz and Lee, 2009, Nikolov et al., 2011]. We motivate this isospin correction by first recalling the isospin dependence of the liquid drop model:

$$\frac{(N-Z)^2}{A}. \tag{4.55}$$

We note this scales as A and therefore has a volume character. However, the final term of Equation (4.53) introduces a surface isospin correction. By looking at the sign of the leading coefficients in the liquid drop model, Equation (4.32), we see increasing the magnitude of the neutron-proton asymmetry decreases the surface tension [Danielewicz and Lee, 2009]. We define the quantity associated with asymmetry in systems in contact at equilibrium as the asymmetric chemical potential μ_a [Danielewicz and Lee, 2009].

$$\mu_a = \frac{\partial E}{\partial (N-Z)} \tag{4.56}$$

Following Reference [Danielewicz and Lee, 2009] we perform a Legendre transform from μ_a to $N - Z$

$$N - Z = \frac{\partial \Phi}{\partial \mu_a} \tag{4.57}$$

where

$$\Phi = \mu_a (N-Z) - E = \mu_a (N-Z) - E_v - E_s \tag{4.58}$$

and note that the energy, E, has both surface (E_s) and volume (E_v) components. Inserting Equation (4.58) into Equation (4.57) we find:

$$\frac{\partial(N-Z)}{\partial\mu_a} = 2\left(\frac{\partial^2 E_v}{\partial\mu_a^2} + \frac{\partial^2 E_s}{\partial\mu_a^2}\right) \tag{4.59}$$

Through dimensionality and scaling [Danielewicz and Lee, 2009] one can finally arrive at an expression for the net energy for a liquid drop description of a nucleus with both surface and volume asymmetry.

$$E = E_0 + \frac{a_{iso}}{A}\frac{(N-Z)^2}{A} \tag{4.60}$$

where E_0 is the volume and surface contributions of symmetric nuclear matter, $N = Z$, and the coefficient a_{iso} is [Danielewicz and Lee, 2009]:

$$a_{iso} = \frac{c_{ss}}{1 + c_{as}A^{-1/3}} \tag{4.61}$$

This provides us with the form of the last term in Equation (4.53). We note the form of Equation (4.61) tends towards c_{ss} for large A and so the isospin term retains a volume character. However, for small A the ratio $\frac{a_{iso}}{A}$ in Equation (4.61) approaches $c_{as}/A^{2/3}$. So we find motivation from the liquid drop model once again in the form of our more complicated $\hbar\omega$ scaling. The two forms, Eqs. (4.53) and (4.54), are found to be crucial in significantly reducing our least-squares error.

4.3 Determination of Relevant Terms

The reader may wonder how we arrived at the particular form of the functional (4.41). Unfortunately, there is no practical recipe available for the construction of the functional. As described in Section 4.1, the guiding principles are saturation, mean-field arguments, algebraic schemes, and insights from analytically solvable systems. However, these arguments do not sufficiently constrain the functional, and we need a

systematic approach rather than a trial-and-error-based, approach to identify terms that should enter into the functional.

Bertsch and coworkers [Bertsch et al., 2005] employed the singular value decomposition and studied the statistical importance of various linear combinations of terms that enter the functional. This method identifies the relative importance of possible combinations of terms and truncates search directions that are flat in the parameter space. Along these ideas, we employ a method that chooses new functional terms based on their correlation to terms already present. New terms are chosen to provide a relatively independent search direction in the parameter space along which the χ^2 of Equation (5.1) is minimized. This approach is presented in detail in Section 4.3.1.

In mass formulae, the addition of new terms (and new fitting parameters) yields a chi-square that is a monotone decreasing function with the number of fit parameters. In fact, adding parameters has been shown to reduce the least-squares error deviation by as much as a factor of five [Möller et al., 1995, Koura et al., 2000, Pomorski and Dudek, 2003, Royer and Gautier, 2006, Mendoza-Temis et al., 2008]. For a functional, however, matters are different. Here, the addition of a new term to the functional guarantees a lowered chi-square only if the term has a perturbatively small effect. This point is demonstrated in Section 4.3.2.

4.3.1 Correlation Test

We first describe our method for selecting new terms to be included in the functional, beyond those strongly motivated by scaling arguments, mean-field arguments, and solutions to simple analytic systems. We seek a systematic method for determining new terms that will provide further insight into the physical system and decrease the overall χ^2.

The independence of new terms in not only important for the reduction of the χ value. Adding *ad hoc* terms, while possibly reducing χ, may alter the value of another parameter that carries physical meaning [Danielewicz and Lee, 2009].

In cases of adding even physically motivated terms there is a danger. Statistical interference [Garthwaite et al., 2002] among combinations of terms can alter the relative size of physical parameters, often resulting from a limited domain of variation in the fitted data set [Kirson, 2008, Danielewicz and Lee, 2009]. By adding only terms with minimal statistical overlap we avoid this issue. In this way we provide a constraint on the forms of the terms, reducing the space of functional forms in which to search.

Consider the addition of a term $c_f f$, with new fit parameter c_f, to the functional F_0. One can expect that this term will be sufficiently useful in lowering the chi-square only when it is independent of the terms already included in the functional.

Let us consider the addition of a term $c_f f$ to the functional

$$F_0(c; n, z) = c_c \frac{Z(Z-1)}{A^{1/3}} + c_P \frac{\delta}{\sqrt{A}} + \sum_{\alpha=1}^{M} c_\alpha f_\alpha(n(c), z(c)) \tag{4.62}$$

of M terms, and let n^*, z^* be the occupation numbers that minimize F_0 for a given nucleus. The occupation numbers depend on the nucleus i under consideration, but we suppress this dependency.

For identification of a new search direction we compute the correlation coefficient

$$R_{f_\alpha, f} \quad = \quad \frac{\mathrm{cov}(f_\alpha, f)}{s_{f_\alpha} s_f}, \tag{4.63}$$

where the covariance is

$$\mathrm{cov}(f_\alpha, f) = \langle f_\alpha f \rangle - \langle f_\alpha \rangle \langle f \rangle \tag{4.64}$$

and the average $\langle \cdot \rangle$ is computed with respect to the N_{pts} nuclei of the nuclear chart. Here N_{pts} represents the number of experimental data points for nuclear binding energies. Similarly, the standard deviations are

$$s_f = \sqrt{\langle f^2 \rangle - \langle f \rangle^2} \text{ and } s_{f_\alpha} = \sqrt{\langle {f_\alpha}^2 \rangle - \langle f_\alpha \rangle^2}. \tag{4.65}$$

In the computation of averages, the terms f and f_α are evaluated at the occupations $(n^*(c), z^*(c))$ that minimize Equation (4.62). Here $(n^*(c), z^*(c))$ depend on the coefficients c that minimize the χ^2 of Equation (4.62). We note that the correlation coefficient is independent of the size of the coefficient c_f of the new term under consideration, though dependent on the other fit coefficients c through the optimal occupations $(n^*(c), z^*(c))$. Should the correlation be sufficiently low for all included terms, the new term can be tested for its performance in lowering the χ value.

This approach allows us to probe many different forms of functional terms and then scan through several hundred iterations without the time-consuming and computationally expensive aspects of performing a full minimization of the chi-square for each new term under question. In this way, we systematically grow the functional term by term. We started from an initial base of about 350 different terms and found that only 18 of them were weakly correlated to the existing terms and had the potential to significantly decrease the least-squares error. Of these 18 terms, 15 were seen to be simply higher-order corrections of three primary forms. We further reduced the set of possible terms through physical arguments and preliminary fits. This approach showed Equation (4.48) to be the best choice for lowering our least-squares deviation. Equations (4.51) and (4.52) were determined similarly, from very large sets of possible terms. In this way we successfully lowered the functional's least-squares error to a meaningful $\chi = 1.31$ MeV with 17 fit parameters. This can be compared to the 28 parameters of the Duflo and Zuker mass formula, which achieves a least-squares error of $\chi \simeq 0.35$ MeV [Duflo and Zuker, 1995].

4.3.2 Perturbative Test

Assume that our functional is F_0 and that we consider the addition of a new term $c_f f$ (with the new fit coefficient c_f taken to be the mean value of the currently determined fit coefficients, where there are no statistical outliers). We will consider the general case where the new term f depends also on the fit coefficients c of F_0. In what follows,

we consider a single nucleus with the ground-state energy

$$E_0 \equiv F_0(c; n^*, z^*) \tag{4.66}$$

obtained from the functional F_0. Let us assume that

$$f(c; n^*, z^*) \ll E_0; \tag{4.67}$$

in other words, the new term is perturbatively small (assuming that the new fit coefficient c_f is of order one). Furthermore, we make the assumption of the naturalness of f and therefore its derivatives in the neighbourhood of (n^*, z^*) is of the same order as f, $f' \sim f$. That is, we insure all terms considered are perturbatively small compared to F_0 in the area around (n^*, z^*), not simply tuned to be small only at the occupations (n^*, z^*). This is motivated by our selection of terms to search and their required scaling. We consider $F = F_0 + c_{\text{new}} f_{\text{new}}$, and it is clear that the minimum of F will be found at some new occupations $n^* + \delta n, z^* + \delta z$ with corrections δn and δz that are much smaller than n^* and z^*, respectively. We expand

$$\begin{aligned}
&\min_{n,z\in\mathcal{D}_i} \Big(F_0(c; n, z) + c_f f(c; n, z)\Big) \\
&\quad = \quad F_0(c; n^* + \delta n, z^* + \delta z) + c_f f(c; n^* + \delta n, z^* + \delta z) \\
&\quad \approx \quad F_0(c; n^*, z^*) + c_f f(c; n^*, z^*) \\
&\qquad + \sum_p \frac{\partial F_0}{\partial n_p}\bigg|_{n^*,z^*} \delta n_p + \sum_p \frac{\partial F_0}{\partial z_p}\bigg|_{n^*,z^*} \delta z_p, \\
&\qquad + c_f \sum_p \frac{\partial f}{\partial n_p}\bigg|_{n^*,z^*} \delta n_p + c_f \sum_p \frac{\partial f}{\partial z_p}\bigg|_{n^*,z^*} \delta z_p \\
&\quad \approx \quad F_0(c; n^*, z^*) + c_f f(c; n^*, z^*),
\end{aligned} \tag{4.68}$$

and the approximation is due to our limitation to first-order corrections. Note that we have expanded to first-order in smallness, eliminating terms that go as derivatives of f since $|f'\delta n| \ll |F_0|$ and $|f'\delta p| \ll |F_0|$. The derivatives of the functional F_0

with respect to the occupation numbers vanish at the optimum occupation numbers (n^*, z^*), where it is understood that the variation is only with respect to those occupation numbers that are not at any of the boundaries (i.e., those occupation numbers for which $n_j^* \neq 0$ or d_j and $z_j^* \neq 0$ or d_j), and that the variation fulfills the equality constraints*. Thus, in leading order of perturbation theory, the functional is simply a mass formula (as it is evaluated at the leading-order occupations), and the chi-square fit cannot yield an increased root-mean-square error for the ground-state energies. In the worst case, $c_f = 0$ will result from the fit.

Therefore, the addition of terms to the functional that cause small changes to the occupation numbers will allow the functional to better reproduce the true ground-state energy. We can expect that this methodology, when coupled with our determination of new search directions, will provide worthwhile reductions in the overall χ.

For quickly evaluating a new candidate term f to be added to the functional, we begin by treating the full functional as a mass formula. That is, we freeze the proton and neutron occupations at the optimal values determined prior to the addition of the new term and approximate the ground-state energy in the presence of the new term as

$$E_i(c; n^*, z^*) \approx F(c; n^*, z^*) + c_f f_{\text{new}}(n^*, z^*). \tag{4.69}$$

We evaluate the energy (4.69) for each nucleus i, perform a χ^2 minimization of the resulting mass formula (4.69), and obtain a new set of test coefficients, c_{test}. Using these coefficients we recalculate the occupations $n^*_{\text{test}}, z^*_{\text{test}}$ and the ground-state energies

$$E_i(c_{\text{test}}; n^*_{\text{test}}, z^*_{\text{test}}) = \min_{n,z \in \mathcal{D}_i} \Big(F(c_{\text{test}}; n, z) + c_f f(c_{\text{test}}; n, z) \Big) \tag{4.70}$$

*Technically, this specification constituting a *reduced* derivative is necessary due to the minimization being performed over the constrained domain $\mathcal{D}_i$ [Mielke and Theil, 2004].

that minimize the functional. The computation of the corrections $(\delta n, \delta z) \approx (n^*_{\text{test}} - n^*, z^*_{\text{test}} - z^*)$ to the occupation numbers shows whether the new term is perturbative in character and thus has the potential to lower the chi-square.

4.3.3 Example of selecting a term

To demonstrate the new method of selecting functional terms detailed in Sects. 4.3.1 and 4.3.2, consider a truncated form of the functional in Equation (4.41):

$$\begin{aligned} F_0 &= c_c \frac{Z(Z-1)}{A^{1/3}} + c_P \frac{\delta}{\sqrt{A}} \\ &\quad + \hbar\omega(V + T_{kin} + I_{2B} + D + D_{4B} + \mathcal{T}) \\ &\quad + \hbar\tilde{\omega}(\tilde{D}_{2B} + L + \tilde{L}). \end{aligned} \tag{4.71}$$

That is, Equation (4.41) without the mean-field, M_{4Bex}, or valence, L_{val}, terms (note the liquid drop bulk terms are kept). Consider the addition of a new generalized term f_{new} to Equation (4.71) that takes a form similar to the M_{4Bex} of Equation (4.51):

$$f_{rmnew}(n,z) = \sum_p \left([z_p(z_p-1)(z_p-2)(z_p-3)]^\gamma + [n_p(n_p-1)(n_p-2)(n_p-3)]^\gamma\right) \tag{4.72}$$

Proposing Equation (4.72) as a form for a new term we first implement a test to insure it is sufficiently independent of the terms already present in Equation (4.71). This independence is determined from the correlation coefficient $R_{f,f_{new}}$ as described by Equation (4.63) in Section 4.3.1.

We allow γ to vary over integer and non-integer values and determine that $\gamma = 3$ produces a correlation coefficient, Equation (4.63), amongst all other terms $R_{f,f_{\text{new}}} < 0.5$, which satisfies our condition for independence. With the specific form

$$f_{\text{new}}(n,z) = \sum_p \left([z_p(z_p-1)(z_p-2)(z_p-3)]^3 + [n_p(n_p-1)(n_p-2)(n_p-3)]^3 \right) \tag{4.73}$$

we are able to confirm that Equation (4.73) causes only small perturbations in the optimal occupations of F_0. In Fig. 4.3 we illustrate the change in optimal occupation numbers $(\delta n, \delta z)$ for each orbital of the nucleus ^{19}Na. We note the largest change occurs in the proton orbitals $p = 3$ and $p = 4$ with $\delta z = -0.8$ and $\delta z = +0.8$, respectively. However, with naive level-filling the $p = 3$ orbital contains three protons. Therefore, a change of $|\delta z| = 0.8$ remains perturbative.

The results of the correlation and perturbation tests identifies Equation (4.73) as a term whose addition will provide a meaningful reduction in the χ value. For the truncated functional F_0, Equation (4.71), we obtain a least-squares error of $\chi_{F_0} = 1.52$ MeV. With the addition of Equation (4.73) the functional $F_0 + f_{\text{new}}$ achieves a least-squares error of $\chi_{new} = 1.32$ MeV. The reduction by 0.2 MeV is meaningful and demonstrates the ability of the correlation and perturbation tests to systematically grow the functional term-by-term.

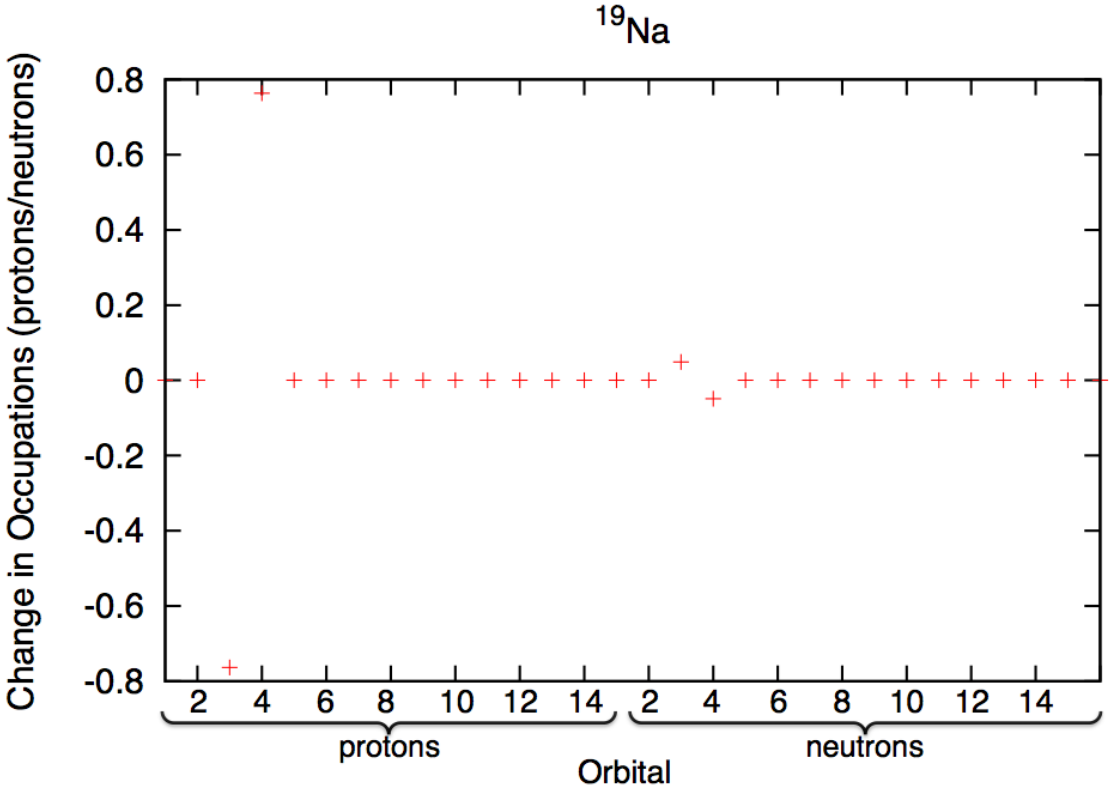

Figure 4.3: Change in proton and neutron occupations $(\delta n, \delta z)$ for ^{19}Na, demonstrating the perturbative effect of adding the term f_{new}. Each orbital is labeled by principle quantum number p. Orbitals $p = 3, 4$ in protons exhibit the greatest change, but still remain perturbative.

Chapter 5

Fitting procedure and numerical implementation

In this chapter we present the numerical optimization that provides us with not only the fit parameters c, but also the occupations numbers (n, z) which minimize the functional and therefore define the ground-state energy for each nucleus a la the Hohenberg-Kohn theorems. To begin, we present the multi-level optimization problem dealt with in this work and show the general theories behind our optimization methods in Section 5.1. Next, we provide the specifics of the functional minimization with respect to orbital occupations (n, z) in Section 5.2.1 and finally, in Section 5.3.1, we discuss the details of the optimization for determining the fit parameters c.

5.1 Multi-level functional optimization

The fit coefficients c are determined by minimizing the sum of squared residuals

$$\chi^2(c) = \sum_{i=1}^{N_{\text{pts}}} \left(\frac{E_i^{\text{th}}(c; n^*(c), z^*(c)) - E_i^{\text{exp}}}{N_{\text{pts}}} \right)^2 \tag{5.1}$$

as a function of c. This is a multi-level optimization problem because each of the theoretical energies, E^{th} are solutions to lower-level minimizations over the occupation

numbers n and z. Obtaining the occupations from an optimization is in stark contrast to previous occupation number-based mass formulae where occupations are input by hand [Duflo and Zuker, 1995].

The multi-level nature of the optimization is non-trivial. Due to the dependency of the sum of squared residuals in Equation (5.1) on the lower-level minimization contained in each E_i^{th} there is a complicated coupling between the two optimizations. This coupling results in a dependency of the fit coefficients c on the optimal occupations (n^*, z^*). The converse is true, where the optimal occupation depend on the current fit coefficients, $(n^*(c), z^*(c))$.

In order to approach the problem of the multi-level optimization we employ two different methods. The first is a constrained optimization for the lower-level problem used to minimize the functional for each nucleus in order to obtain $E_i^{\text{th}}(c; n^*(c), z^*(c))$. The second is an unconstrained optimization for the upper-level problem to determine the fit coefficients c. Details of both the upper- and lower-level optimizations are given in Sects. 5.2.1 and 5.3.1. In Sects. 5.2 and 5.3 we provide the theoretical foundations.

5.2 Lower-level: constrained optimization

Minimization of the functional, Equation (4.41), with respect to the proton and neutron occupations (n, z) provides the binding energy for each nucleus. Obviously, the variables to be optimized, (n, z), can only take restricted values. Therefore, Equation (4.41) must be minimized over a constrained domain. In order to tackle this problem we have chosen to utilize the iterative optimization method of sequential quadratic programming.

Sequential quadratic programming requires that the objective function $f(\mathbf{x})$ be continuous and twice differentiable and solves a sequence of subproblems in order to solve optimizations of the form:

$$\min_{\mathbf{x}} \{ f(\mathbf{x}) : b(\mathbf{x}) \geq 0, c(\mathbf{x}) = 0 \} \tag{5.2}$$

where $b(\mathbf{x})$ and $c(\mathbf{x})$ provide inequality and quality constraints, respectively. The method employed in this work generates a quadratic model of the function's Lagrangian for the optimization. The Lagrangian for Equation (5.2), with Lagrange multipliers $\boldsymbol{\lambda}$ and $\boldsymbol{\sigma}$, is

$$L(\mathbf{x}, \boldsymbol{\lambda}, \boldsymbol{\sigma}) = f(\mathbf{x}) - \boldsymbol{\lambda}^T b(\mathbf{x}) - \boldsymbol{\sigma}^T c(\mathbf{x}). \tag{5.3}$$

The method defines an appropriate search direction $\mathbf{d}$ (with the same dimensionality as $\mathbf{x}$) at each iteration k for the optimization of Equation (5.2). The search direction is found as the solution to the quadratic subproblem at each iteration

$$\begin{aligned} \min_{\mathbf{d}} \{ L(\mathbf{x}_k, \boldsymbol{\lambda}_k, \boldsymbol{\sigma}_k) + \left(\nabla L(\mathbf{x}_k, \boldsymbol{\lambda}_k, \boldsymbol{\sigma}_k)\right)^T \mathbf{d} + \frac{1}{2} \mathbf{d}^T \left(\nabla^2 L(\mathbf{x}_k, \boldsymbol{\lambda}_k, \boldsymbol{\sigma}_k)\right) \mathbf{d} : \\ b(\mathbf{x}_k) + \nabla b(\mathbf{x}_k)^T \mathbf{d} \geq 0, c(\mathbf{x}_k) + \nabla c(\mathbf{x}_k)^T \mathbf{d} = 0 \} \end{aligned} \tag{5.4}$$

The need for continuity and differentiability is clear from the form of the subproblem Equation (5.4). As derivatives of the Equation (4.41) with respect to the optimized variables (n, z) are available, we have chosen to provide them analytically. We found significant advantages in terms of speed and stability using this routines that require analytic expressions for gradients over constrained derivative-free direct-seach methods, such as `COBYLA` (Constrained Optimization BY Linear Approximations) [Powell, 1994]. `COBYLA` operates on the simplex method. In n dimensions a simplex is a polygon of $n+1$ vertices. The function is evaluated at each vertex and the simplex is either rotated of contracted to encompass the region of a local minimum to within a defined accuracy. `COBYLA` constructs linear polynomial approximations to the function and its constraints by interpolation at each vertex. Simplex methods were found to be unstable when the functional was run on various machines and introduced a higher noise level. Details on the routine chosen, and its performance compared to simplex methods is given in Section 5.2.1.

5.2.1 Lower-level specifics: FFSQP

Given coefficients c, for each nucleus $i = 1, \ldots, N_{\text{pts}}$ we obtain the optimal occupation numbers $(n^*(c), z^*(c))$ through a constrained minimization of the functional itself

$$E_i^{\text{th}}(c; n^*(c), z^*(c)) = \min_{(n,z)\in\mathcal{D}_i} F(c; n, z), i = 1, \ldots, N_{\text{pts}}, \tag{5.5}$$

where the linearly-constrained occupation number region is

$$\mathcal{D}_i = \left\{ (n, z) : \sum_p n_p = N, \sum_p z_p = Z, 0 \leq n_p, z_p \leq d_p \right\} \tag{5.6}$$

and $F(c; n, z)$ denotes the functional. We note that the functional and $\mathcal{D}_i$ depend on the nucleus (i) through N, Z, A, T, δ, and the orbital dimensions $\{d_p\}$. This dependency is suppressed in the notation.

The functional F in Eqn. (4.41) is nonlinear but twice continuously differentiable in the occupation numbers (n, z) over the domain $\mathcal{D}$ except when both $\hbar\omega c_9 \neq 0$ and $n_p = z_p$ for some p. Furthermore, given c, we have algebraic derivatives of F with respect to (n, z) and can use this to solve each lower level problem. Hence, we use the sequential quadratic programming code FFSQP (Fortran Feasible Sequential Quadratic Programming) [Zhou et al., 1997], starting from occupation numbers n and z corresponding to the naive level filling, to quickly find a local solution of Equation (5.5).

FFSQP uses a gradient method to find a local minimum within the constraints of $\mathcal{D}$, where we have provided the analytical form of the gradients with respect to (n_j, z_j) (see Section 5.2). The value of the functional is lowered along the direction of steepest descent according to solutions of the subproblem Equation (5.4), and a final value obtained at a location such that further steps result in an increasing gradient. FFSQP has shown to provide a stable result across multiple machines up to machine-precision over the tested direct-search method COBYLA. Additionally, the derivative-based method of FFSQP produced significantly less noise in the full optimization over

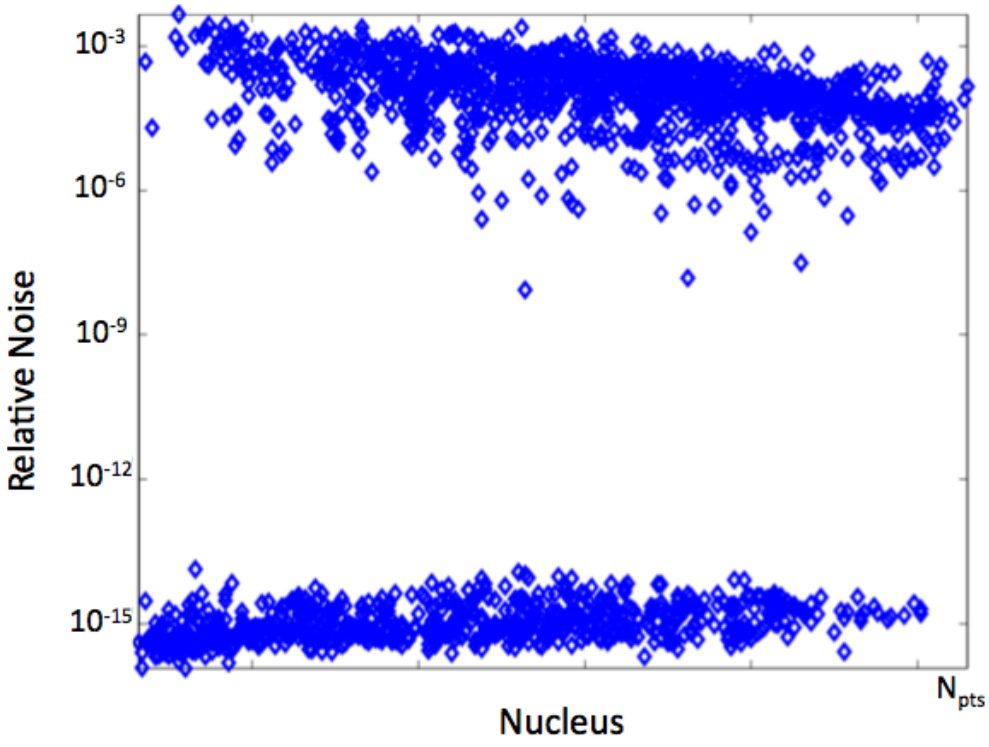

Figure 5.1: Relative noise for each nucleus as calculated by lower-level (constrained) minimization routine `COBYLA`, where derivatives are unavailable. The horizontal axes are arbitrary indexes of the nuclei in the data file. Roughly half of nuclei exhibit significant noise [Moré and Wild, 2011, Wild, 2011].

`COBYLA`. Figures 5.1 and 5.2 show the relative noise for each nucleus using `COBYLA` and `FFSQP` for the lower-level minimization, respectively (horizontal axes are an arbitrary index of the nuclei). In the case of `COBYLA` roughly half of the nuclei exhibit significant noise in the minimization, while `FFSQP` only shows noise above machine precision for four nuclei. These nuclei correspond to the neutron shell closures at $N = 14, 28$.

Relative computational noise of some function $f(\mathbf{x})$ around a point $\mathbf{x}$ is obtained by evaluating the function at small perturbations $\mathbf{h}$ around $\mathbf{x}$ and considering the scaled average of differences [Moré and Wild, 2011]:

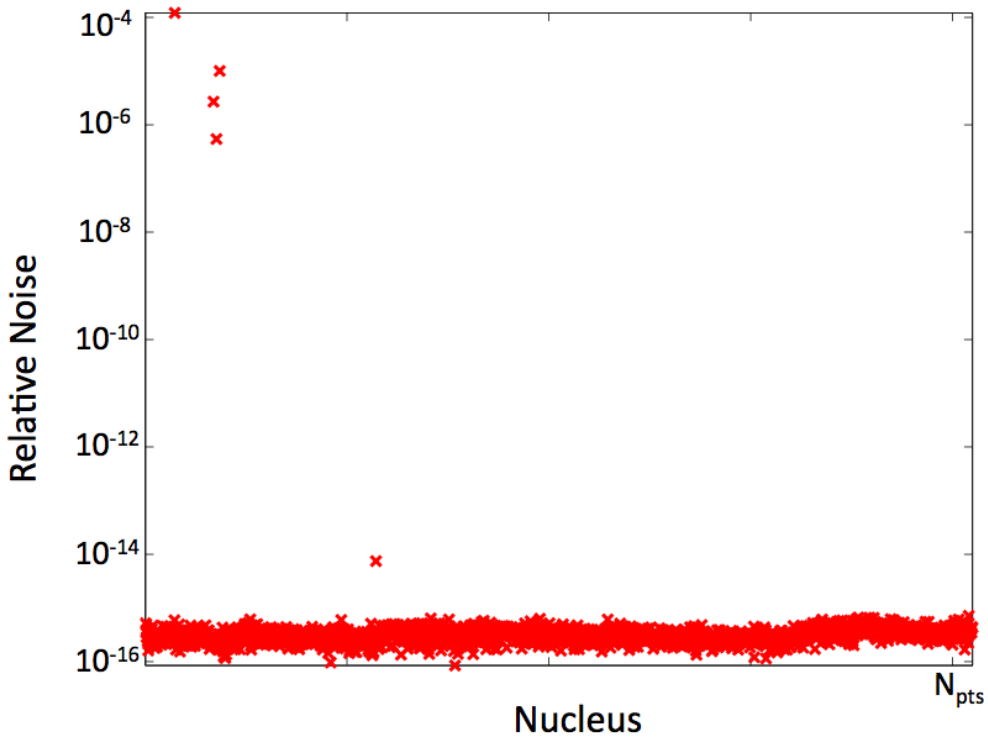

Figure 5.2: Relative noise for each nucleus as calculated by lower-level (constrained) minimization routine `FFSQP`, where derivatives are available. The horizontal axes are arbitrary indexes of the nuclei in the data file. The availability of derivatives significantly reduces noise [Moré and Wild, 2011, Wild, 2011].

$$\frac{1}{|f(\mathbf{x})|}\left(\frac{1}{2m}\sum_{i=1}^{m}|f(x_i+h_i)-f(x_i)|^2\right)^{1/2} \tag{5.7}$$

where m is the number of perturbations taken to be the size of the vector of variables $\mathbf{x}$. In our case we look at Equation (5.7) for the calculated binding energy, E^{th}, for a given nucleus when the optimal occupations (n^*, z^*) are perturbed on the order of 10^{-10} [Moré and Wild, 2011].

In this way we see the computational complexity present in the minimization: for each of the N_{pts} terms of Eqn. (5.1) we must perform a lower level minimization of the functional to determine optimal occupation numbers, which are highly coupled to the coefficients being determined in the upper minimization of χ^2. To reduce the wall time (actual elapsed time) of each χ^2 evaluation, we note that these minimizations can be done in parallel using as many as N_{pts} processors. We provide details of the χ^2 minimization in Section 5.3.1.

5.3 Upper-level: unconstrained optimiztaion

An unconstrained minimization is used to determine the 17 fit coefficients c, which we have termed the upper-level minimization. The objective function of the unconstrained minimization of the sum of squared residuals, Equation (5.1). Equation (5.1) is a special case of the nonlinear least-squares function [Kortelainen et al., 2010b]:

$$f(\mathbf{x}) = \frac{1}{2}\sum_{i=1}^{N_{\text{pts}}} F_i(\mathbf{x})^2 = \frac{1}{2}\|\mathbf{F}(\mathbf{x})\|^2 \tag{5.8}$$

where $\mathbf{x}$ is the vector of variables to be minimized and the function $\mathbf{F} : \mathbb{R}^{N_x} \to \mathbb{R}^{N_{pts}}$. Here N_x is the dimension of the vector of variables $\mathbf{x}$. Optimization of objective functions like Equation (5.8) is performed by first utilizing Taylor's theorem to

approximate the objective function as a quadratic function [Powell, 2003, Kortelainen et al., 2010b]:

$$\begin{aligned} f(\mathbf{x}+\mathbf{d}) &\approx f(\mathbf{x}) + \mathbf{d}^T J(\mathbf{x})^T F(\mathbf{x}) \\ &+ \frac{1}{2}\mathbf{d}^T \left(J(\mathbf{x})^T J(\mathbf{x}) + \sum_{i=1}^{N_x} F_i(\mathbf{x}) \nabla^2 F_i(\mathbf{x}) \right) \mathbf{d} \end{aligned} \tag{5.9}$$

For fixed n and z, the derivatives $\nabla_c E_i^{\text{th}}(c; n, z)$ in Equation (5.1) are known and continuous, except when $c = -A^{1/3}$ for some nucleus. However, the form of the nonlinear lower level minimization in Eqn. (5.5) does not satisfy standard regularity conditions that would ensure existence and continuity of the derivatives $\frac{\partial n^*(c)}{\partial c_j}$ and $\frac{\partial z^*(c)}{\partial c_j}$ (see e.g., [Robinson, 1980]). Thus, unavailability of the residual derivatives in our case comes from the dependence of the optimal occupation numbers (n^*, z^*) on the coefficients c. Therefore, in order to optimize Equation (5.1) we will need a derivative-free method.

Direct search algorithms, such as Nelder-Mead [Kolda et al., 2003], or heuristic models such as genetic algorithms [Goldberg, 1989] are popular derivative-free methods. However, authors of the method used in this work [Moré and Wild, 2009] found that a smooth model-based method accounting for the problem structure yielded better coefficients in fewer simulations than optimization algorithms that can explicitly treat the nonsmoothness. A similar result was found for many of the piecewise smooth problems in Reference. [Moré and Wild, 2009] and the model-based method demonstrated great success in the least-squares optimization of Reference [Kortelainen et al., 2010b].

The derivative-free method used here starts by constructing a quadratic model for each component of the objective function, Equation (5.8) [Powell, 2003, Powell, 2004, Kortelainen et al., 2010b]

$$q_i(\mathbf{x}+\mathbf{d}) = F_i(\mathbf{x}) + \mathbf{d}^T\mathbf{g}_i + \frac{1}{2}\mathbf{d}^T\mathbf{H}_i\mathbf{d} \tag{5.10}$$

where the vector $\mathbf{g}_i \in \mathbb{R}^{N_x}$ and symmetric matrix $\mathbf{H}_i \in \mathbb{R}^{N_x \times N_x}$ approximate the unknown Jacobian and Hessian of Equation (5.9), respectively. These model parameters are determined by requiring that the model q_i is identically the true function F_i on a set $\mathcal{X}$ of $\mathbf{x}$ values. That is, $\mathbf{g}_i$ and $\mathbf{H}_i$ are determined through quadratic interpolation and are the solutions to

$$\min_{\mathbf{g}_i, \mathbf{H_i}} \{\|\mathbf{H}_i\|_F : q_i(\mathbf{x}_k) = F_i(\mathbf{x}_k)\ \forall \mathbf{x}_k \in \mathcal{X}\} \tag{5.11}$$

where $\|\ \|_F$ is the Frobenius norm. The set $\mathcal{X}$ contains $N_x + 1$ to $(N_x + 1)(N_x + 2)/2$ interpolation points [Wild, 2008, Conn et al., 1933]. Of course the model cannot be expected to remain valid far from points in the set $\mathcal{X}$ and so we employ a region of trust. The model is trusted within some trust region radius $\Delta > 0$ of a base point $\hat{\mathbf{x}}$, and we define a spherical neighbourhood $\mathcal{N} = \{\mathbf{x} \in \mathbb{R}^{N_x} : \|\mathbf{x} - \hat{\mathbf{x}}\| \leq \Delta\}$ within which the model Equation (5.10) is trusted.

Within $\mathcal{N}$ we can then generate a model for the second order expansion Equation (5.9)

$$\begin{aligned} m(\hat{\mathbf{x}}+\mathbf{d}) &= f(\hat{\mathbf{x}}) + \mathbf{d}^T \sum_{i=1}^{N_x} F_i(\hat{\mathbf{x}})\mathbf{g}_i \\ &+ \frac{1}{2}\mathbf{d}^T \sum_{i=1}^{N_x} \left(\mathbf{g}_i\mathbf{g}_i^T + F_i(\hat{\mathbf{x}})\mathbf{H}_i\right)\mathbf{d} \end{aligned} \tag{5.12}$$

We are now solving the trust region subproblem $\min_{\mathbf{d}}\{m(\hat{\mathbf{x}}+\mathbf{d}) : \hat{\mathbf{x}}+\mathbf{d} \in \mathcal{N}\}$ which is a quadratic with known derivatives. Therefore, minimizations of the model $m(\hat{\mathbf{x}}+\mathbf{d})$ at each iteration are far simpler than a direct minimization of the objective function Equation (5.8), especially in cases where calls to the object function are

computationally expensive. Minimizations of the quadratic model are performed using a Newtonian method for identifying where the derivatives of the model vanish.

5.3.1 Upper-level specifics: POUNDerS

The POUNDerS (Practical Optimization Using No Derivatives for sums of Squares) algorithm was developed for nonlinear least-squares problems where the derivatives of the residuals are unavailable [Ng et al., 2011] and employs the quadratic model-based method described above. A summary of the algorithm in the context of DFT can be found in Reference [Kortelainen et al., 2010b].

To minimize Equation (5.1), the POUNDerS used in [Kortelainen et al., 2010b] was modified to account for known partial derivatives with respect to some of the coefficients. The optimal occupations $(n^*(c), z^*(c))$ are independent of the three coefficients (c_c, c_P, c_1) because the corresponding terms in the functional Equation (4.41) do not involve n, z. Hence we can algebraically compute the (continuous) derivatives

$$\frac{\partial E_i^{\text{th}}}{\partial c_j}, \frac{\partial^2 E_i^{\text{th}}}{\partial c_j \partial c_k}, \qquad j,k \in \{c, P, 1\}. \tag{5.13}$$

The unavailability of derivatives makes optimization significantly more challenging. Over the course of the optimization, POUNDerS effectively builds up coarse approximations to first- and second-order derivatives of the residuals by interpolating the residuals at previously evaluated coefficient values. Knowing the residual derivatives of three of the 17 coefficients effectively lowers the dimension of the difficult derivative-free optimization problem, resulting in fewer evaluations of χ^2.

To guard against the effects of multiple local χ^2 minima and discontinuities of the computed energies, we found that a sufficient strategy was periodic restarting of POUNDerS in neighborhoods of mild size. This allows the local algorithm to occasionally look beyond the smaller neighborhood it has focused on. While it

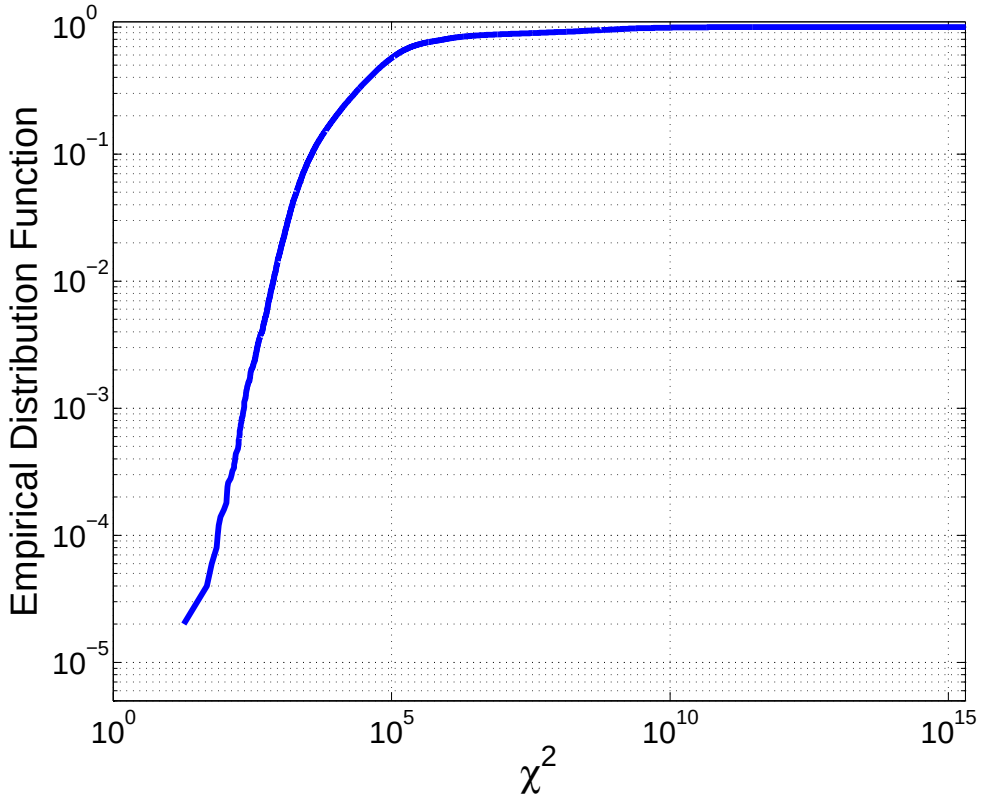

Figure 5.3: $\log - \log$ empirical cumulative distribution function showing the probability of randomly finding a value below the given χ^2 value in the hypercube $[-1, 1]^{17}$ [Bertolli et al., 2011].

is impossible to guarantee that χ^2 has been globally minimized, the local solution reported in the next section is significantly better than the χ^2 values found for other coefficients. Based on $50,000$ c values uniformly drawn from the hypercube $[-1,1]^{17}$, Figure 5.3 shows that roughly 0.01% of c have $\chi^2 \leq 10^2$ and roughly 50% have $\chi^2 \geq 10^5$. This shows that by taking into account the structure of χ^2 and the availability of some derivatives, with POUNDerS we were able to find a proverbial "needle in a haystack" with $\chi \approx 1$. Furthermore, we demonstrate the performance of POUNDerS by comparing it to another derivative-free quadratic-model minimizer NEWUOA [Powell, 2007]. Figure 5.4 compares the number of functional calls by both routines in minimizing the χ^2 for the mass formula version of our functional (that is, the lower-level minimization is not run and occupations are kept at the naive level-filling). POUNDerS not only arrives at a lower minimum χ value, but does so in two orders of magnitude fewer functional calls.

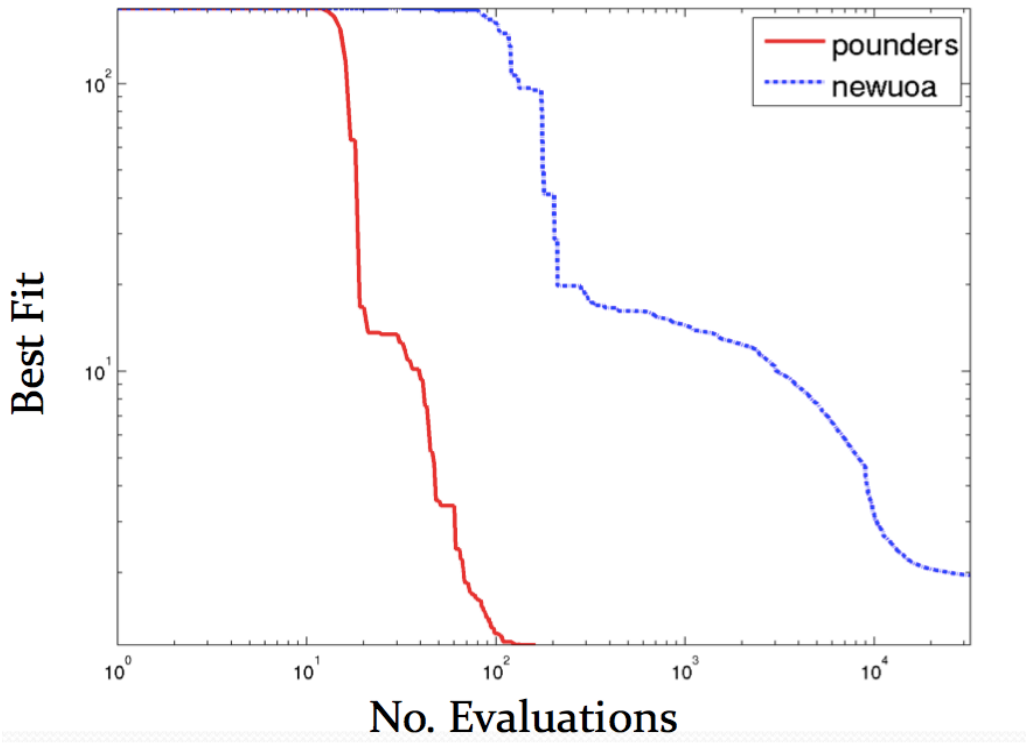

Figure 5.4: log – log comparing minimum χ value vs. functional calls of POUNDerS and NEWUOA for the χ^2 of our functional as a mass mass formula with naive level-filling occupations [Wild, 2011].

Chapter 6

Calculation of nuclear charge radii

We now turn our attention to another bulk nuclear property: the charge radius. Nuclear radii are of interest for a variety of reasons. As a fundamental property, they contribute to our understanding of nuclear structure in their ability to shed light on nuclear potentials and wavefunctions, and thus reaction cross-sections [Alkhazov et al., 2011]. Furthermore, because of the precision available in experimental data radii provide a critical test of the nuclear models available [Papadimitriou et al., 2011].

Elton was the first to calculate the effect of the radius on elastic scattering [Elton, 1950]. He demonstrated that the differential cross-sections for scattering high-energy electrons off of point-like and radially extended nuclei were not equal for all nuclei [Elton, 1950]. The radial dependency for inelastic scattering cross-sections can also be shown [Alkhazov et al., 2011]:

$$\sigma_{\mathrm{NA}} \propto r_{\mathrm{A}}^2 \tag{6.1}$$

$$\sigma_{\mathrm{AB}} \propto (r_{\mathrm{A}}^{1/3} + r_{\mathrm{B}}^{1/3})^2 \tag{6.2}$$

where σ_{NA} is the cross-section for inelastic scattering of a nucleon on some nucleus A with radius r_{A}. Similarly, σ_{AB} is the inelastic cross-section for two nuclei A and

B with radii r_A and r_B, respectively [Alkhazov et al., 2011]. It is clear that nuclear radii are crucial input to reaction calculations [Pain, 2011].

To provide theoretical input to experimentally unknown radii for cross-section calculations there are similar approaches as with masses. From an *ab initio* perspective successful calculations have been made in the framework of Green function Monte Carlo [Pieper, 2008] and no-core shell-model [Caurier and Navrátil, 2006] for light nuclei (as with masses, see Section 1.1). In DFT the charge radius r of a nucleus is computed from the density $\rho(\mathbf{r})$ as

$$\langle r^2 \rangle = \frac{1}{Z} \int d\mathbf{r}^3 \ \mathbf{r}^2 \rho_c(\mathbf{r}). \tag{6.3}$$

where ρ_c is the charge (proton) density. Our development of a functional in the DFT framework, however, requires a model to relate orbital occupation numbers to the nuclear radius. In constructing the functional we employed a harmonic oscillator basis for the shell-model and the scaling arguments. Consequently, we also employ it for the computation of $\langle r^2 \rangle$, as it provides the needed connection to occupations. The expectation value of the radius squared in the harmonic oscillator shell with principal quantum number ν and angular momentum λ is

$$\langle \nu\lambda | r^2 | \nu\lambda \rangle = \ell^2 (2\nu + \lambda + 3/2). \tag{6.4}$$

Here, ℓ is the oscillator length and is set to $\sqrt{492.5 A^{1/3}}$ fm. We use $p = 2\nu + \lambda$ and thus find for the expectation value of the charge radius squared

$$\langle r^2 \rangle = \frac{\ell^2}{Z} \sum_p z_p (p + 3/2). \tag{6.5}$$

In computing charge radii, we must account for the finite size of the nucleons [Friar et al., 1997],

$$\langle r_{ch}^2 \rangle = \langle r_p^2 \rangle + \langle r_{ch,p}^2 \rangle + \frac{N}{Z} \langle r_{ch,n}^2 \rangle. \tag{6.6}$$

Here, the proton and neutron charge radii are $\sqrt{\langle r^2_{ch,p}\rangle} = 0.877$ fm, $\langle r^2_{ch,n}\rangle = -0.1161$ fm^2, respectively.

Following the prescription in Reference [Duflo, 1994] we model in terms of the nuclear volume:

$$\mathcal{V} = v_1 + v_2 r^3 + v_3 \frac{N-Z}{r} + v_4 \frac{(N-Z)^2}{r^3} \tag{6.7}$$

$$r_{\text{fit}}(v;z) = v_5 \mathcal{V}^{1/3} + v_6, \tag{6.8}$$

where $r = \sqrt{\langle r^3_{ch}\rangle}$, and is in units of fm. We perform a simple χ^2 fit of the radii to determine the coefficients $v \equiv (v_1, \ldots, v_6)$ in Eqs. (6.7) and (6.8), whereby we minimize

$$\chi^2_r(v) = \frac{1}{N_{\text{pts}}} \sum_{i=1}^{N_{\text{pts}}} \left(r_{\text{fit},i}(v;z) - r_i^{\text{exp}}\right)^2 . \tag{6.9}$$

This formulation is motivated by the phenomenological work of Myers and Schmidt [Myers and Schmidt, 1983], who express the nuclear radius as

$$r = r_0 A^{1/3}(1 + \bar{\epsilon}) \tag{6.10}$$

where $\bar{\epsilon}$ contains terms related to nuclear diffuseness, Coulomb redistribution and compressibility. Utilizing the nuclear volume, rather than the radius directly, allows us to expand the expressions of Reference [Myers and Schmidt, 1983] in the conveniently parameterized way of Equation (6.8)

Chapter 7

Results

In this chapter we present the results of our research in mass table calculations. We begin in Section 7.1 by showing the performance of our functional Equation (4.41) in calculating the binding energies of nuclei across the nuclear chart. In Section 7.1.1 we highlight the extrapolation properties of the functional in predicting binding energies of nuclei not included in the parameter fit. Following in Sects. 7.2 and 7.2.1 we show the performance and extrapolation properties of the model for nuclear radii based on our functional. Sects. 7.1.2 and 7.2.2 give details on the sensitivity analyses for energy and radii calculations, respectively.

7.1 Binding energies

In collaboration with Stefan Wild, our functional was fit to a set of 2,049 nuclei from the 2003 atomic data evaluation [Audi et al., 2003] whose uncertainty in the binding energy is below 200 keV. The resulting fit produces a least-squares error of $\chi = 1.31$ MeV, and the fit coefficients in units of MeV are given in Table 7.1

Our root-mean-square deviation is competitive with current Skryme interaction-based functionals [Kortelainen et al., 2010b]. For comparison we mention the UNEDF functionals UNEDFnb (12 parameters) and UNEDF0 (10 parameters) of Reference [Kortelainen et al., 2010b] have a least-squares deviation of $\chi = 0.97$ MeV

Table 7.1: The 17 c parameters as fit to the 2,049 nuclei from the 2003 atomic data evaluation with uncertainty in binding energy below 200 keV [Audi et al., 2003].

Parameter	final value
c_c	-0.619948
c_P	11.170908
c_s	0.891816
c_{as}	7.434098
c_{ss}	0.397623
c_2	23.174559
c_3	0.233346
c_4	0.493533
c_5	-10.678202
c_6	-0.353447
c_1	-7.672829
$\tilde{c}_s$	-0.429029
c_8	7.333364
c_7	0.112605
c_9	0.382828
c_{10}	-4.107110
c_{11}	1.383515

and $\chi = 1.46$ MeV, respectively, when fit to a set of 72 even-even nuclei. When applied to 520 even-even nuclei of a mass table, the fitted functionals yield least-squares deviations of $\chi = 1.45$ MeV and $\chi = 1.61$ MeV, respectively. The refit [Bertsch et al., 2005] of the Skyrme functional Sly4 to even-even nuclei exhibits a root-mean-square deviation of about $\chi = 1.7$ MeV. While the current least-squares deviation is greater than the best achieved by a mean-field based functional [Goriely et al., 2009] ($\chi = 0.58$ MeV with 14 parameters), we provide a novel mass functional that uses the orbital occupations of nucleons as the relevant degrees of freedom.

Figure 7.1 shows a nuclear chart of the fit nuclei with colours representing the difference $E^{\text{th}} - E^{\text{exp}}$ between the energies computed from the functional and the experimental data for the 2,049 nuclei employed in the fit. The differences are a smooth function of the neutron and proton numbers. Figures 7.2 and 7.3 display the energy differences as functions of N and Z. There are still systematic deviations

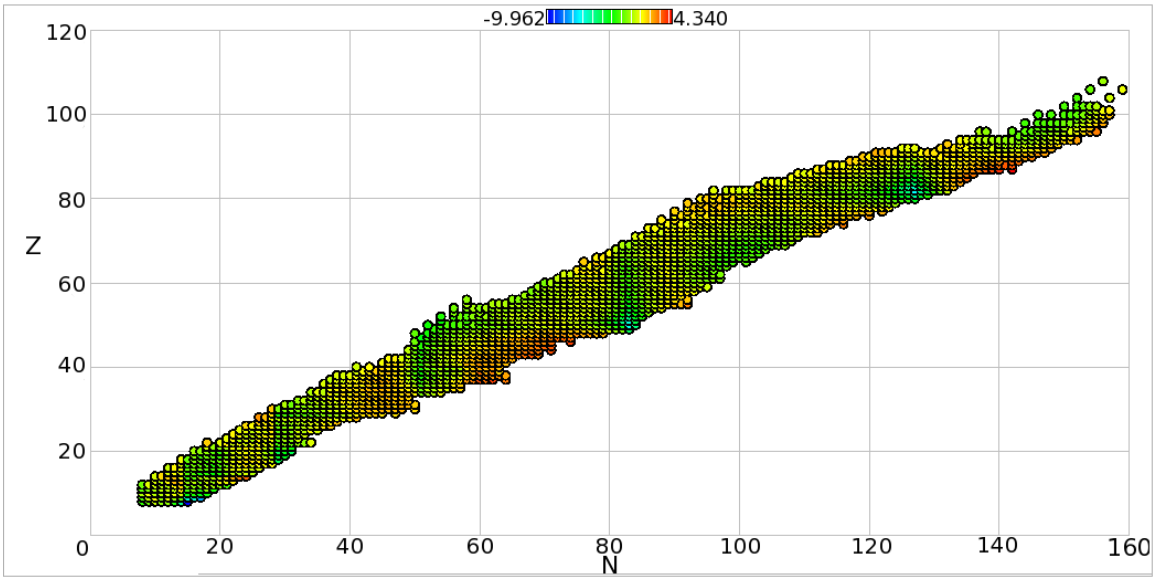

Figure 7.1: Chart of 2,049 well-measured nuclei from the 2003 atomic data evaluation in Reference [Audi et al., 2003], color showing the difference $E^{\text{th}} - E^{\text{exp}}$ between the calculated energy and experimental energy. The energy difference exhibits a smooth behavior across the whole chart. Some overbinding is seen in the area of very heavy nuclei and tin isotopes. Color ranges from -9.962 MeV (blue) to 4.340 MeV (red) [Bertolli et al., 2011].

associated with shell oscillations. Recall that the shell closures are input to our functional through the choice of the single-particle degrees of freedom. Thus, the shell oscillations reflect smaller deficiencies associated with the description of nuclear deformation. This can be seen in comparison to the oscillations in a pure liquid drop model such as the Weizsäcker semi-empirical mass formula, Equation (1.2), in Fig. 7.4. The Weizsäcker semi-empirical mass formula exhibits much larger oscillations due to absence of any shell structure in the formula.

7.1.1 Extrapolation properties of functional

The ability of the functional to extrapolate beyond those nuclei included in the fit is of utmost importance. It is the extrapolation behaviour that demonstrates the predictive power of the functional. As highlighted in Chapter 1, highly predictive models are necessary to provide theoretical descriptions to those nuclei which remain inaccessible

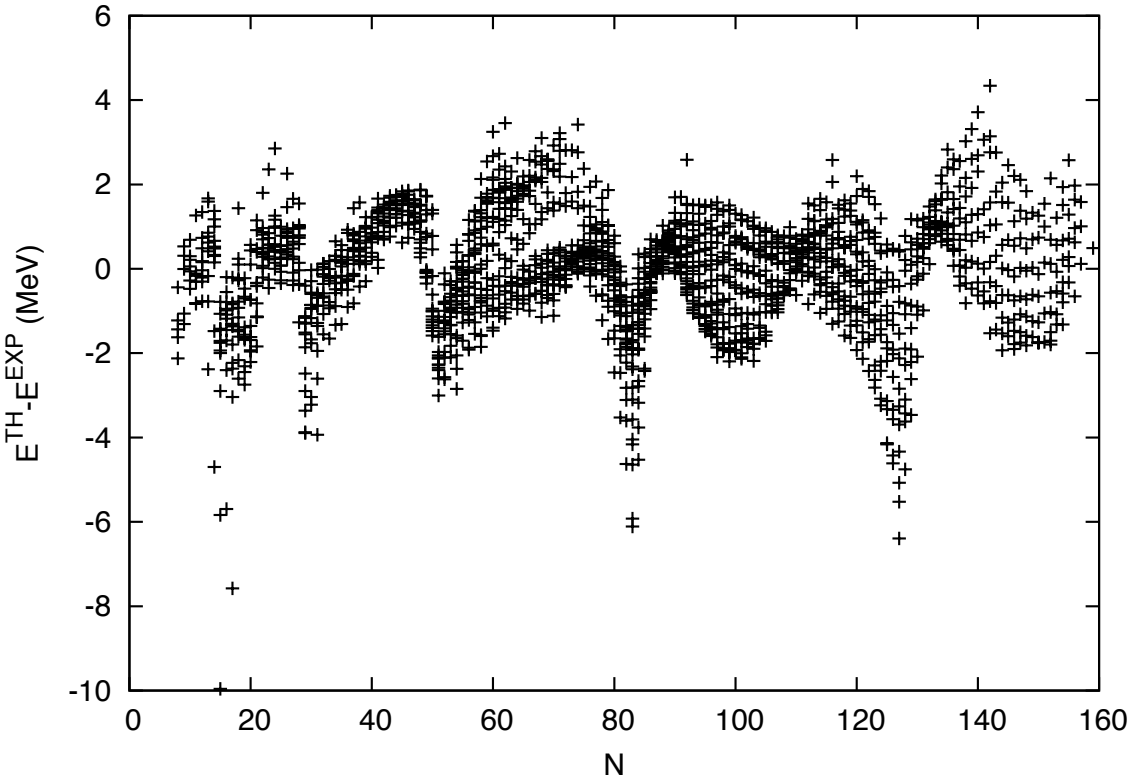

Figure 7.2: Energy difference $E^{\text{th}} - E^{\text{exp}}$ as a function of N for the same nuclei as in Fig. 7.1. The oscillations around zero indicate the nuclear shell structure [Bertolli et al., 2011].

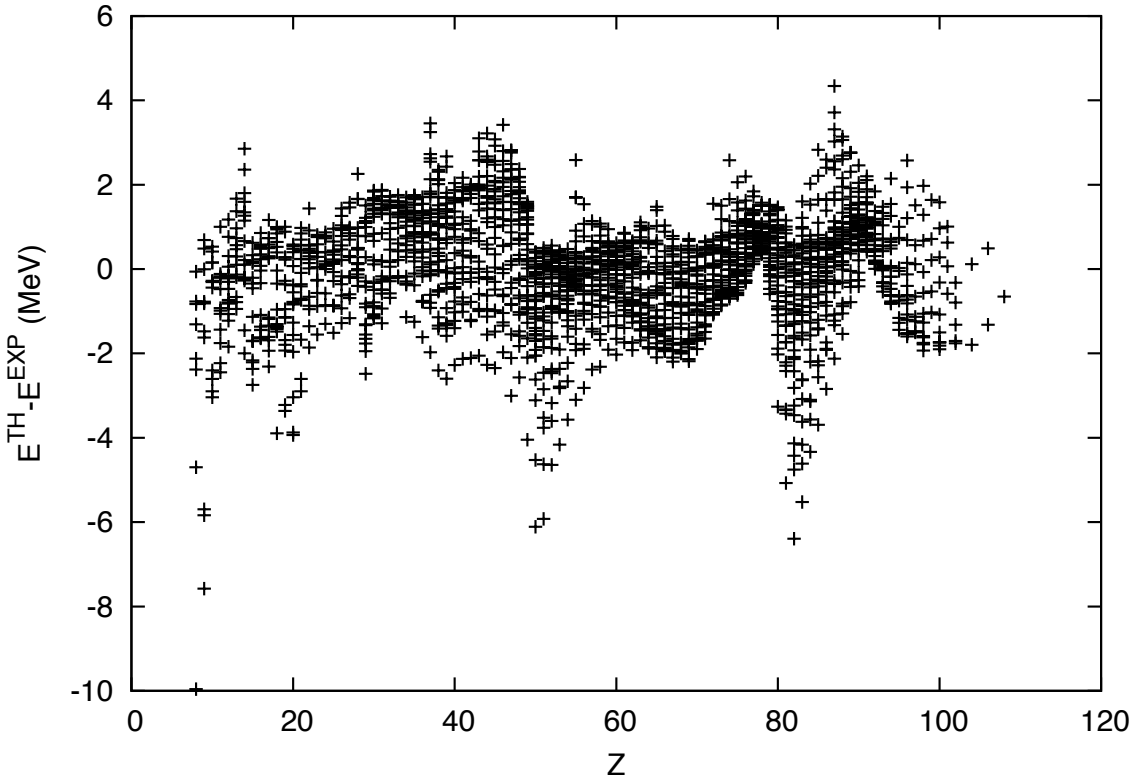

Figure 7.3: Energy difference $E^{\text{th}} - E^{\text{exp}}$ as a function of Z for the same nuclei as in Fig. 7.1. The oscillations around zero indicate the nuclear shell structure [Bertolli et al., 2011].

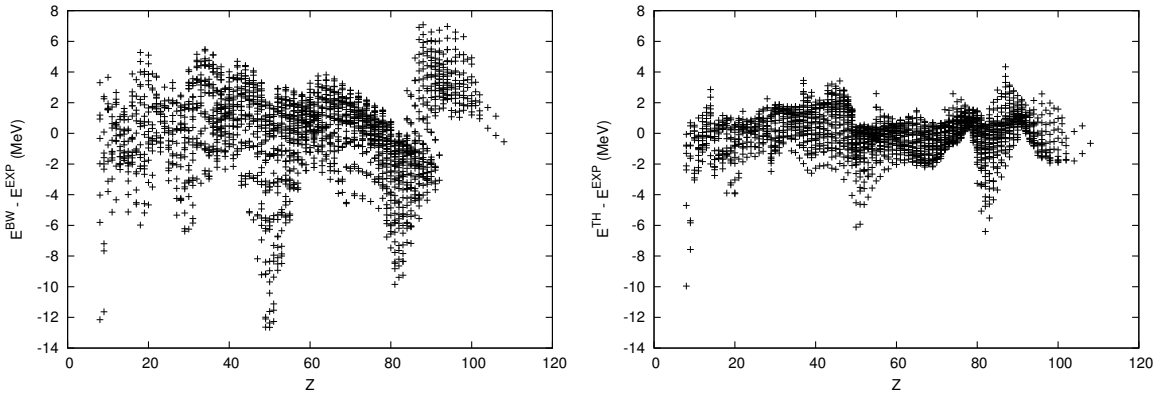

(a) Semi-empirical mass formula, Equation (1.2) **(b)** Functional, Equation (4.41)

Figure 7.4: Energy difference $E^{\text{th}} - E^{\text{exp}}$ as a function of Z for the Weizsäcker semi-empirical mass formula and our functional. Note the decrease in the level of oscillations around magic numbers in our functional as compared to a pure liquid drop model.

to experiment, yet play a crucial role in various astrophysical phenomena. As we will demonstrate in this section our functional is stable with respect to extrapolation, and so retains predictive power.

To test the extrapolation properties of our functional, we fit the functional to a smaller set of 1,837 nuclei taken from the 1993 atomic evaluation data set [Audi and Wapstra, 1993]. For this data set, the root-mean-square error is $\chi = 1.38$ MeV. This least-squares deviation is close to that from a fit to the larger set of 2,049 nuclei, and the deviations are again smooth across the nuclear chart. Employing the functional from the fit to the 1993 data set, we compute the ground-state energies of all 2,049 nuclei and find a root-mean-square deviation of $\chi = 1.34$ MeV. Thus, the functional has good extrapolation properties.

To further test the functional's predictive power, we use the coefficients c from the fit to the 1993 data set ($\chi = 1.38$ MeV) and the coefficients from the fit to the 2,049 nuclei ($\chi = 1.31$ MeV) and compute the binding energies of 2,149 nuclei in the complete 2003 nuclear data set. The functional fit to the 1993 data set yields $\chi = 1.40$ MeV, and the functional from a fit to the 2,049 nuclei yields $\chi = 1.38$ MeV. These values are close to $\chi = 1.37$ MeV that results from a fit of the functional to the full 2003 data set. Thus, the extrapolation properties of the functional are quite good. Table 7.2 summarizes the details of how our functional extrapolates from data set to data set. Figure 7.5 shows the differences between theoretical and experimental ground-state energies across the chart of nuclei employed for the extrapolation.

7.1.2 Sensitivity analysis of functional

We now discuss the quality of fit for our functional. To quantify this we present a sensitivity analysis in terms of statistics on the fit parameters c. This analysis provides an understanding of our functional's sensitivity to changes in c.

Statistically, the least-squares fit of Equation (5.1) is a nonlinear regression of Equation (4.37). There exists some set of coefficients c^* that gives the true

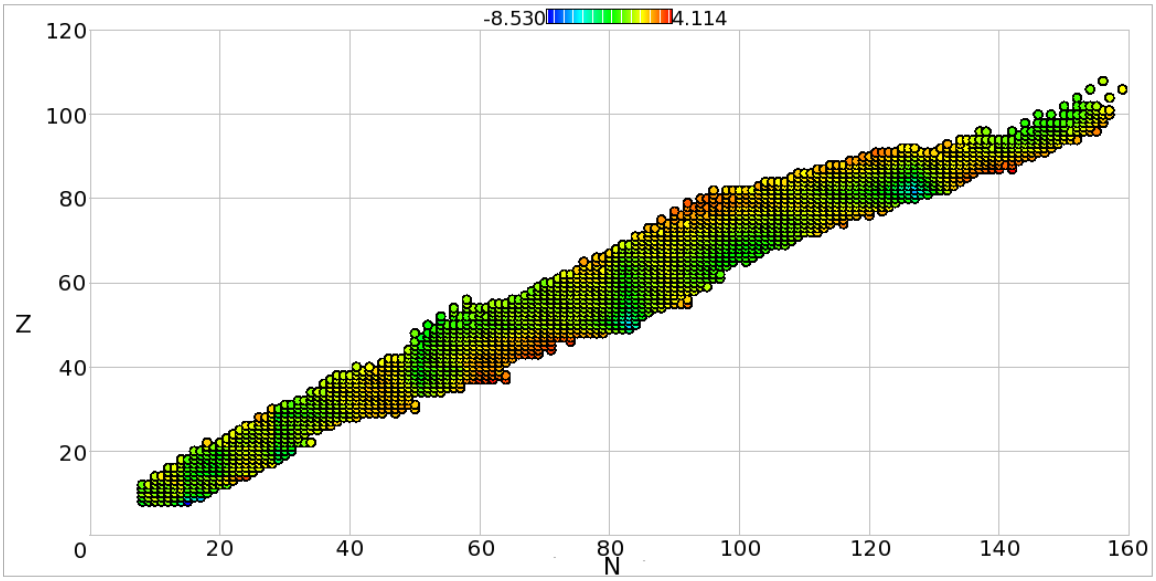

Figure 7.5: Energy difference $E^{\text{th}} - E^{\text{exp}}$ between theoretical and experimental results for the functional that is fit to the 1993 data set and applied to the subset B of well-measured nuclei of the 2003 data set. The deviations are smooth across the nuclear chart and consistent with Fig. 7.1. Color ranges from -8.530 MeV (blue) to 4.114 MeV (red) [Bertolli et al., 2011].

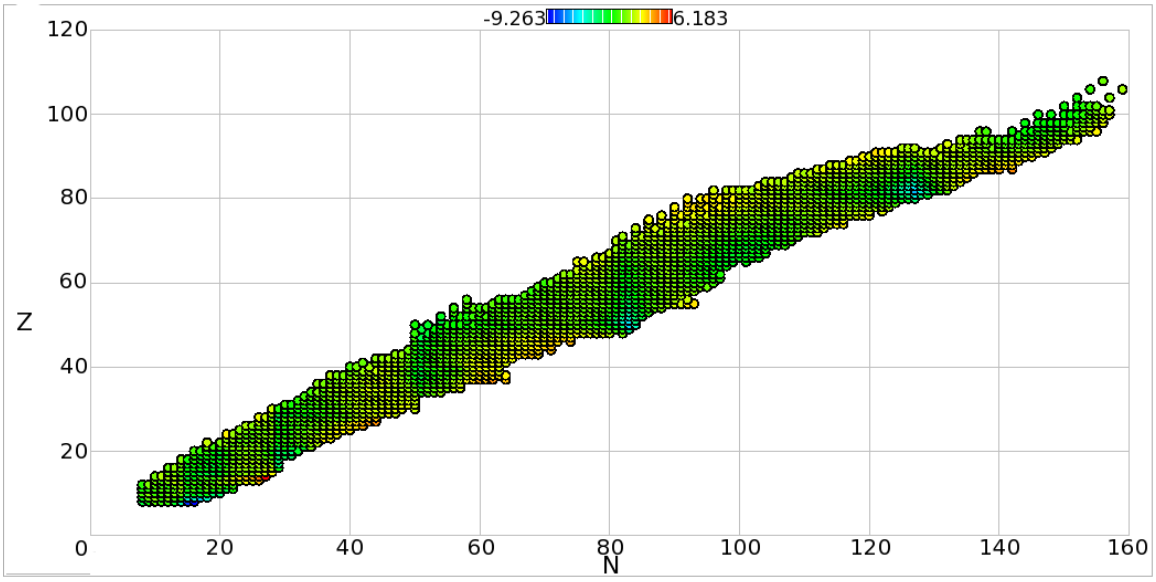

Figure 7.6: Energy difference $E^{\text{th}} - E^{\text{exp}}$ between theoretical and experimental results for the functional fit to the 1993 data set and applied to the 2003 data set. The deviations are smooth across the nuclear chart and consistent with Fig. 7.1. Color ranges from -9.263 MeV (blue) to 6.183 MeV (red) [Bertolli et al., 2011].

Table 7.2: Root-mean-square deviations of binding energies resulting from a global fit of the functional and from extrapolation to larger data sets. Data set A consists of all nuclei of the 1993 mass evaluation [Audi and Wapstra, 1993], data set C consists of all nuclei of the 2003 mass evaluation [Audi et al., 2003], and data set B is a subset of data set C consisting of well-measured nuclei whose uncertainty in the mass is below 200 keV. The number of nuclei in each data set is denoted by N_{pts}.

Data Set	N_{pts}	χ (MeV)		
			Extrapolation to	
		Fit	Data Set B	Data Set C
A	1837	1.38	1.34	1.40
B	2049	1.31	–	1.38
C	2149	1.37	–	–

minimum of the functional at the optimal occupations $(n^*(c^*), z^*(c^*))$. However, these coefficients c^* remain unknown due to model errors. We define the absolute theoretical error between our functional and the experimental data as

$$\varepsilon_i = F_i(c^*; n^*(c^*), z^*(c^*)) - E_i^{\text{exp}} \tag{7.1}$$

where i indicates the nucleus. Each error ε_i is assumed to be random with expectation $\langle \varepsilon_i \rangle = 0$. Furthermore, we assume all ε_i are independent and follow the same normal distribution [Kortelainen et al., 2010b]. In general, theoretical errors are not independent or normally distributed [Toivanen et al., 2008]. These errors prevent us from always obtaining c^* in a statistical setting. However, we can estimate the true parameter set c^* through the minimization in Section 5.3.1:

$$c = \arg\min\{\chi(c; n(c), z(c))\} \tag{7.2}$$

To quantify how well Equation (7.2) estimates c^* we consider the confidence intervals (CI) on the set c. The $1 - \alpha$ confidence interval $\Omega_j \subset \mathbb{R}$ is the region of c_j in which we expect c_j^* to be, with probability $P(c_j^* \in \Omega_j) = 1 - \alpha$ [Kortelainen et al., 2010b].

With our assumed normal distribution we can define the $1-\alpha$ CI half-width, w_j, as [Seber and Wild, 1989]:

$$\{w_j \in \mathbb{R} : \ |w_j - c_j| \leq \sqrt{\text{cov}(c)_{j,j}} t_{N_{\text{pts}}-N_x,1-\alpha/2}\} \tag{7.3}$$

where $t_{N_{\text{pts}}-N_x,1-\alpha/2}$ is the $1-\alpha/2$ quantile of the t-distribution [Montgomery and Taylor, 2003] with $N_{\text{pts}}-N_x$ degrees of freedom. Once again, $N_x = 17$ is the number of coefficients c and the covariance is computed as with Equation (4.64) in Section 4.3.1. A first-order approximation of the covariance matrix is given by Reference [Donaldson and Schnabel, 1987]:

$$\text{cov}(c) \approx \chi^2(c) \left(\sum_i^{N_x} \mathbf{g}_i \mathbf{g}_i^T \right)^{-1} \tag{7.4}$$

The parameters $\mathbf{g}_i$ are the same as in Equation (5.10) and come from calculating central differences on the points $\{c \pm \eta_j e_j\}_{j=1,\ldots,N_x}$. Here η_j is chosen to be small and e_j is the unit vector in the j^{th} direction. Using Equation (7.4) we can generate the 95% CI ($\alpha = 0.05$, $\eta_j \approx 10^{-5}$) half-width. That is, we can say the true parameters c^* have a 95% likelihood of existing in the range $c_j \pm w_j$. Table 7.3 details the confidence intervals on c. In Fig. 7.7 we see what fraction the interval half-widths for each of the 17 parameters c is of the final parameter as determined by the minimization in Section 5.3.1. That is, we plot w_j/c_j. We note most of the half-widths are within 20% of the fitted parameter. Only the parameter c_6, (D_{4B}), and c_{11}, (L_{val}), have half-widths on the order of 80% of their value. This comes as no surprise as both contributions may appear as higher-order corrections to other terms present. This lack of independence not only creates a broader minimum on the energy surface [Bertsch et al., 2005] but is outside our base assumption of independence for Equation (7.1).

We now take a look also at the importance of the multi-level minimization. The computation of ground-state energies via the functional (4.37) with coupled minimizations differs considerably from the uncoupled case. If the proton and neutron

Table 7.3: 95% confidence intervals (CI) and CI half-widths for each of the 17 c parameters as given in Table 7.1.

Parameter	final value	CI	half-width
c_c	-0.619948	$[-0.622018, -0.617881]$	0.002068
c_P	11.170908	$[10.362970, 11.979030]$	0.808030
c_s	0.891816	$[0.885954, 0.897685]$	0.005866
c_{as}	7.434098	$[7.356143, 7.5120568]$	0.077957
c_{ss}	0.397623	$[0.347772, 0.447467]$	0.049847
c_2	23.174559	$[23.063160, 23.286840]$	0.111840
c_3	0.233346	$[0.183108, 0.283592]$	0.050242
c_4	0.493533	$[0.393933, 0.593127]$	0.099597
c_5	-10.678202	$[-10.968490, -10.387510]$	0.290490
c_6	-0.353447	$[-0.656520, -0.050380]$	0.303070
c_1	-7.672829	$[-7.834330, -7.511270]$	0.161530
$\tilde{c}_s$	-0.429029	$[-0.522123, -0.335937]$	0.093093
c_8	7.333364	$[6.996800, 7.670000]$	0.336600
c_7	0.112605	$[0.091259, 0.133961]$	0.021351
c_9	0.382828	$[0.318420, 0.447240]$	0.064410
c_{10}	-4.107110	$[-4.547340, -3.666860]$	0.440240
c_{11}	1.383515	$[0.339700, 2.427300]$	1.043800

occupations are kept fixed to the naive level filling, Eq. (4.37) becomes a mass formula. Performing a chi-square fit with this fixed filling yields coefficients c that can then be used when minimizing the functional with respect to occupations (that is, the lower-level minimization is done independently of the upper-level minimization). The resulting error, $\chi = 3.38$ MeV, is one order of magnitude larger than the residual error of the mass formula by Duflo and Zuker [Duflo and Zuker, 1995]. When including the lower-level optimization in the chi-square fit (and hence dealing with a multi-level optimization), we obtain the considerably reduced $\chi = 1.31$ MeV.

7.2 Charge radii

We now turn to the results for nuclear charge radii. We fit our six-parameter model (6.8) for the charge radii to the experimental data of 772 nuclei from

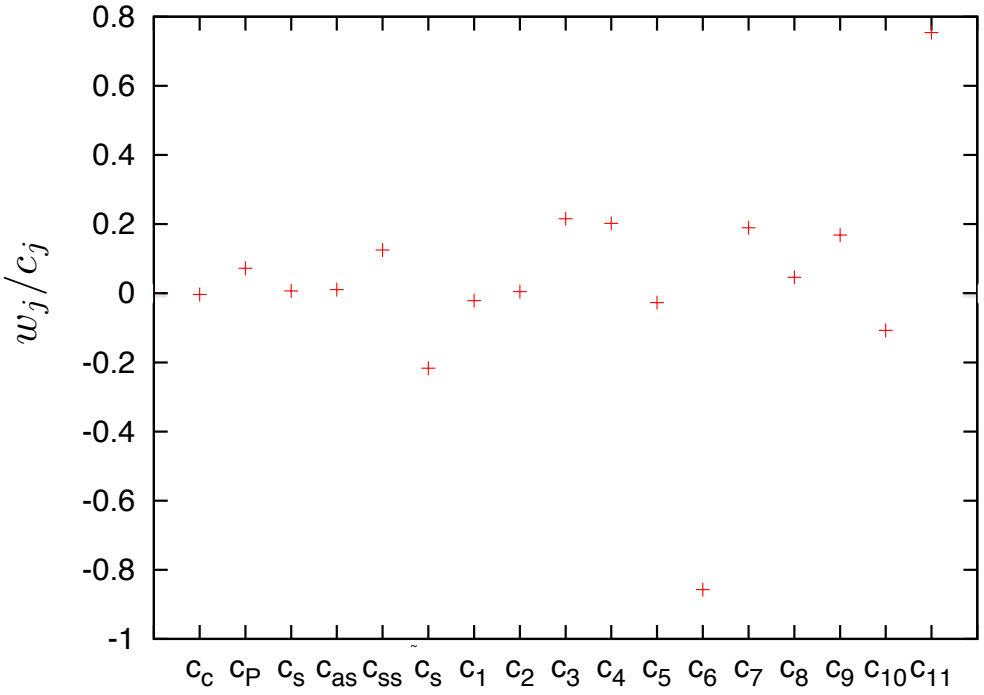

Figure 7.7: Graph of the confidence interval half-widths as fraction of parameter value, w_j/c_j. Most half-widths are within 20% of the parameter value, with the exception of c_6 and c_{11}.

Reference [Angeli, 2004] and obtain a least-squares deviation of $\chi_r = 0.047$ fm. The resulting fit coefficients (with units of fm) are

$$\begin{aligned} v_1 &= 11.004005, \\ v_2 &= 2.000870, \\ v_3 &= -3.248108, \\ v_4 &= -0.279495, \\ v_5 &= 0.775617, \\ v_6 &= -0.557746. \end{aligned}$$

Note that the data set contains both spherical and deformed nuclei. Figure 7.8 shows the difference between the calculated and experimental radii. For a comparison, note that Duflo and Zuker state a least-squares error of about $\chi_r \simeq 0.01$ fm for the charge radii of spherical nuclei [Duflo, 1994]. Radii from Skyrme functionals exhibit a root-mean-square deviation of about 0.025 fm [Stone and Reinhard, 2007]. Figure 7.9 shows the difference between computed and experimental charge radii as a function of neutron number. The outliers seen in Fig. 7.9 correspond to isotopic chain of Tb and the elements Rb, Sr and Zr with neutrons $N = 60 - 62$.

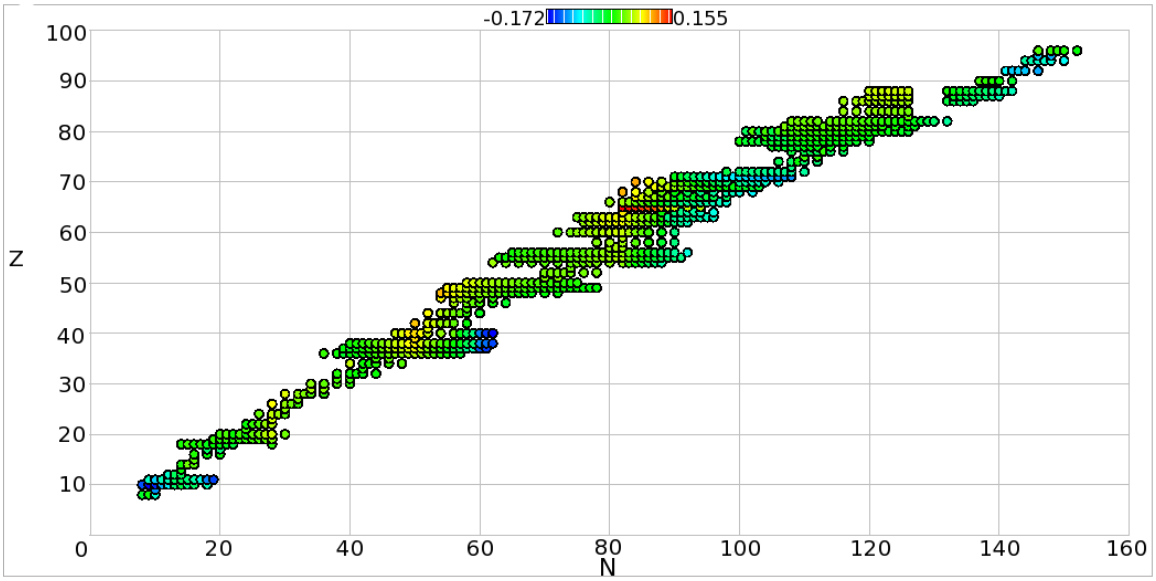

Figure 7.8: Difference between experimental and theoretical charge radii for the set of 772 nuclei from Reference [Angeli, 2004]. Color ranges from -0.172 fm (blue) to 0.155 fm (red) [Bertolli et al., 2011].

7.2.1 Extrapolation properties of model for radii

Let us also study the extrapolation properties of our mass model. We fit the model (6.8) to the charge radii on a subset of 494 nuclei (taken from Reference [Angeli, 2004]) chosen near the valley of stability. This yields a least-squares error of $\chi_r = 0.046$ fm. When using this model to compute the charge radii on the full

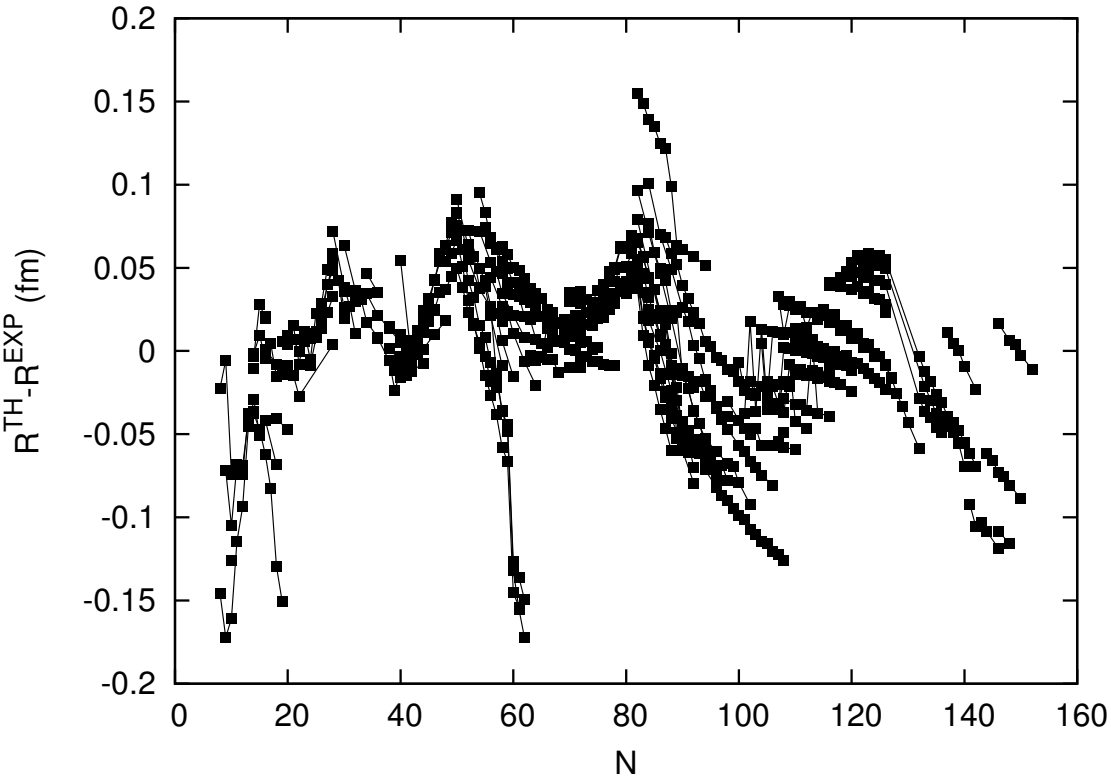

Figure 7.9: Chart of difference between calculated and experimental charge radii for 772 nuclei as a function of N. Lines connect isotopes and outliers correspond to isotopic chain of Tb and the elements Rb, Sr and Zr with neutron number $N = 60 - 62$. [Bertolli et al., 2011].

set of 772 charge radii, we find a slightly increased $\chi_r = 0.048$ fm, indicating that the extrapolation is successful.

7.2.2 Sensitivity analysis of model for radii

For each nucleus, the occupation numbers enter the computation of the charge radius. We thus need to understand how our model for the charge radius depends on the functional employed for the computation of binding energies, in other words, its dependence on the coefficients c. A sensitivity analysis of our fit to binding energies provides us with a confidence interval for each of the coefficients c. We take a randomly chosen sample of five sets of coefficients $\{c_1, \ldots, c_5\}$ within the confidence interval and recompute the structure (i.e., the occupation numbers) and the binding energies. The resulting least-squares deviations for binding energy range from $\chi = 1.34$ MeV to 1.78 MeV. Subsequently, we compute the charge radii for the nuclei of interest (without refitting the coefficients v of our model for the radii). If we refit the coefficients v of our mass model and adjust them to the change in the coefficients c of the energy functional, the least-squares error for the radii changes by at most 4%. Thus, we find the model for radii is relatively independent of the functional's fit coefficients c, as long as the χ value for binding energies is reasonable.

Chapter 8

Conclusions

In this work we developed and explored an energy functional for nuclear masses in a shell-model basis. In our functional, Equation (4.41), the orbital occupations of 15 oscillator shells in protons and neutrons, (n, z), are the relevant degrees of freedom and 17 numerical parameters, c, are determined via a χ^2 fit to experimental data as detailed in Chapter 5. We emphasize that Equation (4.41) is a functional in that the occupations (n, z) are determined through a constrained minimization of the functional (see Section 5.2.1), in accordance with the Hohenberg-Kohn theorem Equation (2.1). This differs from shell-model based mass formulae, such as that given by Reference [Duflo and Zuker, 1995], where the orbital occupations are set by hand.

In the course of developing our functional we highlight the new method proposed for the selection of terms in Sect. 4.3. This method is based on constraining functional terms only to those which provide an independent search direction and are perturbatively small. These two conditions are met by first checking the correlation between a newly proposed term and those terms already present. Second, those terms which are found to be independent are accepted if their addition causes only small changes in the functional's optimal occupation numbers (i.e. the term is perturbative). This method allows us to systematically determine which new terms should be included in the functional.

The final form of the functional, given by Eq. (4.37) along with Eq. (4.41), has 17 parameters c fit to experimental binding energies. The details of solving the numerical challenges of this fit are given in Chapter 5. The least-squares fit of our functional gives an average deviation of $\chi = 1.31$ MeV, which is competitive with current Skyrme interaction-based functionals [Bertsch et al., 2005, Kortelainen et al., 2010b]. Furthermore, the functional presented here exhibits good extrapolation properties (see Sect. 7.1).

As our functional uses orbital occupations as its degrees of freedom, these occupations for a ground-state nucleus are output along with binding energies. Working in a harmonic oscillator basis we are able to develop a model that connects the orbital occupations of protons to the nuclear charge radius (Chapter 6). This model produces a least-squares deviation of $\chi_r = 0.047$ fm from experiment, with good extrapolation away from the line of stability (Sect. 7.2).

8.1 Future directions

The functional developed here presents a novel approach with orbital occupations as the degrees of freedom. Previous implementations of shell-model occupations in mass models as only been done through mass formulae (for example, Reference [Duflo and Zuker, 1995]). While the functional exhibits a promising χ value and good extrapolation, there remains meaningful areas yet to be explored. As the final section of this thesis we take some time to expound upon some possible future directions for this research. We divide the discussion into short-term and long-term objectives.

In the short-term there is further characterization to be done in order to better understand the current form of the functional. The characterization we suggest takes two forms: an analysis of the parameters c, and an investigation of the functional's ability to produce further data. In regards to an analysis of the fit parameters c, we refer specifically to the work in Reference [Kortelainen et al., 2010a]. As there is a concern for using only those terms necessary in a given mass model, we would like to

order those parameters of our functional in a hierarchy of contributions. The naive dimensional analysis of quantum chromodynamics [Friar, 1997] has been adapted for energy functionals [Friar et al., 1996, Rusnak and Furnstahl, 1997, Furnstahl, 2002, Burvenich et al., 2002] as an approach to constructing such a hierarchy. This approach employs a scaling of the parameters to "natural units" of order unity in a scheme that orders by powers of gradients and a density expansion [Kortelainen et al., 2010a]. Such an analysis of our c coefficients provides not only a hierarchy of importance for the functional terms, but a means by which we can directly compare with parameter values of other mass functionals in use.

To further investigate the functional's abilities we consider looking at one- and two-particle separation energies. While a functional may have difficulty in reproducing exact binding energies, it may perform better in computations of relative binding energies [Kortelainen et al., 2010b]. Information on how well the functional reproduces separation energies will provide valuable insight on where further improvement is needed in our description of the nuclear chart. Additionally, we are interested in our functional's ability to answer a key question in nuclear structure: the location of the proton and neutron drip-lines. By calculating binding energies for nuclei beyond those present in experimental compilations we can find at what point the energy of a nucleus with A nucleons is great than that of a nucleus with $A+1$ nucleons. This indicates where the nuclei are no longer stable against particle emission. While the location of the drip-lines is unknown experimentally beyond $Z = 8$ for neutrons and $Z = 50$ for protons (and thus of great interest theoretically), we are able to compare our functional's performance against a robust model such as the FRDM [Möller et al., 1995].

Finally, we outline two long-term objectives for further research. The functional's current χ value is very encouraging for our method. However, a greater goal for this mass model is to cross below the 1 MeV threshold. Maintaining good extrapolation properties and obtaining a least-squares deviation of $\chi < 1$ MeV would make our functional highly competitive. While $\chi = 1.31$ MeV does not seem far off, we remark

that a reduction in the least-squares error of even 0.1 MeV is not trivially achieved (see Sect. 4.3.3 for an example of the hurdles). The above mentioned characterizations may provide some direction in modifications of the functional's current form, but we also propose the addition of new terms. Looking at Fig. 7.1 and similar we see that regions of deformation ($60 \leq N \leq 75,\ 35 \leq Z \leq 45$) are problematic. This is further indicated by the poorly described radii of the deformed nuclei Rb and Sr (Fig. 7.9). It is clear that a more detailed treatment of deformation is needed to improve our functional. Additionally, we employ only a very simplistic treatment of pairing (liquid drop model, Sect. 4.1.1, and seniority model-like, Sect. 4.2.1 Eq. 4.49). More detailed microscopic treatments of pairing have been employed elsewhere with success [Goriely et al., 2009, Kortelainen et al., 2010b], and we suggest further investigation on pairing contributions to this functional. The systematic approach of Sect. 4.3 will aid in this endeavor.

The last avenue of further research we suggest regards the application of our functional to other calculations. As outlined in Chaper 1, a primary motivation for mass model research is for accurate input of nuclear masses that are unavailable experimentally in r-process calculations. As our model is computationally cheap there is interest in implementing it in such astrophysical calculations. This would provide an excellent test of its possible contributions to nuclear structure. So while this work has resulted in insights regarding analytical systems [Bertolli and Papenbrock, 2008], functional development [Bertolli et al., 2011] and optimization of complex energy surfaces [Ng et al., 2011], much work remains to provide ever-better theoretical descriptions of nuclear structure.

Bibliography

Bibliography

[Aalseth et al., 2002] Aalseth, C., III, F. T. A., Barabash, A., Boehm, F., Brodzinski, R. L., Collar, J. I., Doe, P. J., Ejiri, H., Elliott, S. R., Fiorini, E., Gaitskell, R. J., and G. Gratta, e. a. (2002). *Mod. Phys. Lett. A*, 17:1475. 2

[Alkhazov et al., 2011] Alkhazov, G. D., Novikov, I. S., and Shabelski, Y. (2011). *Int. J. Mod. Phys. E*, 20(3):583. 71, 72

[Angeli, 2004] Angeli, I. (2004). *Atomic Data and Nuclear Data Tables*, 87:2. xii, 84, 85

[Anguiano et al., 2001] Anguiano, M., Egido, J. L., and Robledo, L. M. (2001). *Nucl. Phys. A*, 696:467. 11

[Argaman and Makov, 2000] Argaman, N. and Makov, G. (2000). *American Journal of Physics*. 11

[Aston, 1920] Aston, F. W. (1920). *Nature*, 105:617. 1

[Aston, 1933] Aston, F. W. (1933). *Mass Spectra and Isotopes*. Edward Arnold, London. 34

[Audi and Wapstra, 1993] Audi, G. and Wapstra, A. H. (1993). *Nucl. Phys. A*, 565:1. viii, 79, 81

[Audi et al., 2003] Audi, G., Wapstra, A. H., and Thibault, C. (2003). *Nucl. Phys. A*, 729:337. viii, xi, 74, 75, 76, 81

[Beiner et al., 1975] Beiner, M., Flocard, H., Giai, N. V., and Quentin, P. (1975). *Nucl. Phys. A*, 283:29. 14

[Bender et al., 2003a] Bender, M., Heenen, P.-H., and Reinhard, P.-G. (2003a). *Rev. Mod. Phys.*, 75:121. 7, 9

[Bender et al., 2003b] Bender, M., Heenen, P. H., and Reinhard, P. G. (2003b). *Rev. Mod. Phys.*, 75:121. 15

[Bertolli and Papenbrock, 2008] Bertolli, M. and Papenbrock, T. (2008). *Phys. Rev. C*, 78:064310. ix, x, 4, 19, 22, 24, 25, 31, 45, 91

[Bertolli et al., 2011] Bertolli, M. G., Papenbrock, T., and Wild, S. (2011). *arXiv:1110.4305v1 [nucl-th]*. xi, xii, 4, 68, 76, 77, 78, 80, 85, 86, 91

[Bertsch et al., 2007] Bertsch, G. F., Dean, D. J., and Nazarewicz, W. (2007). *SciDAC Review*, (6):42. ix, 5, 7, 9, 10

[Bertsch et al., 2005] Bertsch, G. F., Sabbey, B., and Uusnakki, M. (2005). *Phys. Rev. C*, 71:054311. 8, 50, 75, 82, 89

[Bethe and Bacher, 1936] Bethe, H. and Bacher, R. (1936). *Rev. Mod. Phys.*, 8:82. 4

[Bhattacharyya and Furnstahl, 2005] Bhattacharyya, A. and Furnstahl, R. J. (2005). *Nucl. Phys. A*, 747:268. 11

[Bhattacharyya and Papenbrock, 2006] Bhattacharyya, A. and Papenbrock, T. (2006). *Phys. Rev. A*, 74:041602. 11

[Bohr and Mottelson, 1969] Bohr, A. and Mottelson, B. R. (1969). *Nuclear Structure*, volume 1. W. A. Benjamin, Inc. 40

[Brack et al., 1985] Brack, M., Guet, C., and Hakansson, H. B. (1985). *Phys. Rep.*, 123:275. 14

[Brown and Richter, 2006] Brown, B. and Richter, W. (2006). *Phys. Rev. C.*, 74(034315). 15

[Brueckner and Gammel, 1958] Brueckner, K. A. and Gammel, J. L. (1958). *Phys. Rev.*, 109:1023. 7

[Bulgac, 2007] Bulgac, A. (2007). *Phys. Rev. A*, 76:040502. 11

[Burvenich et al., 2002] Burvenich, T., Madland, D. G., Maruhn, J. A., and Reinhard, P. G. (2002). *Phys. Rev. C*, 65:044308. 90

[Carlson et al., 2003] Carlson, J., Chang, S.-Y., Pandharipande, V., and Schmidt, K. (2003). *Phys. Rev. Lett.*, 91:050401. 11

[Caurier et al., 1999] Caurier, E., Martinez-Pinedo, G., Nowacki, F., Poves, A., Retamosa, J., and Zuker, A. P. (1999). *Phys. Rev. C*, 59:2033. 15

[Caurier et al., 2005] Caurier, E., Martinez-Pinedo, G., Nowacki, F., Poves, A., and Zuker, A. P. (2005). *Rev. Mod. Phys.*, 77:427. 15

[Caurier and Navrátil, 2006] Caurier, E. and Navrátil, P. (2006). *Phys. Rev. C*, 73:021302(R). 72

[Caurier et al., 1998] Caurier, E., Nowacki, F., Poves, A., and Retamosa, J. (1998). *Phys. Rev. C*, 58:2033. 15

[Chabanat et al., 1997] Chabanat, E., Bonche, P., Haensel, P., Meyer, J., and Schaeffer, R. (1997). *Nucl. Phys. A*, 627:710. 14

[Conn et al., 1933] Conn, A. R., Scheinberg, K., and Vicente, L. N. (1933). *Introduction to Derivative-Free Optimization*. MPS/SIAM Series on Optimization. Society for Industrial and Applied Mathematics, Philadelphia, PA, USA. 66

[Danielewicz and Lee, 2009] Danielewicz, P. and Lee, J. (2009). *Nucl. Phys. A*, 818:36. 48, 49, 50, 51

[Dobaczewski et al., 1984] Dobaczewski, J., Flocard, H., and Treiner, J. (1984). *Nucl. Phys. A*, 422:103. 11, 14

[Donaldson and Schnabel, 1987] Donaldson, J. R. and Schnabel, R. B. (1987). *Technometrics*, 26:67. 82

[Duflo, 1994] Duflo, J. (1994). *Nucl. Phys. A*, 576:29. 42, 73, 85

[Duflo and Zuker, 1995] Duflo, J. and Zuker, A. P. (1995). *Phys. Rev. C*, 52:R23. 8, 16, 17, 33, 34, 42, 45, 52, 59, 83, 88, 89

[Duguet et al., 2001a] Duguet, T., Bonche, P., Heenen, P. H., and Meyer, J. (2001a). *Phys. Rev. C*, 65:014310. 3

[Duguet et al., 2001b] Duguet, T., Bonche, P., Heenen, P. H., and Meyer, J. (2001b). *Phys. Rev. C*, 65:014311. 3

[Duguet et al., 2002] Duguet, T., Bonche, P., Heenen, P.-H., and Meyer, J. (2002). *Phys. Rev. C*, 65:014310. 11

[Elsasser, 1933] Elsasser, W. (1933). *J. Phys. Radium*, 4:549. 16

[Elsasser, 1934a] Elsasser, W. (1934a). *J. Phys. Radium*, 5:389. 16

[Elsasser, 1934b] Elsasser, W. (1934b). *J. Phys. Radium*, 5:635. 16

[Elton, 1950] Elton, L. R. B. (1950). *Proc. Phys. Soc.*, A63:1115. 71

[Eschrig, 2003] Eschrig, H. (2003). *The Fundamentals of Density Functional Theory (revised and extended version)*. Edition am Gutenbergplatz, Leipzig, Germany. 9

[Feynman, 1939] Feynman, R. (1939). *Phys. Rev.*, 56(4). 13

[Fiolhais et al., 2003] Fiolhais, C., Nogueira, F., and Marques, M., editors (2003). *A Primer in Density Functional Theory*. Springer. 12

[Friar, 1997] Friar, J. L. (1997). *Few Body Syst.*, 22:161. 90

[Friar et al., 1996] Friar, J. L., Madland, D. G., and Lynn, B. W. (1996). *Phys. Rev. C*, 53:3085. 90

[Friar et al., 1997] Friar, J. L., Martorell, J., and Sprung, D. W. L. (1997). *Phys. Rev. A*, 56:4579. 72

[Fritz et al., 1993] Fritz, R., Müther, H., and Machleidt, R. (1993). *Phys. Rev. Lett.*, 71:46. 7

[Furnstahl, 2002] Furnstahl, R. J. (2002). *Nucl. Phys. A*, 706:85. 90

[Furnstahl et al., 2007] Furnstahl, R. J., Hammer, H.-W., and Puglia, S. J. (2007). *Annals Phys.*, 322:2703. 11

[Gamow, 1930] Gamow, G. (1930). *Proc. R. Soc. London, Ser. A*, 126:632. 37

[Garthwaite et al., 2002] Garthwaite, P. H., Jones, B., and Jolliffe, I. T. (2002). *Statistical Inference*. Oxford Science Publications, Oxford. 51

[Giovinazzo et al., 2002] Giovinazzo, J., Blank, B., Chartier, M., Czajkowski, S., Fleury, A., Jimenez, M. J. L., Pravikoff, M. S., Thomas, J. C., de Oliveira Santos, F., Lewitowicz, M., and V. Maslov, e. a. (2002). *Phys. Rev. Lett.*, 89:102501. 2

[Goldberg, 1989] Goldberg, D. E. (1989). *Genetic Algorithms in Search, Optimization, and Machine Learning*. Addison-Wesley, Reading, MA, USA. 65

[Gomes et al., 1958] Gomes, L. C., Walecka, J. D., and Weisskopf, V. F. (1958). *Ann. Phys.*, 3:241. 16

[Goriely et al., 2009] Goriely, S., Chamel, N., and Pearson, J. M. (2009). *Phys. Rev. Lett.*, 102:152503. 8, 14, 75, 91

[Goriely et al., 2002] Goriely, S., Samyn, M., Heenen, P. H., Pearson, J. M., and Tondeur, F. (2002). *Phys. Rev. C*, 66:024326. 8, 14, 17

[Hagino and Bertsch, 2000] Hagino, K. and Bertsch, G. (2000). *Phys. Rev. C*, 61:024307. 19, 21, 26, 27

[Hartree, 1929] Hartree, D. R. (1929). *Math. Proc. Cambridge Phil. Soc.*, 25(2):225. 7

[Haxel et al., 1950] Haxel, O., Jensen, J. H. D., and Suess, H. E. (1950). *Z. Phys.*, 128:295. 16

[Hellman, 1937] Hellman, H. (1937). *Einfuehrung in die Quantenchemie*. Deuticke, Leipzig. 13

[Hohenberg and Kohn, 1964] Hohenberg, P. and Kohn, W. (1964). *Phys. Rev.*, 136:B864. 9, 12, 13

[Holozwarth and Yukawa, 1974] Holozwarth, G. and Yukawa, T. (1974). *Nucl. Phys. A*, 219:125. 19

[Kirson, 2008] Kirson, M. W. (2008). *Nucl. Phys. A*, 798:29. 51

[Klapdor-Kleingrothaus et al., 2001] Klapdor-Kleingrothaus, H., Dietz, A., Harney, H. L., and Krivosheina, I. V. (2001). *Mod. Phys. Lett. A*, 16:2409. 2

[Kohn and Sham, 1965] Kohn, W. and Sham, L. J. (1965). *Phys. Rev.*, 140:A1133. 11

[Kolda et al., 2003] Kolda, T., Lewis, R., and Torczon, V. (2003). *SIAM Review*, 45:385. 65

[Kortelainen et al., 2010a] Kortelainen, M., Furnstahl, R. J., Nazarewicz, W., and Stoitsov, M. V. (2010a). *Phys. Rev. C*, 82:011304. 89, 90

[Kortelainen et al., 2010b] Kortelainen, M., Lesinski, T., Moré, J., Nazarewicz, W., Sarich, J., Schunck, N., Stoitsov, M. V., and Wild, S. (2010b). *Phys. Rev. C*, 82:021603. 8, 14, 64, 65, 67, 74, 81, 89, 90, 91

[Koura et al., 2000] Koura, H., Uno, M., Tachibana, T., and Yamada, M. (2000). *Nucl. Phys. A*, 674:47. 50

[Kruppa et al., 2000] Kruppa, A., Bender, M., Nazarewicz, W., Reinhard, P. G., Vertse, T., and Cwiok, S. (2000). *Phys. Rev. C*, 61:034313. 5

[Kutzelnigg, 2006] Kutzelnigg, W. (2006). *Journal of Molecular Structure: THEOCHEM*, 768(1-3):163–173. 14

[Lacroix and Hupir, 2010] Lacroix, D. and Hupir, G. (2010). *Phys. Rev. B*, 82:144509. 45

[Li et al., 1970] Li, S. Y., Klein, A., and Dreizler, R. M. (1970). *J. Math. Phys.*, 11:975. 19

[Lieb, 1983] Lieb, E. H. (1983). *Int. J. Quant. Chem.*, 24:243. 14

[Lipkin et al., 1965] Lipkin, H. J., Meshkov, N., and Glick, A. J. (1965). *Nucl. Phys.*, 62:188. 19

[Lunney et al., 2003] Lunney, D., Pearson, J. M., and Thibault, C. (2003). *Rev. Mod. Phys.*, 75:1021. 1, 5, 7, 9

[Machleidt, 1989] Machleidt, R. (1989). *Adv. Nucl. Phys.*, 19(189). 7

[Mang, 1975] Mang, H. J. (1975). *Phys. Rep.*, 18:325. 7

[Martinez-Pinedo and Langanke, 1999] Martinez-Pinedo, G. and Langanke, K. (1999). *Phys. Rev. Lett.*, 83:4502. 2

[Mayer and Jensen, 1955] Mayer, M. and Jensen, J. H. D. (1955). *Elementary Theory of Nuclear Shell Structure*. Wiley, New York. 7, 15, 16, 41

[Mayer, 1966] Mayer, M. G. (1966). *Nucl. Phys.*, 81:1. 16

[Mendoza-Temis et al., 2008] Mendoza-Temis, J., Frank, A., Hirsch, J. G., Vieyra, J. C., Morales, I., Barea, J., Isacker, P. V., and Velazquez, V. (2008). *Nucl. Phys. A*, 799:84. 50

[Mendoza-Temis et al., 2010] Mendoza-Temis, J., Hirsch, J. G., and Zuker, A. P. (2010). *Nucl. Phys. A*, 843:14. 8

[Meredith et al., 1988] Meredith, D. C., Koonin, S. E., and Zirnbauer, M. R. (1988). *Phys. Rev. C*, 37:3499. 19, 20, 21

[Mielke and Theil, 2004] Mielke, A. and Theil, F. (2004). *NoDEA*, 11:151. 54

[Möller et al., 1995] Möller, P., Nix, J. R., Myers, W. D., and Swiatecki, W. J. (1995). *Atomic Data and Nuclear Data Tables*, 59:185. 8, 17, 50, 90

[Montgomery and Taylor, 2003] Montgomery, D. C. and Taylor, G. C. (2003). *Applied statistics and probability for engineers*. John Wiley and Sons. 82

[Moré and Wild, 2011] Moré, J. and Wild, S. (2011). *SIAM J. Scientific Computing*, 33:1292. x, 62, 63, 64

[Moré and Wild, 2009] Moré, J. J. and Wild, S. M. (2009). *SIAM J. Optim.*, 20:172. 65

[Myers and Schmidt, 1983] Myers, W. A. and Schmidt, K. H. (1983). *Nucl. Phys. A*, 410(1):61. 73

[Myers and Swiatecki, 2001] Myers, W. D. and Swiatecki, W. J. (2001). *Phys. Rev. Lett.*, 87:172502. 3

[Navrátil et al., 2001] Navrátil, P., Vary, J. P., and Ormand, W. E. (2001). *Phys. Rev. Lett.*, 87:172502. 7

[Ng et al., 2011] Ng, E., Sarich, J., Wild, S. M., Munson, T., Aktulga, H., Yang, C., Maris, P., Vary, J. P., Schunck, N., Bertolli, M. G., Kortelainen, M., Nazarewicz,

W., Papenbrock, T., and Stoitsov, M. V. (2011). *arXiv*, 1110.1708v1:[cs.CE]. 67, 91

[Nikolov et al., 2011] Nikolov, N., Schunck, N., Nazarewicz, W., Bender, M., and Pei, J. (2011). *Phys. Rev. C*, 83:034305. 48

[Oliveira et al., 1988] Oliveira, L. N., Gross, E. K. U., and Kohn, W. (1988). *Phys. Rev. Lett.*, 60:2430. 11

[Otsuka, 2001] Otsuka, T. (2001). *Hyperfine Interact.*, 132:409. 15

[Otsuka et al., 2001] Otsuka, T., Utsuno, Y., Mizusaki, T., and Honma, M. (2001). *Nucl. Phys. A*, 685:100. 15

[Ozawa et al., 2000] Ozawa, A., Kobayashi, T., Suzuki, T., Yoshida, K., and Tanihata, I. (2000). *Phys. Rev. Lett.*, 84:5493. 3

[Pain, 2011] Pain, S. (2011). *Private Communication*. 72

[Pandharipande et al., 1997] Pandharipande, V. R., Sick, I., and deWitt Huberts, P. K. A. (1997). *Rev. Mod. Phys.*, 69:981. 7

[Papadimitriou et al., 2011] Papadimitriou, G., Kruppa, A. T., Michel, N., Nazarewicz, W., Poszajczak, M., and Rotureau, J. (2011). *arXiv:1109.0223v2 [nucl-th]*. 71

[Papenbrock, 2006] Papenbrock, T. (2006). *Phys. Rev. A*, 72:041603. 11

[Papenbrock and Bhattacharyya, 2007] Papenbrock, T. and Bhattacharyya, A. (2007). *Phys. Rev. C*, 75:014304. 23, 45

[Pfützner et al., 2002] Pfützner, M., Badura, E., Bingham, C., Blank, B., Chartier, M., Geissel, H., Giovinazzo, J., Grigorenko, L. V., Grzywacz, R., Hellström, M., Janas, Z., and J. Kurcewicz, e. a. (2002). *Eur. Phys. J. A*, 14:279. 2

[Pieper, 2008] Pieper, S. C. (2008). *Riv. Nuovo Cim.*, 031:709. 72

[Pieper et al., 2001] Pieper, S. C., Pandharipande, V. R., Wiringa, R. B., and Carlson, J. (2001). *Phys. Rev. C*, 64:014001. 7

[Pomorski and Dudek, 2003] Pomorski, K. and Dudek, J. (2003). *Phys. Rev. C*, 67:044316. 50

[Powell, 1994] Powell, M. J. D. (1994). A direct search optimization method that models the objective and constraint functions by linear interpolation. In Gomez, S. and Hennart, J.-P., editors, *Advances in Optimization and Numerical Analysis*, page 51, Dordrecht. Kluwer Academic. 60

[Powell, 2003] Powell, M. J. D. (2003). *Math. Programming*, 97:605. 65

[Powell, 2004] Powell, M. J. D. (2004). *Optim. Meth. Software*, 19:399. 65

[Powell, 2007] Powell, M. J. D. (2007). *Report DAMTP 2007/NA05, CMS, University of Cambridge, Cambridge CB3 0WA, UK.* 69

[Puglia et al., 2003] Puglia, S. J., Bhattacharyya, A., and Furnstahl, R. J. (2003). *Nucl. Phys. A*, 723:145. 11

[Reinhard et al., 2006] Reinhard, P. G., Bender, M., Nazarewicz, W., and Vertse, T. (2006). *Phys. Rev. C*, 73:014309. 5

[Retamosa et al., 1997] Retamosa, J., Caurier, E., Nowacki, F., and Poves, A. (1997). *Phys. Rev. C*, 55:1266. 15

[Ring and Schuck, 1980] Ring, P. and Schuck, P. (1980). *The Nuclear Many-Body Problem*. Springer. 35

[Robinson, 1980] Robinson, S. M. (1980). *Math. of O.R.*, 5:43. 65

[Roy and Nigam, 1967] Roy, R. R. and Nigam, B. P. (1967). *Nuclear Physics: Theory and Experiment*. John Wiley and Sons, Inc., NY, USA. 38

[Royer and Gautier, 2006] Royer, G. and Gautier, C. (2006). *Phys. Rev. C*, 73:067302. 50

[Rusnak and Furnstahl, 1997] Rusnak, J. J. and Furnstahl, R. J. (1997). *Nucl. Phys. A*, 627:495. 90

[Satula et al., 1997] Satula, W., Dean, D., Gary, J., Mizutori, S., and Nazarewicz, W. (1997). *Phys. Lett. B*, 407:103. 46

[Seber and Wild, 1989] Seber, G. A. F. and Wild, C. J. (1989). *Nonlinear Regression*. Wiley. 82

[Skyrme, 1956] Skyrme, T. H. R. (1956). *Phil. Mag.*, 1:1043. 11, 14

[Sorlin et al., 2000] Sorlin, O., Leenhardt, S., Donzaud, C., Duprat, J., Azaiez, F., Nowacki, F., Grawe, H., Dombradi, Z., Amorini, F., Astier, A., Baiborodin, D., and M. Belleguic, e. a. (2000). *Phys. Rev. Lett.*, 88:092501. 3

[Stone and Reinhard, 2007] Stone, J. R. and Reinhard, P.-G. (2007). *Prog. Part. Nucl. Phys.*, 58:587. 2, 7, 8, 85

[Strutinsky, 1967] Strutinsky, V. M. (1967). *Nucl. Phys. A*, 95(2):420. 5, 45

[Talmi, 1962] Talmi, I. (1962). *Rev. Mod. Phys.*, 34:704. 46

[Thielemann et al., 2001] Thielemann, F. K., Brachwitz, F., Freiburghaus, C., Kolbe, E., Martinez-Pinedo, G., Rauscher, T., Rembges, F., Hix, W., Liebendorfer, M., Mezzacappa, A., Kratz, K. L., Pfeiffer, B., Langanke, K., Nomoto, K., Rosswog, S., Schatz, H., and Wiescher, W. (2001). *Prog. Part. Nucl. Phys.*, 46:5. 2

[Toivanen et al., 2008] Toivanen, J., Dobaczewski, J., Kortelainen, M., and Mizuyama, K. (2008). *Phys. Rev. C*, 78:034306. 81

[Tondeur et al., 1984] Tondeur, F., Brack, M., Farine, M., and Pearson, J. M. (1984). *Nucl. Phys. A*, 420:297. 14

[Vautherin, 1973] Vautherin, D. (1973). *Phys. Rev. C*, 7:296. 11, 14

[Vautherin and Brink, 1972] Vautherin, D. and Brink, D. M. (1972). *Phys. Rev. C*, 626. 11, 14

[Wigner, 1937] Wigner, E. (1937). *Phys. Rev.*, 51:106. 46

[Wild, 2011] Wild, S. (2011). *Private Communication*. Sep.-Oct. x, xi, 62, 63, 70

[Wild, 2008] Wild, S. M. (2008). *10th C. M. Conf. Iter. Meth.* 66

[Wiringa et al., 2000] Wiringa, R. B., Pieper, S. C., Carlson, J., and Pandharipande, V. R. (2000). *Phys. Rev. C*, 62:014001. 7

[Zeldes, 1998] Zeldes, N. (1998). *Phys. Lett. B*, 429:20. 46

[Zhou et al., 1997] Zhou, J. L., Tits, A. L., and Lawrence, C. T. (1997). User's guide for ffsqp version 3.7. Technical Report RC-TR-92-107r5, Institute for Systems Research, University of Maryland. 61

Vita

Michael Bertolli was born in 1987 and lived with his family in various locations before attending university at the Colorado School of Mines (Golden, CO). At the School of Mines he immediately enrolled as a physics major where he earned both his Bachelor and Master of Science degrees. After a brief year in experimental nuclear physics research as an undergraduate, Michael was introduced to nuclear theory by Dr. James McNeil. Completing his Master's degree in few-body nuclear structure theory under Dr. McNeil, Michael moved on to a PhD program at the University of Tennessee (Knoxville, TN) in the Fall of 2007. While few-body nuclear theory had held great interest to Michael, he obtained his desired opportunity to begin the study of many-body nuclear theory at the University of Tennessee. The opportunity allowed him to grow intellectually through work with his thesis advisor and collaborators at Oak Ridge and Argonne National Laboratories.

Michael was awarded a full graduate research assistantship his first year at the University of Tennessee, and was afforded opportunities to work along side many of the greatest in his field. Through many conferences, courses and exams he continued to study both nuclear theory in the realm of mass models and the various necessary numerical techniques. In the course of his work he met Alicia Caputo to whom became engaged to in 2011. Awarded his PhD in December of 2011, Michael will be joining the Theory Division at Los Alamos National Laboratory.